USGS
science for a changing world

Structure and Velocities of the Northeastern Santa Cruz Mountains and the Western Santa Clara Valley, California, from the SCSI-LR Seismic Survey

By R.D. Catchings, M.R. Goldman, and G. Gandhok[1]

Open-File Report 2006-1014

U.S. Department of the Interior
U.S. Geological Survey

[1]U.S. Geological Survey, 345 Middlefield Rd, MS 977, Menlo Park, CA 94025

U.S. Department of the Interior
Gale A. Norton, Secretary

U.S. Geological Survey
P. Patrick Leahy, Acting Director

U.S. Geological Survey, Reston, Virginia 2006
Revised and reprinted: 2006

For product and ordering information:
World Wide Web: http://www.usgs.gov/pubprod
Telephone: 1-888-ASK-USGS

For more information on the USGS—the Federal source for science about the Earth, its natural and living resources, natural hazards, and the environment:
World Wide Web: http://www.usgs.gov
Telephone: 1-888-ASK-USGS

Introduction

The Santa Clara Valley is located in the southern San Francisco Bay area of California and generally includes the area south of the San Francisco Bay between the Santa Cruz Mountains on the southwest and the Diablo Ranges on the northeast (**Fig. 1a**). The area has a population of approximately 1.7 million including the city of San Jose, numerous smaller cities, and much of the high-technology manufacturing and research area commonly referred to as the Silicon Valley (**2000 U. S. Census; http://quickfacts.census.gov/qfd/states/06/06085.html**). Major active strands of the San Andreas Fault system bound the Santa Clara Valley, including the San Andreas fault to the southwest and the Hayward and Calaveras faults to the northeast; related faults likely underlie the alluvium of the valley (**CWDR, 1967**). This report focuses on subsurface structures of the western Santa Clara Valley and the northeastern Santa Cruz Mountains and their potential effects on earthquake hazards and ground-water resource management in the area. Earthquake hazards and ground-water resources in the Santa Clara Valley are important considerations to California and the Nation because of the valley's preeminence as a major technical and industrial center, proximity to major earthquakes faults, and large population.

To better assess the earthquake hazards of the Santa Clara Valley, the U. S. Geological Survey (USGS) has undertaken a program to evaluate potential earthquake sources and potential effects of strong ground shaking within the valley. As part of that program, and to better assess water resources of the valley, the USGS and the Santa Clara Valley Water District (SCVWD) began conducting collaborative studies to characterize the faults, stratigraphy, and structures beneath the alluvial cover of the Santa Clara Valley in the year 2000. Such geologic features are important to both agencies because they directly influence the availability and management of groundwater resources in the valley, and they affect the severity and distribution of strong shaking from local or regional earthquakes sources. As one component of these joint studies, the U. S. Geological Survey acquired more than 28 km of combined seismic reflection/refraction data from the Santa Cruz Mountains to the central Santa Clara Valley in December 2000 (**Fig. 1a**). The seismic investigation included both high-resolution (~5-m shot and sensor spacing) and relatively lower-resolution (~50-m sensor) seismic surveys from the central Santa Cruz Mountains to the central part of the valley (**Fig. 1a-c**). Collectively, we refer

to these seismic investigations as the 2000 western Santa Clara Seismic Investigations (SCSI). Results of the lower-resolution study, referred to as SCSI-LR, are presented in this report, and results of the high-resolution seismic study (SCSI-HR) are presented in a separate report by **Catchings et al. (2005).**

Local Geology, Tectonics, and Hydrogeology

The Santa Clara Valley is part of the topographic depression that forms the San Francisco Bay between the Santa Cruz Mountains and the Diablo Range (**Fig. 1a**). Surficial and near-surface sediments within the Santa Clara Valley largely consist of Plio-Pleistocene to Holocene clastic deposits (clay, silt, sand, and gravel) from the adjacent mountain ranges and marine sediments (**CDWR, 1967; Wagner, 1990; Wentworth et al., 1998; McLaughlin et al., 2001**). The composition of basement rocks beneath the valley is not known but is assumed to be the same as those in the adjacent mountain ranges (**Fig. 1d**). These rocks include the Jurassic to Cretaceous Franciscan Complex (marine sediments, largely mélanges, including serpentine, volcanic, and metamorphic rocks), the Coast Ranges Ophiolite (ultramafic to intermediate igneous rocks), and the Great Valley Sequence (**McLaughlin et al., 2001**). The Jurassic-Cretaceous rocks are, in places, overlain by Eocene to Pliocene marine sediments and intercalated volcanic rocks. At least one recently drilled borehole near the center of the valley encountered serpentinite at about 225 m depth (**Orze et al., 2003**), which is likely part of the Coast Ranges Ophiolite.

Within the adjacent mountain ranges, rocks are highly faulted and folded (Fig. 1d) due to tectonism, much of which is associated with the San Andreas fault system (**CDWR, 1967**; **McLaughlin et al., 2001**). Similarly faulted and folded rocks underlie the Santa Clara Valley beneath the near-surface Quaternary alluvium, as evidenced by strike-slip and reverse faults and folded strata that have been mapped on uplifted ridges (for example, Santa Teresa Hills and the Sierra Azul) within the valley (**McLaughlin et al., 2001)**. Some of the buried faults are active, as shown by seismic events recorded beneath the valley (**Zoback et al., 1995; ANSS Catalog, 2003-** anss@quake.geo.berkeley.edu). Differential movement on these faults may have produced a series of basement highs and lows, several-kilometer-deep basins near the margins (i.e., Cupertino and Evergreen basins), and a relative basement high near the center of the valley (**CWDR, 1967; Stanley et al., 2002**).

Near-surface consolidated and low-permeability Franciscan Complex rocks are regarded as non-water bearing and not a significant contributor to the hydrogeology of the valley. Fresh-water-bearing deposits that form the ground-water reservoir within the Santa Clara Valley are chiefly of Quaternary age, and they include the semi-consolidated, Plio-Pleistocene non-marine Santa Clara Formation (SCFm), associated marine deposits of Pliocene and Pleistocene age, and the overlying Pleistocene-to-Holocene unconsolidated alluvial and bay deposits (**CWDR, 1967**). Lateral variations in the thickness of the SCFm are poorly known, but the SCFm has been encountered in boreholes at depths ranging from about 30 m to several hundred meters within the valley. Where exposed in the adjacent Santa Cruz Mountains, the SCFm is locally tightly to mildly folded and faulted and consists of poorly sorted conglomerate, sandstone, siltstone, and clay that is as much as 600 m thick in outcrop (**Dibblee, 1966; McLaughlin et al., 2001**). Where it crops out on the southwest flanks of the valley, the SCFm dips 10 to 30 degrees to the east (**CDWR, 1967**), but locally, the SCFm dips at 60 degrees to vertical or is overturned where associated with faulting along the southwest Santa Clara Valley margin. The SCFm is assumed to similarly dip beneath the alluvial cover. The unconsolidated alluvial and bay deposits (clay, silt, sand, and gravel) that overlie the SCFm contain the most productive aquifers of the ground-water reservoir (**Poland, 1971**). Minimum depths to the water table are highly variable within the valley, but generally range from about 10 to 40 m below ground surface (**CWDR, 1967**).

SCSI Data Acquisition

The SCSI survey consisted of two seismic surveys along nearly the same transect, an ~18-km-long, lower-resolution (50-m sensor; 1-km shot spacing) survey from the San Andreas fault to downtown San Jose (**Fig. 1a**), and an ~10-km-long, high-resolution (5-m shot and sensor spacing) survey between shot points 1 and 10 of the lower-resolution survey (**Fig. 1b,c**). Each survey was acquired in a manner that yields both seismic refraction and seismic reflection images of the subsurface. This report describes data acquisition, processing, and analysis for the lower-resolution (SCSI-LR) survey.

We used 11 buried explosions (shot points 1-11) ranging in size from about 12 to 23 kg to generate seismic sources approximately every kilometer along the central part of the N-60^{o}-E-trending profile (**Fig. 1)**. To record the blasts, we placed 416 "Texan" seismographs, with single-element, Mark Products 1-10B^{TM}, vertical-component, 4.5-

and 40-Hz geophones, every 50 m along the profile. The 4.5-Hz and 40-Hz geophones alternated in sequence along the profile, such that there was 100 m spacing between geophones of the same frequency. The Texan seismographs were programmed to record the 11 blasts during specific time windows between the hours of 12:00 am and 5:00 am, when cultural noises were relatively low. Sixty seconds of data were recorded for each shot at a sampling rate of 1 ms. Seismographs were then retrieved the following day, and the data were downloaded to a computer. The internal timing of the seismographs was checked using Global Positioning System (GPS) clocks before and after deployment, and a linear drift was assumed. Acquisition parameters for the SCSI-LR survey are given in Table 1.

To account for variations in the SCSI profile geometry, each shot point and geophone location was surveyed using an electronic distance meter (EDM) or Global Positioning System (GPS) with theoretical accuracies of a few centimeters (see **Appendices 1-3**). Seismograph elevations varied by about 250 m along the profile (**Fig. 2a**). Lateral variations in the seismograph array (with respect to a line connecting the first and last shot points) were less than about 500 m within the shot array (**Fig. 2b**). However, northeast and southwest of the shot array, the seismograph array varied from this line by about 2.5 km. Relative to the seismograph array length (17.7 km), individual seismographs varied by about 2.8% and 14% within and outside of the shot array, respectively. Because the major deviation from an ideally linear profile was not within the shot array (**Fig. 2c**), the non-linearity of seismographs outside of the shot-point array has a minimal effect on the modeled structure of the Santa Clara Valley. The shot array was about 12.4 km long (**Fig 2c**), and shot point elevations varied by about 150 m (**Fig. 2d**). Relative to a line connecting the end points of the shot array, individual shots varied laterally from an ideal profile by about 200 m or 1.6% of the shot line length. Most of the non-linearity of the seismic profile was required because of the high degree of urbanization in the study area.

For velocity modeling and reflection stacking, we redefined arrays to remove redundant stations as shown in **Appendix 2**.

Table 1. Acquisition parameters for the SCSI low-resolution seismic profile. Distance is relative to the first seismograph.

Parameter	Length	Number	Type	Spacing
Profile	17.7 km	1	2-D	
Geophone	17.7 km	416	4.5 & 40 Hz, Vertical	50 m
Shot Points	12.4 km	11	Explosion	1 km
Seismograph	17.7 km	416	Reftek RT125 (Texan)	50 m
Record	60 s	4576	SEGY	
Sample Rate	1 ms			

Data Processing

We minimally processed the shot gathers presented in this report (**Fig. 3**). After individual shot gathers were assembled, we used trace editing to remove noisy or dead traces, and we bandpass-filtered the data to accommodate the varying frequency ranges of the geophones.

Seismic Data

Unreduced SCSI-LR shot gathers are shown in **figure 3a-k,** with low bandpass filtering (2-4-10-20 Hz) applied. A total of 60 s of data were acquired, but we present only the first 6 s in **figure 3**. Although the urban environment was noisy, useful seismic energy from the shots propagated across the seismic profile for most shots. Surface-wave, air-wave, and some shear-wave arrivals are also present on most shot gathers. Near-vertical and wide-angle reflections are also observed on all shot gathers, which allow low-fold reflection images to be developed. The complex topography on the pre-Cenozoic basement structure beneath the Santa Clara Valley is inferred from the non-linear moveout of refracted arrivals (**Fig. 3**).

Seismic Velocity Modeling

To develop P-wave tomographic seismic velocity models of the subsurface along the SCSI seismic profile, we inverted first-arrival refractions from usable seismograms using a modified version of an algorithm by **Hole (1992**). The velocity inversion method uses 2- or 3-D raytracing (**Fig. 4a**) to match observed and calculated travel times until a suitable fit is obtained for all arrivals from all shots. A total of about 4500 first-arrival

picks were available from the data. We used reciprocal shot and receiver travel times to improve accuracy of the first-arrival picks. A maximum error of 10 ms was allowed between reciprocal P-wave travel time picks. In parameterizing the P-wave model, we used 50-m by 50-m horizontal and vertical grid spacings and a 2-D starting model derived from composite 1-D velocity models, calculated from shot gathers. We used multiple 2-D starting velocity models, but regardless of the starting model used, successive velocity inversions yielded similar final 2-D velocity models, suggesting that velocity structure is fairly well resolved. In general, the model is best resolved where we have the highest density of ray coverage (**Fig. 4a**). We applied a smoothing routine to the inversion that yielded an approximately 100- to 300-m vertically and horizontally smoothed final model (**Fig. 4b**). The ray density diagram is colored white (masking) where we have less than 2 ray paths within a given $50m^2$ grid. The corresponding $50m^2$ areas of the velocity model have similarly limited ray coverage, but to better visualize the velocity model, we present the model without masking.

The minimum depth of velocity imaging is related to the shot (1 km) and geophone (50 m) spacing, the model grid spacing (50 m), and the amount of smoothing used in modeling. Therefore, velocities in the upper 100 m are a smoothed average of the velocities within those depth ranges. The maximum depth of velocity imaging was limited by the maximum distance that clear first arrivals could be measured on the shot gathers (**Fig. 3**). Because of the noisy urban environment, clear first arrivals were measurable to varying distances for each shot, but first arrivals were measurable to minimal distances greater than 10 km from the source for most shots.

Although we used vertical-component geophones and explosive-source shots, shear-wave energy was generated and recorded for some of the shots, particularly those shots within or near bedrock (**Fig. 3**). We used the same picking parameters and tomographic modeling code to develop an S-wave velocity model of the subsurface along the SCSI seismic profile (**Fig. 5b**). The secondary shear-wave arrivals were not as clearly measurable to distances as great as those of the first-arrival P-wave, resulting in shallower depths for the S-wave model. The secondary S-wave arrivals were also less reliably picked, and as a result, we have less confidence in the S-wave model than the P-wave model, particularly at depths below 1.5 km. For both the P-wave and S-wave arrivals, we used reciprocity between shot and receiver pairs to increase accuracy.

Seismic Velocity and Related Images

P-Wave Velocity Model

First-arrival refractions were measurable to sufficient distances to develop a P-wave velocity model to maximum depths of about 3 km (**Fig. 4b**). Observed velocities are highly variable across the model but are generally highest (~ 5- to 6.5 km/s) at depth below the Santa Cruz Mountains and also near the base (~3 km) of the velocity model below the Santa Clara Valley. Velocities are lowest (< 1600 m/s) at the surface within the Santa Clara Valley, where Quaternary sediments are exposed at the surface. Relatively low velocities (< 3 km/s) persist to the greatest depths (~1.5 km) near the central part of the seismic profile (Cupertino Basin), but there are appreciable lateral and vertical variations in velocity. For example, one prominent feature of the model is the velocity anomaly near Los Gatos, where relatively high-velocity (~4.5 km/s) rocks overlie lower-velocity (~4.0 km/s) rocks. Such reversals in velocity indicate complex structures because on crustal scales, lower-velocity rocks usually overlie higher-velocity rocks. The general upper-crustal (3 km) pattern along the profile consists of relatively high velocities within the Santa Cruz Mountains and the central Santa Clara Valley (San Jose area) and low velocities beneath the Cupertino Basin.

S-Wave Velocity Model

S-wave arrivals are observed best near the southwestern part of the seismic profile within harder rocks. Within the alluvium of the Santa Clara Valley, limited generation and/or propagation of S-wave arrivals resulted in poor resolution of the deeper structure on the northeast end of the seismic profile. The S-wave model is most reliably developed for the upper 1.5 km of the profile, but a poorly resolved model, resulting from uncertainties in picking secondary arrivals, was determined for the upper 3 km near the center of the seismic profile. Velocities range from 0.5 km/s near the surface to about 3.5 km/s within the base of the model. Low- and high-velocity features within the S-wave velocity model are similar to those of the P-wave model, including relatively higher near-surface velocities in the Santa Cruz Mountains and thicker, low-velocity deposits in the Cupertino Basin. The S-wave velocity model also shows a velocity inversion similar to that observed for the P-wave velocity model beneath the Los Gatos area. The lowest S-wave velocities (0.5 km/s) correspond to near-surface sediments, which appear to be

thickest within the Cupertino basin. The highest S-wave velocities (~3.5 km/s) are observed in the Santa Cruz Mountains and at the base of the model.

Models of Vp/Vs and Poisson's Ratios

Variations in Poisson's and Vp/Vs ratios can yield information about crustal composition and physical conditions of the crust, such as water saturation and crack density (faulting). We developed a Vp/Vs ratio model from the P- and S-wave velocity models (**Fig. 6a**). The Vp/Vs ratio model was calculated to the maximum depths of the S-wave velocity model (~3 km), but the Vp/Vs ratios are probably most reliably determined at depths less than 1.5 km. Vp/Vs ratios vary from about 1.5 to about 3.6, with the highest ratios occurring near the surface, particularly in the vicinity of water reservoirs in the Los Gatos area, and near the northeastern part of the seismic profile. The lowest ratios (~1.5) are calculated for depths between 0.5 and 1 km below Lexington Reservoir and at depths in excess of 1.5 km near the northeastern part of the seismic profile. Although such low Vp/Vs ratios could be related to faulting (**Catchings, 1999**), Vp/Vs ratios below 1.5 km on the northeastern part of the profile are not well constrained due to the poor constraints on S-wave velocities in that part of the profile.

A model of Poisson's ratio was developed along the SCSI profile using the P- and S-wave velocities (**Fig. 6b**). Due to properties of P- and S-wave propagation, Poisson's ratio (v) can be determined using the following relations (**Thomsen, 1990; Schon, 1996**):

$$v = (E/2u) - 1 = (3K-2u)/(6K+2u) = [(Vp/Vs)^2] - 2/[2(Vp/Vs)^2] - 2$$

Where u = shear modulus, E= Young's modulus, K = Bulk modulus, Vp = compressional or P-wave velocity, and Vs = shear or S-wave velocity.

The modeled Poisson's ratios (PR) show considerable lateral variation along the SCSI-LR profile, with the highest values (~0.46) near the surface and lowest values of about 0.05. Due to the poor S-wave measurements on the northeastern end of the model below about 1.5 km depth, very low PR values (~0.05) in that area of the model are probably not reliable. Some other areas of the PR model, however, show relatively low PR values (~0.26), which are consistent with average values (~0.24-0.29) for common plutonic rocks (**Christensen, 1996**).

Seismic Reflection Processing

In acquiring the seismic data, we used a shoot-through geometry, whereby shots were systematically fired through a stationary recording array. The combination of multiple sources and multiple receivers, which were spread over long distances, permitted both reflection and refraction data to be simultaneously acquired.

In seismic-reflection data processing, we followed procedures similar to those outlined by **Brouwer and Helbig (1998**). Processing steps included geometry installation, independent trace editing, timing corrections, elevation static corrections, automatic gain control (AGC), bandpass filtering, F-K filtering (or surgical muting), velocity analysis (from refractions, semblence, and borehole-velocity measurements), normal-move-out (NMO) correction, stretch muting, common-depth-point (CDP) stacking, post-stack AGC, post-stack bandpass filtering, and post-stack deconvolution. For depth-migrated sections, we used Kirchoff pre-stack depth migration after velocity analysis. Principal parameters used in processing are shown in **Table 2**.

In trace editing, noisy traces (due to cultural noises) or redundant traces (due to geometry) were removed from the shot gathers before stacking or migrating, leaving approximately 366 channels per shot gather. We surgically muted first-arrival refractions, and we applied bottom muting by surgically removing all arrivals between the surface waves. Elevation statics, migration, and velocity analysis were accomplished using the tomographic velocity model from both the lower- and higher-resolution SCSI profiles. For velocities at depths in excess of those determined by the tomography velocity model, we used parabolic methods, and we inferred velocities based on laboratory-determined velocity-depth (pressure) relations (**Carmichael, 1989**).

Table 2. Reflection Processing Parameters for the SCSI Profile

Maximum Fold	11
CDP Spacing	25 m
AGC Prestack Poststack	 2000 ms 300 ms
Bandpass Filter Prestack Poststack Low	 5-10-80-160 Hz 5-10-50-100 Hz
Deconvolution (filter length, prediction dist., application gate)	700 ms, 65m, 0-5000 m
Migration (frequency, aperture, angle)	200, 8000, 30

Seismic Reflection Images

A migrated seismic reflection image along the SCSI profile was developed from about meter 2300 to about meter 17000 of the SCSI-LR profile (**Fig. 7**). The length of the reflection image was largely determined by the position of the shot point array, and to a lesser extent, by the curvature of the recording array on the southwestern part of the seismic profile. In general, the seismic reflection image shows that the Santa Clara Valley is more reflective to greater depths than the Santa Cruz Mountains, but appreciable lateral variations in reflectivity are observed both within the valley and the mountains. The seismic image also shows that the upper few kilometers of the crust is complex, with folded and faulted strata. Because of the complexity of the structure, interpretation of the seismic reflection image is difficult. However, in the discussion section below, we combined the available data (velocities, velocity ratios, reflection, and geologic) to develop an interpretative model.

Combined Velocity and Seismic Reflection Images

We superimposed the velocity models onto the seismic reflection image so that direct comparisons between P- and S-wave velocities, their ratios, and the reflection image could be made (**Figs. 8a-d**). The combined P-wave velocity and reflection image shows appreciable variation in the velocities of the layered rocks (**Fig. 8a**). Near the southwestern end of the profile (meters 2300 to 5000), near-surface, layered rocks have velocities ranging from about 3000 to 5000 m/s in the upper 500 m depth. However, layered rocks beneath the Cupertino Basin (~meter 9000) have velocities less than 3000 m/s in the upper 1.5 km depth. Higher velocities (>3500 m/s) at relatively shallow (< 1000 m) depths are also observed near meter 11000. Deeper, less reflective rocks generally have velocities in excess of 3500 m/s, and a prominent northeast-dipping reflector generally marks the boundary between the higher-velocity rocks and the low-velocity rocks. As discussed below, the higher-velocity and less-reflective rocks probably correlate with basement rocks.

Similar variations in the S-wave velocity structure are observed (**Fig. 8b**). Most of the highly reflective rocks have S-wave velocities less than 2000 m/s in the upper 1.5 km beneath the Santa Clara Valley. The high reflectivity and low S-wave velocities are consistent with the presence of sedimentary rocks in that depth range. The rocks

underlying these probable sediments at depth (> 3 km) beneath the Cupertino Basin are not as reflective and have lower S-wave velocities (<3000 m/s) than rocks at similar depths in the adjacent Santa Cruz Mountains and central Santa Clara Valley. Because these rocks are poorly reflective, they are probably not horizontally layered sedimentary rocks (i.e., probably mélange or related Franciscan rocks or massive Coast Ranges Ophiolitic rocks), and as discussed below, the low S-wave velocities are probably related to fractured and faulted rocks beneath the Cupertino Basin. There are similar variations in Vp/Vs and Poisson's ratios, whereby high Vp/Vs (> 2.8) and Poisson's (0.38) ratios are largely confined to the highly reflective near-surface (probably water saturated) deposits in the Santa Clara Valley (**Figs. 8c and 8d, respectively**). Low Vp/Vs (< 2.0) and Poisson's (0.25) ratios are largely limited to poorly reflective deeper rocks. These Vp/Vs and Poisson's ratios are more consistent with common igneous rocks than sedimentary rocks (**Christensen, 1982; 1996**).

Geologic Maps and Cross Sections

The near-surface geology along the SCSI profile includes deposits and rocks ranging in age from Holocene to Jurassic (**McLaughlin et al., 2001**). As many as seven recognizable fault zones, each with multiple fault strands, are mapped at the surface within the Santa Cruz Mountains between the San Andreas fault and the center of the SCSI profile (**Fig. 1d**). Each of the fault zones may be several tens of meters wide and includes folded and faulted rocks of varying geologic ages. Published cross sections (**McLaughlin et al., 2001**) for the Santa Cruz Mountains show a series of near-vertical strike-slip and lower-angle reverse faults (with associated antithetic faults). Many of these faults dip to the southwest at the surface where exposed and are inferred to dip southwestward toward (and presumably join with) the San Andreas fault at depth (**McLaughlin et al., 2001**). Along the Santa Clara Valley segment of the SCSI profile, rocks are covered by Holocene-to-Pleistocene alluvial deposits (**Helley et al., 1994**), and the lithology of the subsurface rocks and associated structures are poorly known below the surface. However, the shallow-depth subsurface lithology and structures can be inferred from geophysical data and lithologic logs from a number of nearby boreholes (**Stanley et al., 2002**). The lithology and structure beneath part of the Santa Clara Valley can also be inferred from rock exposures within the Santa Teresa Hills, approximately 5 km east-southeast of the SCSI profile. Rocks within the Santa Teresa

Hills range in age from Quaternary to Jurassic and include geologic materials ranging from sediments to ophiolitic rocks. Similar rocks conceivably underlie the Santa Clara Valley along the SCSI profile. Structures observed in the Santa Teresa Hills may also provide clues to the subsurface structure beneath part of the SCSI profile, including the dips of some faults and stratigraphic units. **McLaughlin et al. (2001**) interpret a predominant northeasterly dip for most faults and stratigraphic units in the Santa Teresa Hills. Thus, similar structures may underlie the Santa Clara Valley segment of the SCSI profile.

Comparison with Available Well Data

Data from two recently drilled wells (McGlincey and Willow wells - see **Fig. 1a,c**) along and adjacent to the SCSI profile can be compared with the SCSI seismic data. The 240-m-deep McGlincey well was located near meter 12500 (shot point 9) of SCSI profile, and the 254-m-deep Willow well was located at the northeast end of the SCSI profile (**Orze et al., 2003**). Borehole data from the McGlincey well included P- and S-wave velocity measurements and lithologic well logs, which can be compared with SCSI velocity data (**Fig. 9**). In general, there is close agreement between the borehole sonic velocities and the SCSI refraction velocities. Seismic P-wave velocities in the McGlincey well range from about 1500 m/s at 5 m depth to about 2500 m/s at 100 to 200 m depth (**Hansen et al., 2004**), with an average P-wave velocity ~2200 m/s in the 20 m to 240 m depth range. Where the McGlincey well projects to the SCSI profile, SCSI P-wave velocities range from about 2050 m/s within 50 m of the surface to about 2200 m/s at 250 m depth, with an average velocity of about 2100 m/s. SCSI S-wave velocities in the vicinity of the McGlincey well range from about 500 m/s at the surface to about 850 m/s at 240 m depth, with an average S-wave velocity of about 700 m/s. S-wave velocities measured in the McGlincey well vary from about 500 to 1000 m/s, with an average S-wave velocity of about 750 m/s in the upper 250 m. Thus, both P-wave and S-wave velocities from the SCSI profile and those from the McGlincey well are comparable, given the relatively low resolution of the SCSI data. Velocity data are not available for the Willow well, but comparisons can be made based on lithologic logs from both wells.

We also used the lithologic information from oil wells (**Stanley et al., 2002**) and the McGlincey and Willow wells (**Newhouse et al., 2004; Fig. 1c**) to constrain probable

rock types at shallow depths along the SCSI profile. Near the central part of the SCSI profile, **Stanley et al. (2002)** used lithologic logs from oil wells that were drilled during the late 19th and early 20th centuries to interpret the lithology in the upper 800 m. They interpret Quaternary sediments to overlie Miocene sediments in the upper few hundred meters along the central part of the SCSI profile, with Miocene rocks extending to more than 800 m below the surface in the deepest oil well. We plotted the interpreted well logs in their approximate locations on the SCSI-LR reflection image (**Fig. 7**). The well logs indicate that the Quaternary-Miocene boundary correlates with a prominent reflector that extends across most of the western Santa Clara Valley. Because of the relatively low resolution of the SCSI-LR reflection images, reflective layers are averaged over about depth ranges of about 100 m. Thus, SCSI-LR reflection image would generate reflections that are approximately centered on the Quaternary-Miocene boundary where the Quaternary sediments are less than about 100 m thick.

In all but one of the well logs analyzed, **Stanley et al. (2002)** interpreted Miocene sediments at the bottom of the wells. In the one excepted well, they interpret Franciscan or Coast Ranges Ophiolitic rocks at about 100 m depth in the vicinity of Vasona Reservoir. However, we interpret the seismic data as being more consistent with the presence of Miocene sediments at 100 m depth in the vicinity of Vasona Reservior because apparent Miocene layers appear laterally continuous in that area (**Fig. 7**).

A hard, relatively low-velocity (~2200 m/s) rock, which correlates with the base of the ground-water aquifer (**Newhouse et al., 2004**), was encountered in the McGlincey well at about 240 m depth, and this rock correlates with a reflector at the same depth in the SCSI reflection image (**Fig. 7**). Paleontological data from the McGlincey well indicate that Miocene rocks underlie SCFm rocks (**C. Wentworth, Pers. Comm., 1994**) at about the depth (240 m) of our SCSI reflector. The reflector is largely continuous across the Santa Clara Valley northeast of SP 5 (~meter 8000) along the SCSI profile. The correlation between the ground-water aquifer (as revealed in the various wells) and the SCSI reflector suggests that the base of the ground-water aquifer may be traced laterally across most of the western Santa Clara Valley on the SCSI reflection image (**Fig. 7, 8b**). This reflector and others above and below it appear to be vertically offset by at least tens of meters in several places along the profile, suggesting that the ground-water aquifer system is faulted in places along the profile.

Only sedimentary rock was observed at the base of the McGlincey well at ~240 m, but serpentinite was found at the base of the Willow well at about 245 m depth. The two wells are separated laterally by about 5 km, and the difference in lithology at the base of the two wells suggests that there is a major lithologic change in shallow subsurface rocks over the 5-km distance. The change in shallow-depth (~upper 250 m) lithology between the McGlincey well and the Willow well (which is located about 0.7 km ENE of the northeast end of the SCSI profile; **Fig. 1c**) is indicated by an abrupt change in the reflectivity pattern near meter 15000 of the SCSI profile (**Fig. 7**).

Interpretation and Discussions

The complex tectonic setting and history of the eastern Santa Cruz Mountains and the western Santa Clara Valley makes interpretation of seismic velocity and reflection images difficult. Multiple fault zones with northeast- and southwest dips and both strike-slip and reverse motions are superimposed upon rocks ranging in composition from sedimentary to ultramafic (**Dietz and Ellsworth, 1997; Simpson, 2004; McLaughlin et al., 2001**). Because similar tectonism and structural complexity are likely beneath the alluvium of the western Santa Clara Valley, seismic reflection images are difficult to interpret, especially for the deeper (older) structures. By combining the reflection and refraction images with other data, such as seismicity data, geologic mapping, and borehole data, we present non-unique interpretations of the upper 3 km of the crust that may be important in evaluating water resources and earthquake hazards.

Structure of the Groundwater Aquifer System

The maximum depth of the ground-water aquifer in the Santa Clara Valley is poorly determined, but it is generally assumed to correlate with the maximum depth of the Pliocene to Holocene semi-consolidated and unconsolidated sediments (**CDWR, 1967**). Although older consolidated rocks, such as Franciscan rocks, may contain water, they are unlikely to be a major part of the ground-water aquifer system because of their low permeabilities. Therefore, the seismic P-wave velocities, which increase with ground-water saturation or consolidation, can be used to help constrain lateral variations in the ground-water aquifer system across the Santa Clara Valley. Vp/Vs and Poisson's ratios are also sensitive to the presence of water in unconsolidated sediments, and therefore, these measures should also be indicative of lateral variations in the ground-

water aquifer system. Due to the relatively low resolution of the SCSI-LR profile, however, the velocities and their ratios may be indicative of structures over vertical and lateral ranges of 50 to 300 m.

Because compressional-wave velocities (Vp) greatly increase in unconsolidated sediments which are more than 90% water saturated (**Nur, 1982**), saturated unconsolidated sediments generally have minimum P-wave velocities of about 1500 m/s (**Schon, 1996; Catchings et al., 1999a;b; Gandhok et al., 1999**). The shallowest P-wave velocities imaged along the SCSI profile range from about 1500 m/s to about 2000 m/s in the upper 100 m (**Fig. 4b, 8a**). These velocities, which are averaged over at least 50-m intervals, are consistent with velocities expected of the shallow ground-water aquifer along SCSI profile, as the minimum depths to the ground-water aquifer along the SCSI profile is known to range from about 10 to 50 m (**Table 3**). Because of the wide (50 m) spacing of seismographs (low resolution), the velocity images do not provide information about the upper ~25 m, and therefore, the minimum depth of the ground-water aquifer cannot be inferred from the SCSI-LR P-wave velocity data alone. However, minimum depths are inferred from the SCSI-HR velocity data to be about 5 to 40 m along the SCSI profile (**Catchings et al., 2005**). The maximum depth of the ground-water aquifer along the SCSI profile, however, can be inferred on the basis of higher-velocity rocks (~2200 to 2300 m/s), which are typically too consolidated (impermeable) to act as efficient ground-water aquifers. Within the McGlincey well, consolidated sedimentary rocks (~2200 m/s) form the base of the ground-water aquifer at about 240 m depth (**Hansen et al., 2004**). If similar rocks extend across the western Santa Clara Valley at the base of the ground-water aquifer, lateral variations in the depth to ground water may be inferred on the basis of the rocks (faulted or fractured), degree of saturation, and compositional variations. In particular, for similar sequences of rocks, those rocks that have experienced significant faulting would have lower P-wave velocities than rocks that have not been faulted. Another problem with using the P-wave velocities to infer lateral variation in the ground-water aquifer system is the probable lateral variation in ground-water saturation. Because the SCSI-LR profile was situated along and between recharge ponds, reservoirs, and the Los Gatos Creek, some of the velocity measures are likely averages of velocities within a few hundred meters of major sources of ground-water recharge. For example, within the Santa Clara Valley, areas along the SCSI-LR profile near major recharge ponds, reservoirs, or Los Gatos Creek

appear to have relatively high velocities at relatively shallow depths, suggesting relatively saturated sediments at relatively shallow depths (**Fig. 4b**). Conversely, those areas that are more distant from recharge ponds, reservoirs, or Los Gatos Creek have relatively low velocities at shallow depths. In places, both the ground-water aquifer system and the underlying Miocene sediments are probably variable in saturation and the degree of faulting, resulting in laterally variable velocities.

Shear-wave velocities (Vs) are much less sensitive to water saturation. Thus, unconsolidated saturated sediments tend to have higher Vp/Vs ratios than consolidated saturated sediments, and both have higher Vp/Vs ratios than unsaturated sediments. For example, **Gibbs et al. (2000)** show Vp/Vs ratios that range from about 3 to about 5 for most unconsolidated and saturated sediment sites surveyed in southern California, but they show most consolidated sediments to have Vp/Vs ratios of about 2.5 or less. Consolidated and saturated sediments would have significantly lower Vp/Vs ratios, such as those (~2.2) for 100% saturated Massilon sandstone (**Nur, 1982),** than unconsolidated and saturated sediments.

Because both Vp and Vs data are available from the SCSI profile, Vp/Vs ratios can be used to infer lateral variation and depth of water-saturated sediments, which may be indicative of the degree of water recharge into the subsurface along the SCSI profile (**Fig. 6a, 8a**). However, high Vp/Vs ratios can also be caused by features other than fluid saturation, such as the presence of highly faulted strata or serpentinite, both of which have been found within the Santa Clara Valley and the eastern Santa Cruz Mountains. At the McGlincey well (shot point 9), a Vp/Vs ratio of 2.7 correlates with the base of the ground-water aquifer (**Fig. 6a, 8a**). If one assumes that the sedimentary rocks underlying the shallow subsurface are not highly faulted, then the 2.7 Vp/Vs contour may infer lateral variations in the ground-water aquifer. The thickest deposits with Vp/Vs ratios of 2.7 or higher occur between shot point 1 and 3, near shot point 5, and northeast of shot point 10. Between shot points 5 and 10, it is unlikely that there are significant deposits of serpentinite at shallow depths; thus, the 2.7 Vp/Vs ratio contour is probably indicative of lateral variations in the base of the ground-water aquifer in that area. However, because of the possible presence of serpentinite in various other areas along the profile, the 2.7 Vp/Vs ratio contour may not correlate with the base of the ground-water aquifers in those areas along the SCSI profile.

Poisson's ratio is also sensitive to high levels of groundwater saturation. For crustal materials, Poisson's ratio typically varies between about 0.15 and 0.5 (**Schon, 1996**), where a Poisson's ratio of 0.5 is indicative of fluids. In the shallow crust, high values (> ~0.43) of Poisson's ratio probably correlate with saturated sediments or unusual rock types. In the vicinity of the McGlincey well, the base of the ground-water aquifer (~240 m) correlates with a Poisson's ratio of about 0.43, but faulting and the presence of serpentinite may also affect the Poisson's ratios. As with the Vp/Vs ratios, however, the lateral variations in Poisson's ratio (0.43, as measured at the base of the McGlincey well) likely outline the ground-water aquifer between shot points 5 and 10, where near surface deposits are probably sedimentary.

On the basis of the Vp, Vp/Vs, and Poisson's ratios found at the base of unconsolidated deposits in the McGlincey well and lateral variations in these values along the SCSI profile, we suggest that the thickest (up to 300 m) ground-water aquifer is located between shot points 9 and 10. If, however, there are not significant serpentinite deposits or faulting near shot point 3, the velocity data are also consistent with the presence of a thick aquifer in that area.

Near-Surface (< 250 m) Structure

Near-surface strata along the SCSI profile are dominated by a series of faults and folds in the Santa Cruz Mountains (**Fig. 1d**) (**McLaughlin et al., 2001**). The SCSI seismic reflection images show folds that persist into the subsurface to several hundred meters depth or more. Between meters 3000 and 7000 of the SCSI profile, the shallow (~50 to 250 m) strata appear folded, with dips as high as 45 degrees, and associated faults may dip both northeastward and southwestward as much as 80 degrees (**Fig. 7**).

Within the Santa Clara Valley, the folds are largely covered at the surface by unfolded or mildly folded alluvium, but the deeper (older) strata below about 200 m depth appear similarly faulted and folded as those in the Santa Cruz Mountains. The SCSI reflection image suggests that some subsurface strata in the Santa Clara Valley have dips greater than 30 degrees. The similarity in faulting and folding between the deeper valley structure and the near-surface mountain strata suggests that both areas have experienced similar tectonism. However, either the tectonism may have slowed in the valley, or deposition of near-surface Pliocene to Holocene sediments in the valley is sufficiently high that ongoing tectonism remains covered.

Strata above about 200 m depth in the Santa Clara Valley are gently folded (**Fig. 7**), with wavelengths of about 2 km or more and both southwest and northeast dips (3 to 10 degrees). From about meter 7000 to about meter 9000, the shallow-depth strata largely dip (3 to 6 degrees) northeastward, but from about meter 9000 to meter 10000, the shallow-depth strata dip (~6 degrees) southwestward along the limb of an apparent fold that apexes at about meter 10200. From meter 10200 to about meter 11500, the shallow-depth strata also dip (~6 degrees) northeastward. Between meters 11500 and 13000, the shallow-depth strata are largely horizontal to about meter 13000, where they dip (~3-7 degrees) southwestward to the end of the SCSI profile. Some of the near-surface strata beneath the alluvium appear to be faulted, but because the SCSI reflection image does not image the near surface (upper few tens of meters) strata, it is not possible to determine the minimum depth of faulting from these data. However, the seismic image shows evidence of faulting near the base of the ground-water aquifer. Such faults may affect ground-water recharge and flow across the valley.

Basin Depth and Structures

Basement rocks beneath the Santa Clara Valley are presumed to be the same as those in the eastern Santa Cruz Mountains, the Santa Teresa Hills, and the New Almaden areas, which consist of Franciscan Complex rocks and parts of the Coast Ranges Ophiolitic sequence, strata of the Great Valley sequence, and early Tertiary (Eocene) to mid-Tertiary (Miocene) rocks (**McLaughlin et al., 2001**). The Franciscan Complex is composed of a variety of penetratively sheared rocks including Cretaceous and Jurassic basaltic volcanic rocks, cherts, and sandstone, Cretaceous melange (blueshist, amphibolite, chert, basaltic volcanics, conglomerate and metadiorite), limestone, volcanics, and tuff. Within the Santa Clara Valley, the basement rocks are overlain by Miocene to Holocene sediments (**Stanley et al., 2002**). Basement rocks and the overlying sediments are likely to have significantly different velocities, which can be used to infer basement depth along the SCSI profile.

Shot point 1 was located within basement rocks consisting of Franciscan melange rocks (**McLaughlin et al., 2001**). At the surface, these rocks have a P-wave velocity of about 3000 m/s (**Fig. 4b**), but at depths of 2 km or less, these rocks would experience lithostatic pressures of about 50 KPa, resulting in P-wave velocity increases due to compaction (**Carmichael, 1989**). Laboratory measurements on pressurized Franciscan

rocks show that compressional velocities (~4.35 to about 6.0 km/s) vary widely in the upper few kilometers (**Stewart and Peselnick, 1977**). When pressurized to about 0.5 kbar, the Franciscan rocks used in **Stewart and Peselnick's (1977)** investigation increased in velocity an average of about 0.4 km/s. Assuming similar Franciscan basement rocks beneath the valley as at the surface at shot point 1, and assuming an increase in velocity of about 0.4 to 0.5 km/s due to lithostatic pressure, such Franciscan mélange rocks beneath the Cupertino Basin would have velocities of about 3400 to 3500 m/s. The 3500 m/s velocity contour is located at about 1600 m depth in our velocity image, suggesting basement is about 1600 to 1800 m deep along the SCSI profile between shot points 5 and 6 and between shot points 9 and 10 (**Fig. 4b**), if basement beneath the Cupertino Basin is composed of such Franciscan rocks.

A similar analysis of the velocities of the Miocene sediments within the Santa Clara Valley can be made. On the basis of numerous P-wave measurements in deep boreholes, **Press (1966)** showed the range of velocities typical of sandstones and shales of various ages and varying depths of burial (**Fig. 10**). Miocene sandstones and shales typically have P-wave velocities that range from about 2200 m/s at about 300 m depth to about 2900 m/s at 2 km depth (**Press, 1966**). In contrast, the SCSI P-wave velocity image shows that velocities beneath the central Cupertino Basin are approximately 4500 m/s at 2 km depth. Comparison of the borehole sonic velocities and the SCSI refraction velocities suggest that sandstone and shale sediments of any age between Miocene and Jurassic are probably no deeper than about 1600 to 1800 m in the Cupertino Basin (**Figs. 10a**). **Brocher et al. (1997**) made a similar analysis of sonic velocities as a function of depth from boreholes in the San Francisco Bay area. They show that the average velocity for sedimentary rocks at about 1800 m depth is less than 3500 m/s, but at depths in excess of 1800 m, the SCSI refraction data show that velocities are more than 4500 m/s (**Fig. 10b**). Both comparisons of the SCSI refraction velocities with sonic velocities suggest that the deepest sediments along the SCSI profile are probably not more than about 1800 m.

We also interpret a maximum depth to basement of 1600 to 1800 m along the SCSI profile from the SCSI reflection image (**Fig. 7**). The reflectivity pattern, which is indicative of layered sedimentary rocks, abruptly changes to a pattern of en echelon northeast-dipping reflectors at depths of approximately 1600 to 1800 m depth near the central Cupertino Basin (meter 9000). These en echelon reflectors are part of a high-

amplitude series of reflectors that extend to the near surface southwest of Lexington Dam, where geologic mapping shows a northeast-dipping thrust fault separates Franciscan rocks from Coast Ranges Ophiolitic rocks (**McLaughlin et al., 2001**). Because of its upward projection toward the thrust fault and because of the high basement velocities (up to 6.5 km/s at 3.5 km depth) in the northeastern Santa Cruz Mountains, we interpret the high-amplitude, northeast-dipping reflector as a contact between the Coast Ranges Ophiolite and Franciscan Complex rocks. As the Franciscan and Coast Ranges Ophiolite are considered basement rocks, the en echelon reflectors at about 1800 m depth beneath the Cupertino Basin, which may have resulted from tectonic wedging of Coast Ranges Ophiolitic rocks into Franciscan Complex rocks (**R. McLaughlin, Pers. Comm., 2004**), are also likely to be basement rocks.

Our velocity- and reflectivity-based estimates to the top of basement (or maximum depth of Miocene sediments) are consistent with at least one other estimate of the minimum thickness of Miocene sediments beneath the western Santa Clara Valley. Based on chemical analysis of oil from a well along the seismic profile, **Stanley et al. (2002)** suggest that the oil producing rocks (top of the oil-generative window) could be buried as shallowly as 1600 to 1800 m below the surface, although their preferred depth range is between 2100 and 2500 m (p. 36). Thus, the chemical analyses do not require present-day sediments below 1600 to 1800 m depth in the western Santa Clara Valley.

On the basis of gravity modeling, the depth to basement beneath the Cupertino Basin in the vicinity of the SCSI-LR profile has been estimated at about 3.5 to 4 km depth (**R. Jachens, Pers. Comm., 2001; Stanley et al., 2002**). However, the velocity and reflectivity data from out study suggest that sediments of the Cupertino Basin are less than about 1800 m thick in the vicinity of the SCSI-LR profile.

Faulting Relationships:

Numerous faults are mapped at the surface in the eastern Santa Cruz Mountains (**McLaughlin et al., 2001**), and beneath the alluvium cover of the western Santa Clara Valley, faults are also inferred from previous geophysical and borehole investigations (**CDWR, 1967**). Most of the prominent reverse faults in the eastern Santa Cruz Mountains are interpreted to dip southwestward toward the San Andreas fault, with some antithetic, northeast-dipping normal faults that merge with the southwest-dipping faults at depth **(McLaughlin et al., 2001)**. In contrast, many of the mapped faults and

stratigraphic units near the edge of the Santa Clara Valley and within the Santa Teresa Hills (~ 5 km south of the seismic profile) dip steeply to the northeast **(McLaughlin et al., 2001).**

Because of the relatively low resolution of the SCSI-LR profile and the complexity of the subsurface structure, fault structures to depths of several hundred meters along the SCSI-LR profile are best determined from the SCSI-HR profile images (**Catchings et al., 2005**) and from known surface faults (**Fig. 7**). Although the SCSI-LR and SCSI-HR profiles are not everywhere coincident, when SCSI-HR interpreted faults are superimposed on the SCSI-LR reflection image, apparent stratigraphic offsets on the SCSI-LR reflection image coincide with most of the interpreted faults to depths of about 600 m (**Fig. 7**). Below about 600 m, the fault structures are not well resolved on the SCSI-LR reflection image, but there appear to be near-vertical offsets of stratigraphic layers that extend to several kilometers depth (**Fig. 11**). On the basis of offset layers and the dips of faults at shallow depths, we suggest that many of the near-surface faults merge at depths of one to three kilometers into several discrete, largely southwest-dipping fault zones.

Surface and near-surface (trenching) geologic mapping (**McLaughlin et al., 2001**) shows that most of the faults along the SCSI profile dip at high angles (~75 to 80 degrees), and our seismic images also indicate that the high-angle (75 to 80 degrees) faults extend to at least 600 m depth (**Fig. 7**). Focal mechanisms for the best-recorded earthquakes within a few kilometers of the SCSI-LR profile also show that most of the faults between about 1 to 20 km depth are relatively high-angle, reverse faults (**Figs. 7 and 11**). Thus, it is likely that many of the fault zones within the western Santa Clara Valley merge with the San Andreas fault zone at depths of 3 to 15 km. However, seismic events centered northeast of the Cupertino Basin indicate that there may also be one or more fault zones that either merge with the San Andreas fault at depths of 15 to 30 km, or they are separate fault zones that do not merge with the San Andreas at all (**Fig. 12**).

Summary

The seismic images from this study show the larger-scale features of the upper few kilometers of the crust. The seismic images provide structural constraints, including (1) the thickness of the sedimentary rocks within the Santa Clara Valley, (2) depth to and

lateral variations in basement rocks, (3) distribution and structure of subsurface faults, and (4) probable lateral variations in the ground-water aquifer system.

We suggest that Miocene sandstone and shales are thickest (1600 to 1800 m) beneath the central Cupertino Basin, but thin rapidly toward the center of the basin and near its southwestern edge. In places in the northeastern Santa Cruz Mountains surface mapping shows that the Miocene rocks are underlain by Franciscan Complex rocks (**McLaughlin et al, 2001**), and the same structural relationship may exist beneath the Santa Clara Valley. However, serpentinite observed at relatively shallow depths (~245 m) in the Willow well (**Orze et al., 2003**), near the northeast end of the SCSI-LR profile, suggests that at least parts of the Santa Clara Valley are underlain by rocks of the Coast Ranges Ophiolite. This observation is somewhat consistent with our seismic reflection image, whereby a high-amplitude northeast-dipping reflector extends from surface exposures of the Coast Ranges Ophiolite in the Santa Cruz Mountains to the base of the Cupertino Basin, and back toward the shallow subsurface in the vicinity of the Willow well (**Fig. 11**). On the basis of the reflection image, we suggest that Miocene sediments of the western Santa Clara Valley may be underlain by a wedge of Coast Ranges Ophiolitic rocks that has been thrust beneath the valley. These rocks have relatively high velocities (~6.5 km/s) within the Santa Cruz Mountains. Similar high-velocity (~6.4 to 6.5 km/s) rocks have been observed to the north of the SCSI-LR profile, beneath the San Francisco Bay, (**Catchings et al, 2004**) and below the eastern side of the Santa Clara Valley (**Catchings et al., unpublished data**). Such high-velocity rocks are consistent with ultramafic rocks that compose parts of the Coast Ranges Ophiolite (**Carmichael, 1989**), but such high velocities are not consistent with most Franciscan rocks at that depth (**Stewart and Peselnick, 1977**).

Offset reflectors and folded Pre-Pliocene strata suggest multiple faults beneath the alluvium of the Santa Clara Valley. Offset strata imaged on the SCSI-LR reflection image show that some of the faults offset the base of the ground-water aquifer system. Such shallow-depth faulting implies at least post-Pliocene movement on faults beneath the Santa Clara Valley, and SCSI-HR images show that many of these fault extend to the near surface or to within about 10 m of the surface (**Catchings et al., 2005**). Furthermore, earthquakes recorded over the past 30 years show that similar faults are presently active at depths of 1 to 30 km. These stratigraphic relationships and earthquakes recorded beneath the valley clearly indicate the presence of potentially

hazardous earthquake faults beneath the Santa Clara Valley. These faults represent a potential hazard both from the standpoint of local sources beneath a large population base and increased ground amplification due to regional sources, such as the San Andreas fault. The maximum magnitudes of earthquakes that can be generated from the imaged faults are unknown but are related to the lengths of the faults. The seismicity pattern and mapped faults near the base of the mountains suggest that the valley faults may extend 70 km or more. Where they extend to the shallow depths, these faults probably cause lateral variations in the ground-water aquifer by acting as barriers to lateral flow across the valley.

Lateral variations in P-wave velocities, Vp/Vs and Poisson's ratios, and reflection images, correlated with borehole data, indicate that the maximum depth of the ground-water aquifer is variable across the Santa Clara Valley, varying from less than 50 m to about 300 m. Quaternary deposits that form the ground-water aquifer system appears to thicken eastward of Vasona Dam, with the thickest deposits in the area northeast of the city of Campbell (shot point 11). The thinnest Quaternary deposits are located southwestward of Vasona Reservoir, with the possible exception of isolated basins, such as that beneath the city of Los Gatos. Most lateral variations in the depth of the ground-water aquifer system correlate with apparent fault offsets in subsurface reflectors, suggesting that the ground-water aquifer is faulted in multiple locations across the western part of the valley. The SCSI reflection images suggest that the Quaternary rocks are faulted at various locations along the length of the SCSI-LR profile, including the central part of the valley between Campbell and San Jose. A short seismic profile acquired farther to the northeast of the end of the SCSI-LR profile suggests similar faulting extends beneath the eastern downtown area of San Jose (**Catchings et al., 2000**), but our 2000 SCSI-LR seismic profile did not extend far enough to the northeast to address that area.

The dimensions and velocities of the low-velocity Cupertino Basin are important parameters needed to understand potential ground shaking resulting from movement on regional and/or local faults. The velocity and reflection images suggest that the Cupertino Basin is about 1600 to 1800 m deep, which is about one-half the depth previously suggested from potential fields studies (**R. Jachens, Pers. Comm., 2001**; **Stanley et al., 2002).** Although other factors, such as basin shape, velocities, location of the sources, type of fault, etc., are important contributors, the shallower depth of the Cupertino Basin

may also indicate less hazard from amplification of seismic waves in the valley than previously believed. However, the seismic images also suggest multiple faults beneath the valley, some of which are active, as indicated by earthquakes recorded over the past few decades (**Fig. 12**) and by near-surface traces of the faults imaged on the seismic reflection images (**Fig. 11**). Slip on any one of the major faults may trap fault-zone guided waves into the general fault system, and produce amplified seismic waves within the each of the fault zones. However, the principal hazard for the Santa Clara Valley may be the high-amplitude seismic energy generated by the reverse faults that underlie the valley.

Acknowledgements:

This work was jointly funded by the U.S. Geological Survey's (USGS) Earthquake Hazards Program and the Santa Clara Valley Water District (SCVWD). We than IRIS-PASSCAL for providing the Texan seismographs, and we especially thank Bob Greschke and Pete Ulbricht, who provided technical support during the seismic investgation. We thank numerous individuals and organizations, including the SCVWD, the City of Los Gatos, City of Campbell, Open Space District, Los Gatos High School, Del Mar High School, and the San Jose Water Company, who provided permits and access to their properties. We thank Alonzo Aballo, Joe Catchings, Coye Criley, Coyn Criley, Courtney Criley, Ed Criley, Samuel V. Gudino, Samuel R. Gudino, Silvia Gudino, Ron Kaderabek, Grey Jensen, Shawn Hanson, Lora Kiger, David Reneau, Jose Rodriguez, Paul Singh, Jeffrey Thacker, and John VanSchaack, who assisted in data acquisition. We thank Lora Kiger for helping with many of the logistical challenges of this investigation, and we also thank Lora Kiger and John Hamilton for providing precision survey data. We thank Carl Wentworth, David Schwartz, and Jack Boatwright, who provided administrative assistance. We thank Bob Mclaughlin for scouting and recommending the Santa Cruz Mountains segment of the SCSI profile northeast of Lexington Reservoir. Thanks to Tom Brocher, Bob McLaughlin, and Peter Martin, who provided reviews of this manuscript.

References

Advanced National Seismic System (ANSS) Catalog (2004). anss@quake.geo.berkeley.edu

Bortugno, E.J., McJunkin, R.D., and Wagner, D.L. (1991). Map showing recency of faulting, San Francisco-San Jose quadrangle, 1:250,000: Department of Conservation, Division of Mines and Geology Regional Geologic Map Series, Map 5A, Sheet 5

Brocher, T. M., A. L. Ruebel, and E. E. Brabb (1997). Compilation of 59 sonic and density logs from 51 oil test wells in the San Francisco Bay area, California. U.S. Geological Survey Open-File Report 97-987 75 pp.

Brouwer, J., and K. Helbig (1998). Shallow high-resolution reflection seismics. In: Helbig, K., Treitel, S. (Eds.), Handbook of Geophysical Exploration: Seismic Exploration, Vol. 19, Elsevier, New York, New York, 391 pp.

California Department of Water Resources (CDWR) (1967). Evaluation of Ground Water Resources, South Bay, Appendix A: Geology: Bulletin 118-1, 153 p.

California Department of Water Resources (CDWR) (1975). Evaluation of groundwater resources, south San Francisco Bay, Volume III, northern Santa Clara County area: Bulletin No. 118-1, various pagination

Catchings, R. D. (1999). Regional Vp, Vs, Vp/Vs, and Poisson's ratios across earthquake source zones from Memphis, Tennessee to St. Louis, Missouri. Bull. Seism. Soc. Am, 89, 1591-1605

Catchings, R. D., G. Gandhok, M. R. Goldman, E. Horta, M. J. Rymer, P. Martin, and A. Christensen (1999a). Subsurface, high-resolution, seismic images from Cherry Valley, San Bernardino County, California: Implications for Water Resources and Earthquake Hazards, US Geological Survey Open-File Report 99-26, 57 pp.

Catchings, R. D., M. R. Goldman, G. Gandhok, E. Horta, M. J. Rymer, P. Martin, and A. Christensen (1999b). Structure, velocities, and faulting relationships beneath San Gorgonio Pass, California: Implications for water resources and earthquake hazards, US Geological Survey Open-File Report 99-568, 53 pp.

Catchings, R.D., and Goldman, M.R., Gandhok, G., Rymer, M.J., and Underwood D.H. (2000). Seismic imaging evidence for faulting across the northwestern projection of the Silver Creek Fault, San Jose, California: U.S. Geological Survey Open-File Report 00-125, 29 p.

Catchings, R. D., M. R. Goldman, C. E. Steedman, and G. Gandhok (2004). Velocity models, first-arrival travel times, and geometries of the 1991 and 1993 USGS land-based controlled-source seismic investigations in the San Francisco Bay area, California: In-line shots, U.S. Geological Survey Open-File Report 2004-1423, 32 pp.

Catchings, R. D., G. Gandhok, M. R. Goldman, C. E. Steedman, and R. Hanson (2005). Near-surface structure and velocities of the northeastern Santa Cruz Mountains and the western Santa Clara Valley, California from seismic imaging, U.S. Geological Survey Open-File Report, in press.

Carmichael, R. S. (1989) Practical Handbook of Physical Properties of Rocks and Minerals, CRC Press, Boca Raton, Ann Arbor, Boston

Christiansen, N.I. (1982). Seismic Velocities in R.S. Carmichael ed., Handbook of Physical Properties of Rocks, v. II, CRC Press, Boca Raton.

Christiansen, N. I. (1996). Poisson's ratio and crustal seismology, J. Geophys. Res., 101, p. 3139-3156

Dibblee, T.R., Jr. (1966). Geology of the Palo Alto quadrangle, Santa Clara and San Mateo Counties, California: California Division of Mines and Geology Map Sheet 8, scale 1:62,500.

Dietz, Lynn D., and William L. Ellsworth (1997). Aftershocks of the Loma Prieta Earthquake and their tectonic implications, in The Loma Prieta, California Earthquake of October 17, 1989: Earthquake Occurrence. Aftershocks and Postseismic Effects, U.S. Geological Survey Profess. Paper 1550-D, p. D5-D47

Gandhok, G., R. D. Catchings, M. R. Goldman, E. Horta, M. J. Rymer, P. Martin, and A. Christensen (1999). High-Resolution Seismic Reflection/Refraction Imaging from Interstate 10 to Cherry Valley Boulevard, Cherry Valley, Riverside County, California: Implications for Water Resources and Earthquake Hazards, U.S. Geological Survey Open-File Report 99-320, 52 pp.

Gibbs, J. F., J. C. Tinsley, D. M. Boore, and W. B. Joyner (2000). Borehole velocity measurements and geological conditions at thirteen sites in the Los Angeles, California region, U.S. Geological Survey Open-File Report 00-470, 118 pp.)

Hanson, R.T., Newhouse M.W., Wentworth, C.M., Williams, C.F., Noce, T.E., Bennett, M.J. (2002b). Santa Clara Valley Water District multi-aquifer monitoring-well site, Coyote Creek Outdoor Classroom, San Jose, California: U.S. Geological Survey Open-File Report OFR 02- 369, 4 p.

Helley, E.J., R.W. Graymer, G.A. Phelps, P.K.Showalter, and C.M. Wentworth (1994). Quaternary geology of the Santa Clara Valley, Santa Clara, Alemeda, and San Mateo counties, California: A digital database. U.S. Geological Survey Open-File Report 94-231.

Hole, J. A. (1992). Nonlinear high-resolution three-dimensional seismic traveltime tomography. J. Geophys. Res. 97, 6553–6562.

Lin, Wunan, and Wang, C.-Y., 1980, P-wave velocity in rocks at high pressure and temperature and the constitution of the central California crust: Royal Astronomical Society Geophysical Journal, v. 61, no. 2, p. 379-400.

McLaughlin, R. J., J. C. Clark, E.E. Brabb, E.J. Helley, and C.J. Colon (2001). Geologic maps and structure sections of the southwestern Santa Clara Valley and southern Santa Cruz Mountains, Santa Clara and Santa Cruz Counties, California, U.S. Geol. Surv. Misc. Field Studies Map MF-2373

Newhouse, M.W., R.T. Hanson, C.M. Wentworth, Rhett R. Everett, C.F. Williams, J.C.Tinsley, T.E. Noce, B.A. Carkin (2004). Geologic, Water-Chemistry, and Hydrologic Data from Multiple-Well Monitoring Sites and Selected Water-Supply Wells in the Santa Clara Valley, California, 1999-2003, U.S. Geological Survey Scientific Investigations Report, 2004-5250

Nur, A. (1982). Notes on wave propagation in porous rocks, Stanford Rock Physics Progress Report, January 1982, vol. 13, 121 pp. Stanford University, Stanford, CA,

Orze, C. J., M. J. LaForce, C. M. Wentworth, R. T. Hanson, D. K. Bird, and R. G. Coleman (2003). Chromium geochemistry of serpentinous sediment in the Willow Core, Santa Clara County, California, U.S. Geological Survey Open-File Report 03-251, 24 pp.

Press, F. (1966). Seismic Velocities, In Handbook of Physical Constants, S.P. Clark SP, ed., pp. 195-218, Geol. Soc. Am. Mem. 97, Geol. Soc. Am., New York**.**

Poland, J.F. (1971). Land subsidence in the Santa Clara Valley, Alameda, San Mateo, and Santa Clara Counties, California: U.S. Geological Survey Open-File Report, Map Scale 1:125,000

Schmidt, D.A. (2002).The kinematics of faults in the San Francisco Bay area inferred from geodetic and seismic data: unpublished PhD dissertation, University of California at Berkeley, 200 p.

Schon, J. H. (1996). Physical Properties of Rocks. Fundamentals and principals of petrophysics, in Handbook of Geophysical Exploration V. 18 (K. Helbig and S. Treitel, eds.), Pergamon Press, Elsevier Science, Inc. New York, New York, 583 pp.

Simpson, R. (2004). http://ehzweb-menlo.wr.usgs.gov/DD_Eq_Plots/Eqs_scvbt/)

Stanley, R.G., Jachens, R.C., Lillis, P.G., McLaughlin, R.J., Kvenvolden, K.A., Hostettler, F.D., McDougall, K.A., and Magoon, L.B. (2002). Subsurface and Petroleum Geology of the Southwestern Santa Clara Valley ("Silicon Valley"), California: U.S. Geological Survey Professional Paper 1663, 55 p.

Stewart, R.M., and Peselnick, Louis, 1977, velocity of compressional waves in dry Franciscan rocks to 8 kbar and 300° C: Journal of Geophysical Research, v. 82, no. 14, p. 2027-2039.

Thomsen, Leon (1990). Poisson was not a geophysicist, The Leading Edge of Exploration, December 1990, p. 27-29

Wagner, D.L., K.J. Bortugno, and R.D. McJunkin (1990). Geologic map of the San Francisco-San Jose quadrangle: California Department of Conservation, Division of Mines and Geology, Regional Geologic Map Series, Map No. 5A, 5 sheets.

Wentworth C.M. (1997). General distribution of geologic materials in the San Francisco Bay region, California: a digital map database: U.S. Geological Survey Open File Report 97-744.

United States Census Bureau (2003). http://quickfacts.census.gov/qfd/states/06/06085.html

Zoback, M.L., J. A. Olson, and R. C. Jachens (1995). Seismicity and basement structure beneath the south San Francisco Bay, California, in Sangines, E.M., Anderson, D.W., and Busing, A.V., eds., Recent geologic studies in the San Francisco Bay area: Scoeity of Economic Paleontologists and Mineralogists, Pacific Section Special Publication 76, p. 31-46.

Figures

Fig. 1 (a) Location map of the southern San Francisco Bay area and the Santa Clara Seismic Imaging (SCSI) profile. Shot points and seismograph locations for the SCSI profile are shown in the inset. Major faults (from Bortugno et al., 1991), roadways, and selected cities are also shown. Inferred faults that cross the SCSI profile in the Santa Clara Valley are shown only at their inferred crossing. The Cupertino (CB) and Evergreen (EB) Basins (from Stanley et al., 2002) are outlined as dashed lines. (b) Shot points (Shot point #) of the southwestern half of the SCSI low-resolution (SCSI-LR) seismic profile. The brown asterisks show the locations of individual seismographs of the southwestern part of the SCSI-LR profile. The green asterisks show the locations of shot points along the southwestern part of the SCSI high-resolution (SCSI-HR) seismic profile. Where the profile overlap, the SCSI-HR (green) shot points are shown on top. The base map is from the USGS 7.5 minute Los Gatos quadrangle. (c) The locations of the northeastern parts of the SCSI-LR and SCSI-HR seismic profiles, plotted as in figure 1b. The base map is from the USGS 7.5 minute Los Gatos quadrangle. Recently drilled USGS/SCVWD water wells (McGlincey, Willow, and STPK) are shown by the red dots, with distances to the wells shown. (d) Geologic map (from McLaughlin et al., 2001) of the northeastern Santa Cruz Mountains with the southwestern part of the SCSI profiles plotted as in figure 1b. Note the numerous faults mapped along the seismic profile. See McLaughlin et al. (2001) for map legend.

Fig. 2. Geometry of the SCSI-LR profile. Variation in seismograph array (a) elevation and (b) linearity. Variation in shot-point array (c) elevation and (d) linearity. Note that most of the non-linearity occurs outside of the shot-point array. (e) Fold as a function of common depth point (CDP) along the SCSI profile.

Fig. 3. (a-k) Shotgathers for SCSI-LR shot points 1-11, respectively. Several prominent reflectors are highlighted on the southwestern end of the seismic profile. Some of these reflectors project to the surface at a fault contact between rocks of the Coast Ranges Ophiolite and Franciscan rocks.

Fig. 4. (a) Ray density diagram showing raypaths for P-waves and redundancy for shot and receiver pairs along the SCSI profile. (b) P-wave velocity model for the upper 3 km along the SCSI profile. Distance is relative to the southwestern most geophone, located near the San Andreas fault. Depth is relative to the lowest elevation along the SCSI profile. The shallow depth white contour denotes the 2200 m/s velocity contour, which correlates with the base of the ground-water aquifer system in the McGlincey water well, located approximately at meter 12500 of the velocity model. The other white velocity contour denotes the 3000 m/s velocity contour, which correlates with Franciscan basement rocks at the surface at shot point 1 (meter 3500). The red contour denotes the 3500 m/s contour, which is the probably the maximum velocity for similar basement rocks at 2 km depth.

Fig. 5. (a) Ray density model showing raypaths for S-waves and redundancy for shot and receiver pairs along the SCSI profile. (b) S-wave velocity model for the upper 5 km along the SCSI profile. Depth and distance are the same as those in figure 4b. Velocities below about 1500 m depth are poorly constrained due to uncertain picks on the shot gathers.

Fig. 6 Vp/Vs ratio model along the SCSI profile. Depth and distance are the same as those in figure 4b. The 2.7 Vp/Vs ratio contour, which correlates with the base of the ground-water aquifer in the McGlincey well (~meter 12500) is shown in white. Due to the presence of serpentinite and faults along the profile, high values of Vp/Vs ratios in various places are not necessarily related to the ground-water aquifer along all of the SCSI profile. (b) Poisson's ratio model along the SCSI profile. Depth and distance are the same as those in figure 4b. The 0.43 Poisson's ratio contour, which correlates with the base of the ground-water aquifer in the McGlincey well (~meter 12500) is shown in white. Low values of Poisson's ratio below 1.5 km depth are not well constrained.

Fig 7. (a) Migrated seismic reflection image of the upper 1000 m along the SCSI profile. Red vertical arrows above the reflection image denote the locations of mapped faults (McLaughlin et al., 2001) along the SCSI-LR profile. Blue arrows indicate interpreted faults. (b) Migrated reflection image from figure 7a, with the locations of faults as interpreted on the SCSI-HR reflection images (Catchings et al., 2005). Focal mechanisms for earthquakes within about 3 km of the SCSI profile are shown below the reflection image. Most focal mechanisms indicate northeast striking, high-angle (~75 to 90 degrees) faults. (c) Migrated reflection image from figure 7a, with interpretative strata, derived from surface mapping and wells along the profile. Yellow indicates Quaternary sediments, blue indicates Miocene strata, and green indicates Franciscan rocks.

Fig. 8. (a) Seismic reflection image from figure 7 with the unmasked P-wave velocity model from figure 4b superimposed. (b) Seismic reflection image from figure 7 with the unmasked S-wave velocity model from figure 5b superimposed. (c) Seismic reflection image from figure 7 with the Vp/Vs model from figure 6a superimposed. (d) Seismic reflection image from figure 7 with the Poisson's ratio model from figure 6b superimposed. Wells located along or near the seismic profile are shown in yellow. See Stanley et al. (2002) for well descriptions.

Fig. 9. Comparison of P- and S-wave sonic velocities from the McGlincey well (see fig. 1) with SCSI refraction velocities. The SCSI velocities, which are averaged over 50-100 m intervals are comparable to the sonic logs over similar depth ranges.

Fig. 10. (a) Average P-wave velocities of sandstone and shale as a function of age (from Press, 1966) and comparison with velocities determined along the SCSI-LR profile beneath the Cupertino Basin (meter 9000). Tertiary sandstone and shale are known to underlie the near-surface Quaternary deposits in the western Santa Clara Valley (Stanley et al, 2002). This comparison suggests that sandstones and shales are probably confined to the upper 1600 m beneath the Santa Clara Valley. (b) Comparison of velocity-depth relationships from sonic velocities obtained from boreholes in the San Francisco Bay area (from Brocher et al., 1998) and SCSI refraction velocities. Sonic velocities are derived from boreholes drilled in various sedimentary basins in the San Francisco Bay area, and refraction velocities are from a vertical profile at meter 9000 of the SCSI velocity model (fig. 4b). The SCSI and average sonic velocities differ significantly at about 1600 to 1800 m depth, suggesting that sediments of the Cupertino Basin are probably not deeper than 1600 to 1800 m.

Fig. 11 Seismic reflection image from figure 7, with probable rock types and interpretative faults outlined at shallow depths. Interpretative rock types are based on known stratigraphy at the surface, borehole data, and continuity of reflectors. Interpretative faults are based on fault mapped at the surface, SCSI-HR reflection images (Catchings et al., 2005), and offset reflectors on the SCSI-LR image. Focal mechanism for well-recorded earthquakes within 3 km of and along the seismic profile are shown below the SCSI-LR reflection image.

Fig 12 Interpreted seismic image figure 11 with earthquakes that have been recorded over the past 3 decades within 3 km of the SCSI profile. Although locations are not precise, there are at least two separate zones of seismicity along the SCSI profile. Seismicity below each of these zones extend to depths greater than 25 km, but only earthquakes in the upper 14 km are shown here.

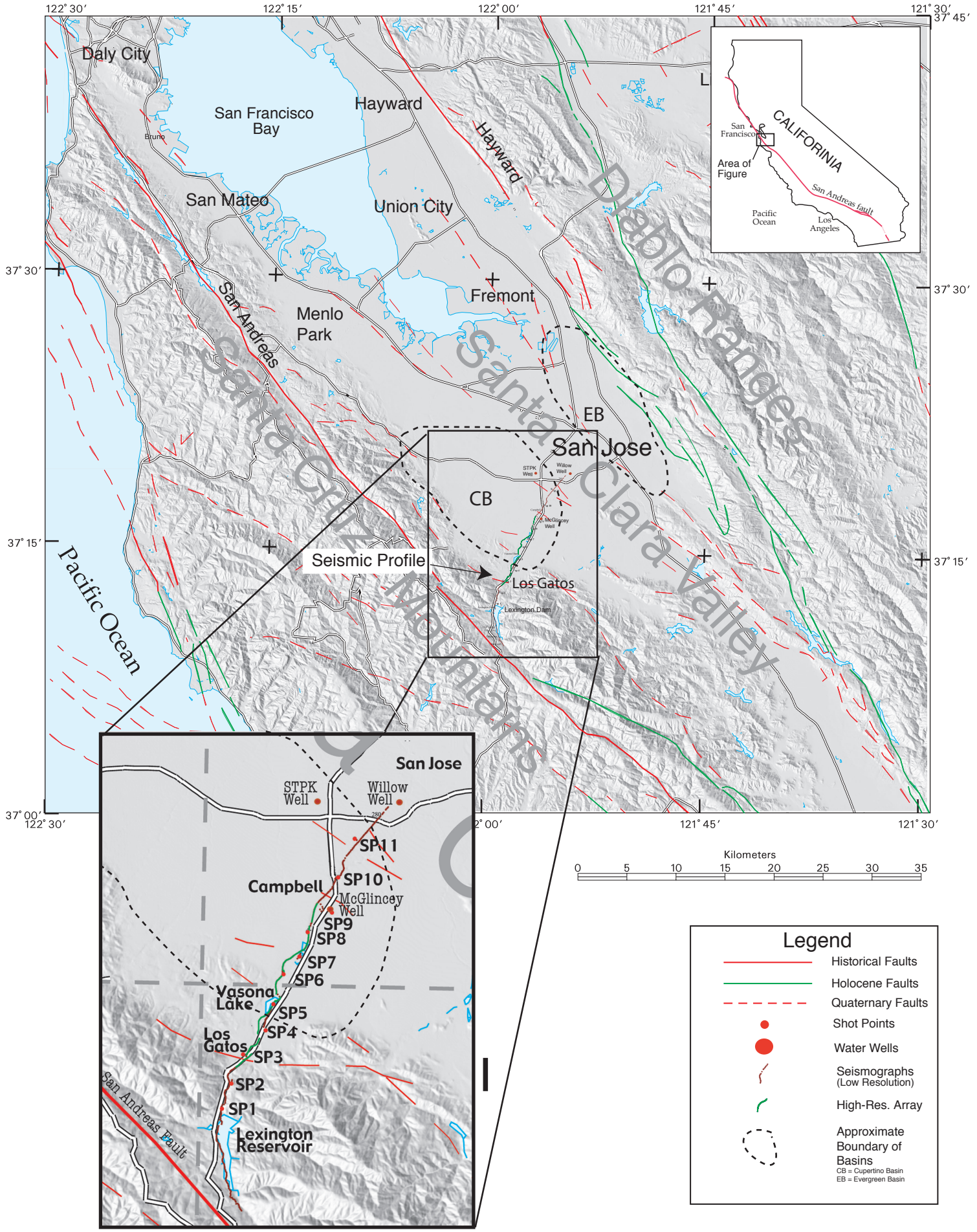
122° 30′
122° 15′
122° 00′
121° 45′
121° 30′
37° 45′
37° 30′
37° 15′
37° 00′
Daly City
San Francisco Bay
Hayward
Hayward
San Mateo
Union City
Fremont
Menlo Park
San Andreas
Pacific Ocean
Santa Cruz Mountains
Santa Clara Valley
Diablo Ranges
EB
San Jose
CB
Seismic Profile
Los Gatos
Lexington Dam
STPK Well
Willow Well
McGlincey Well
CALIFORNIA
San Francisco
Area of Figure
San Andreas fault
Pacific Ocean
Los Angeles
Kilometers
0 5 10 15 20 25 30 35
San Jose
STPK Well
Willow Well
SP11
SP10
Campbell
McGlincey Well
SP9
SP8
SP7
SP6
Vasona Lake
SP5
SP4
Los Gatos
SP3
SP2
SP1
Lexington Reservoir
San Andreas Fault
Legend
Historical Faults
Holocene Faults
Quaternary Faults
Shot Points
Water Wells
Seismographs (Low Resolution)
High-Res. Array
Approximate Boundary of Basins
CB = Cupertino Basin
EB = Evergreen Basin

Fig. 1a

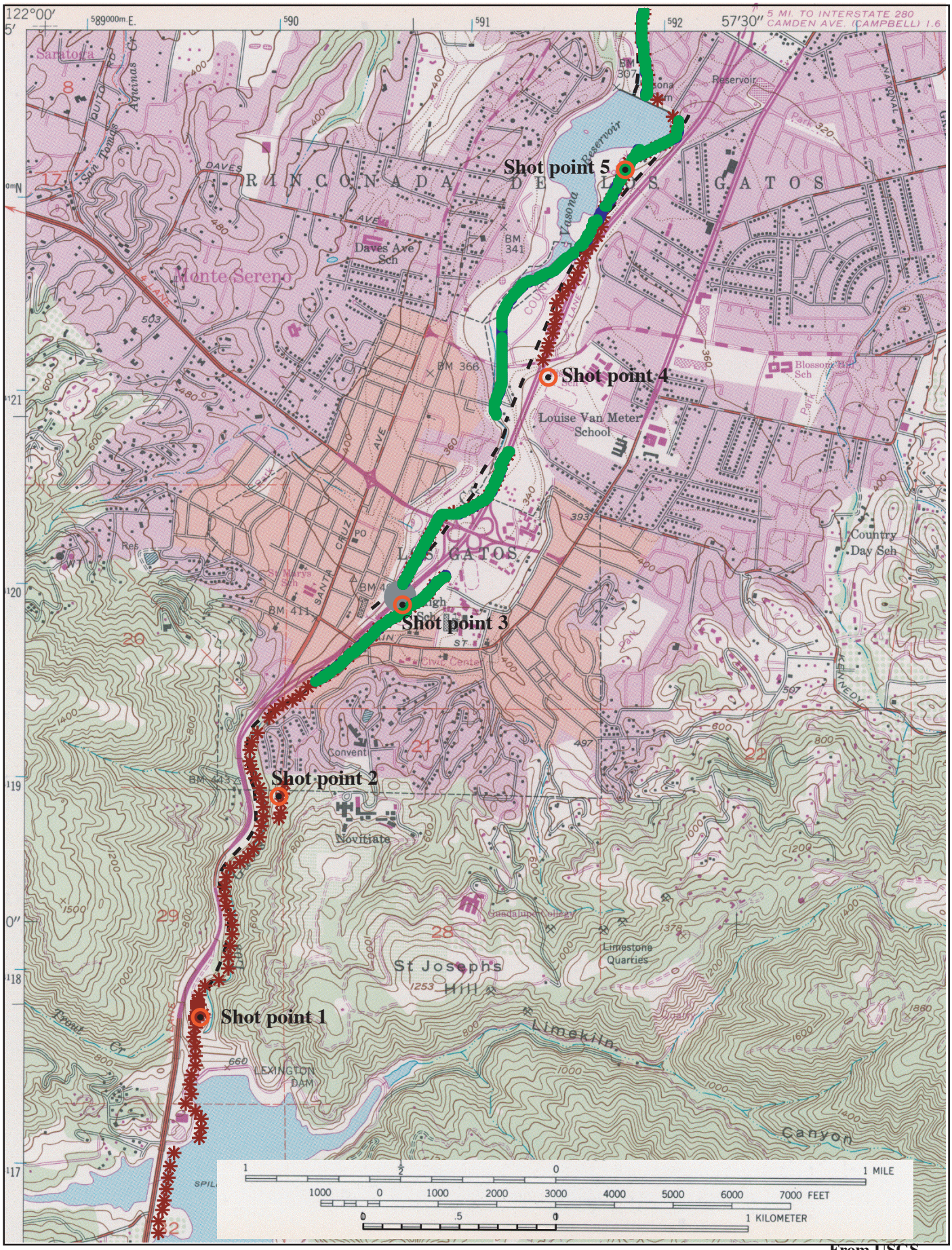

SCSI-HR Profile

SCSI-LR Seismograph

SCSI-LR Shot Point

From USGS San Jose West Quadrangle

Fig. 1b

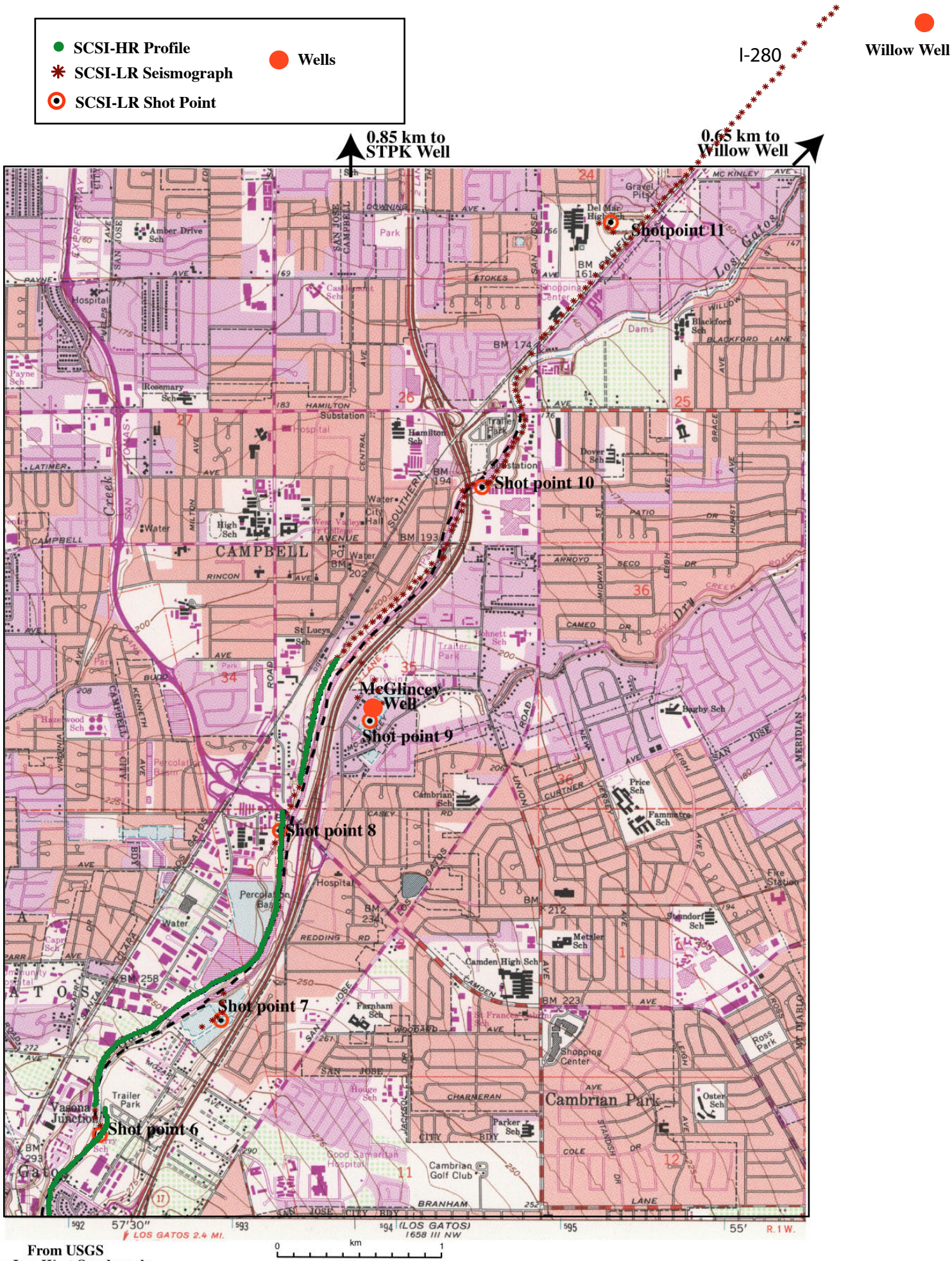
SCSI-HR Profile
SCSI-LR Seismograph
SCSI-LR Shot Point
Wells
I-280
Willow Well
0.85 km to STPK Well
0.65 km to Willow Well
Shotpoint 11
Shot point 10
McGlincey Well
Shot point 9
Shot point 8
Shot point 7
Shot point 6
CAMPBELL
Cambrian Park
Los Gatos
From USGS
San Jose West Quadrangle
0
km
1

Fig. 1c

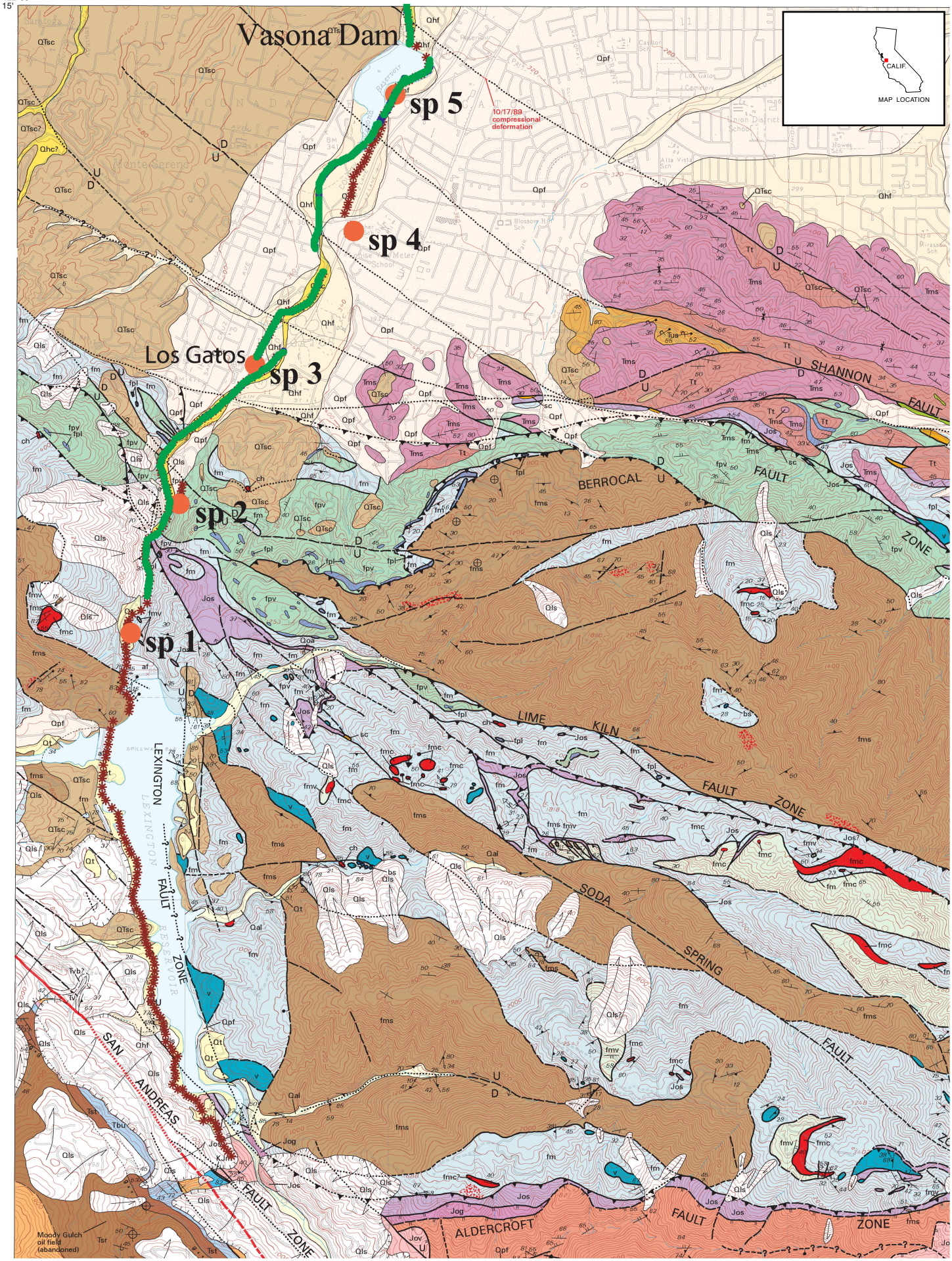

- SCSI-HR and/or LR Profiles
- SCSI-Seismographs
- SCSI-LR Shot Points

Fig. 1d

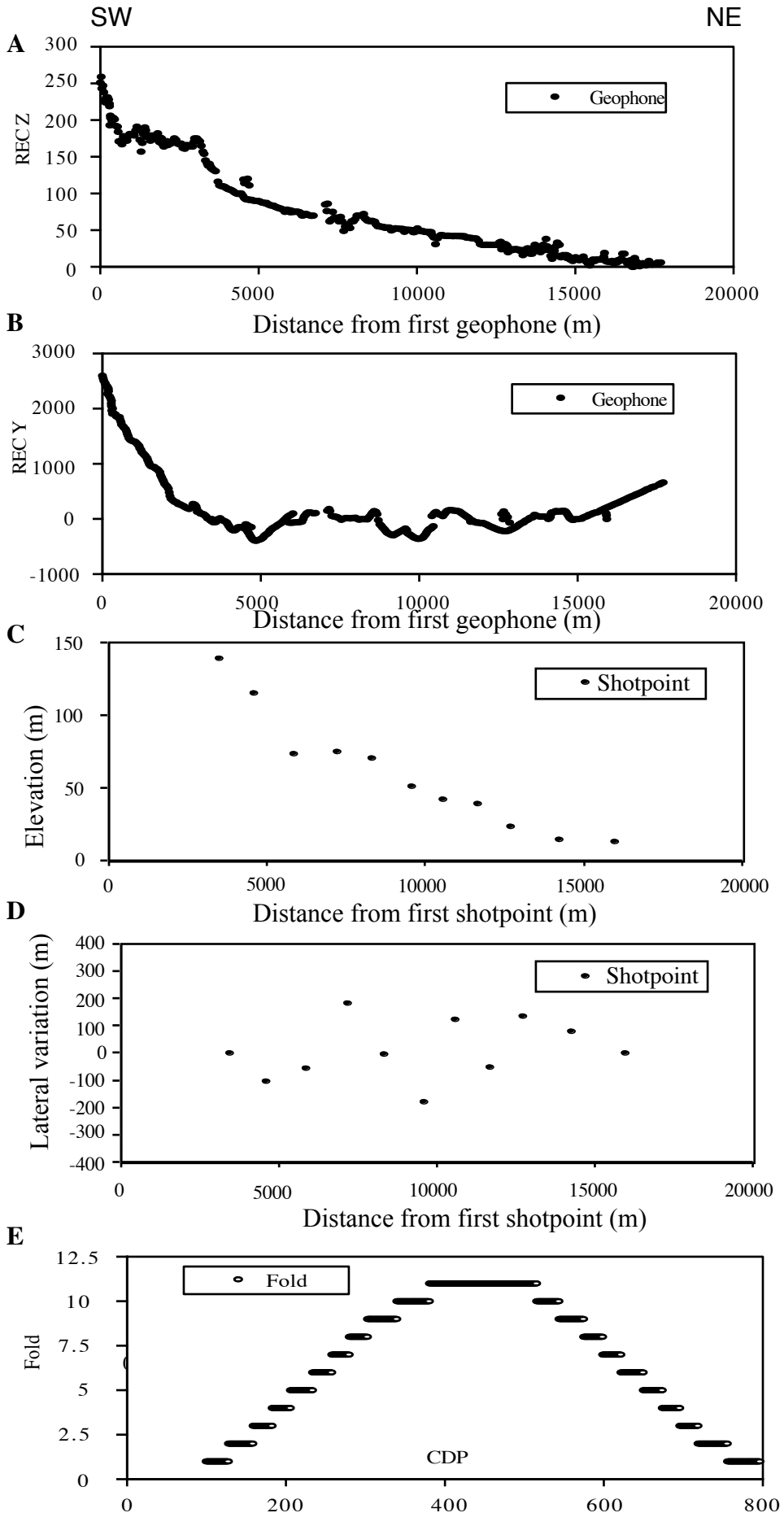
SW
NE
A
REC Z
Geophone
Distance from first geophone (m)
B
REC Y
Geophone
Distance from first geophone (m)
C
Elevation (m)
Shotpoint
Distance from first shotpoint (m)
D
Lateral variation (m)
Shotpoint
Distance from first shotpoint (m)
E
Fold
Fold
CDP

Fig. 2

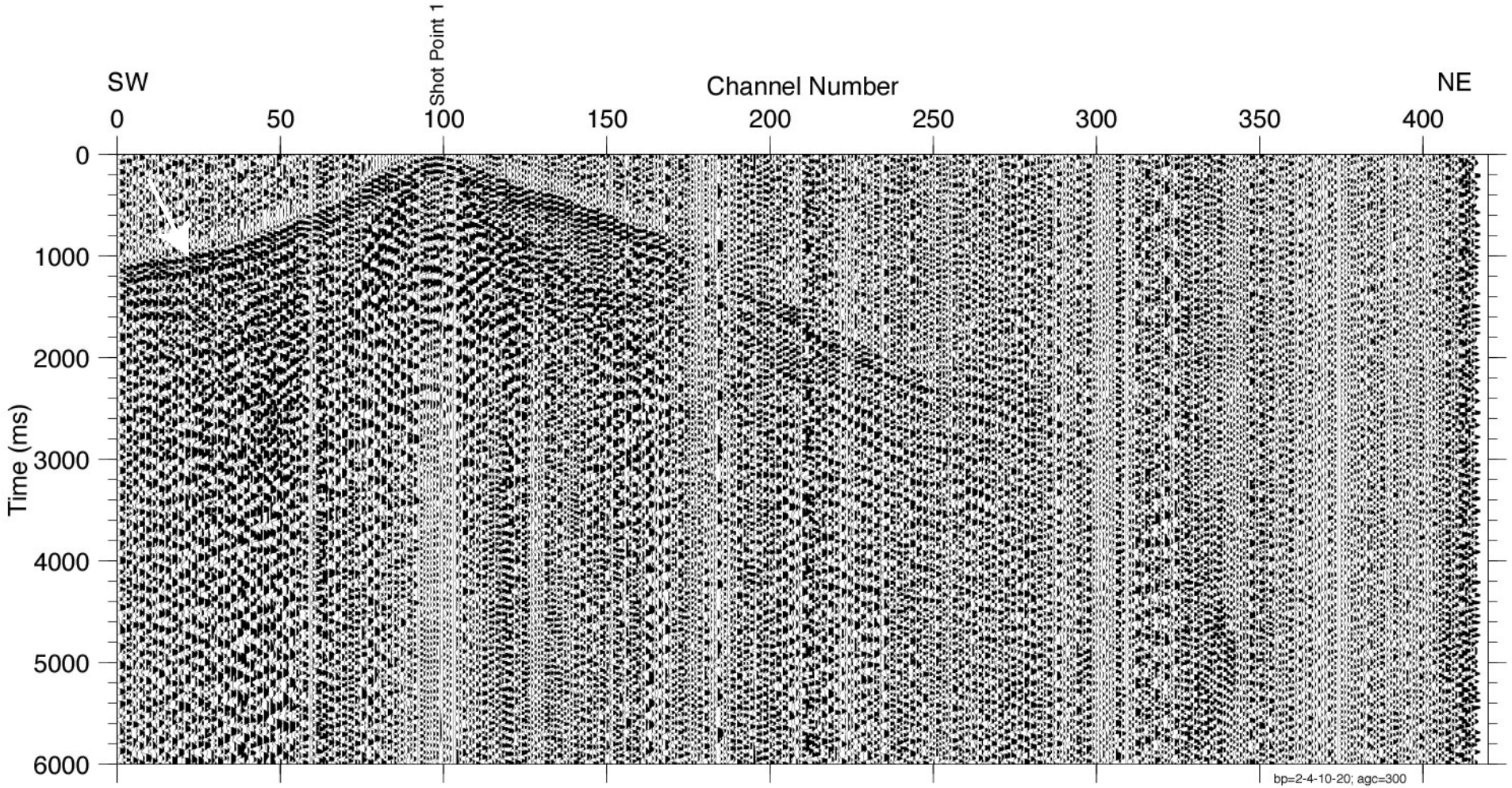
SW
Shot Point 1
Channel Number
NE
0
50
100
150
200
250
300
350
400
0
1000
2000
3000
4000
5000
6000
Time (ms)
bp=2-4-10-20; agc=300

Fig 3a

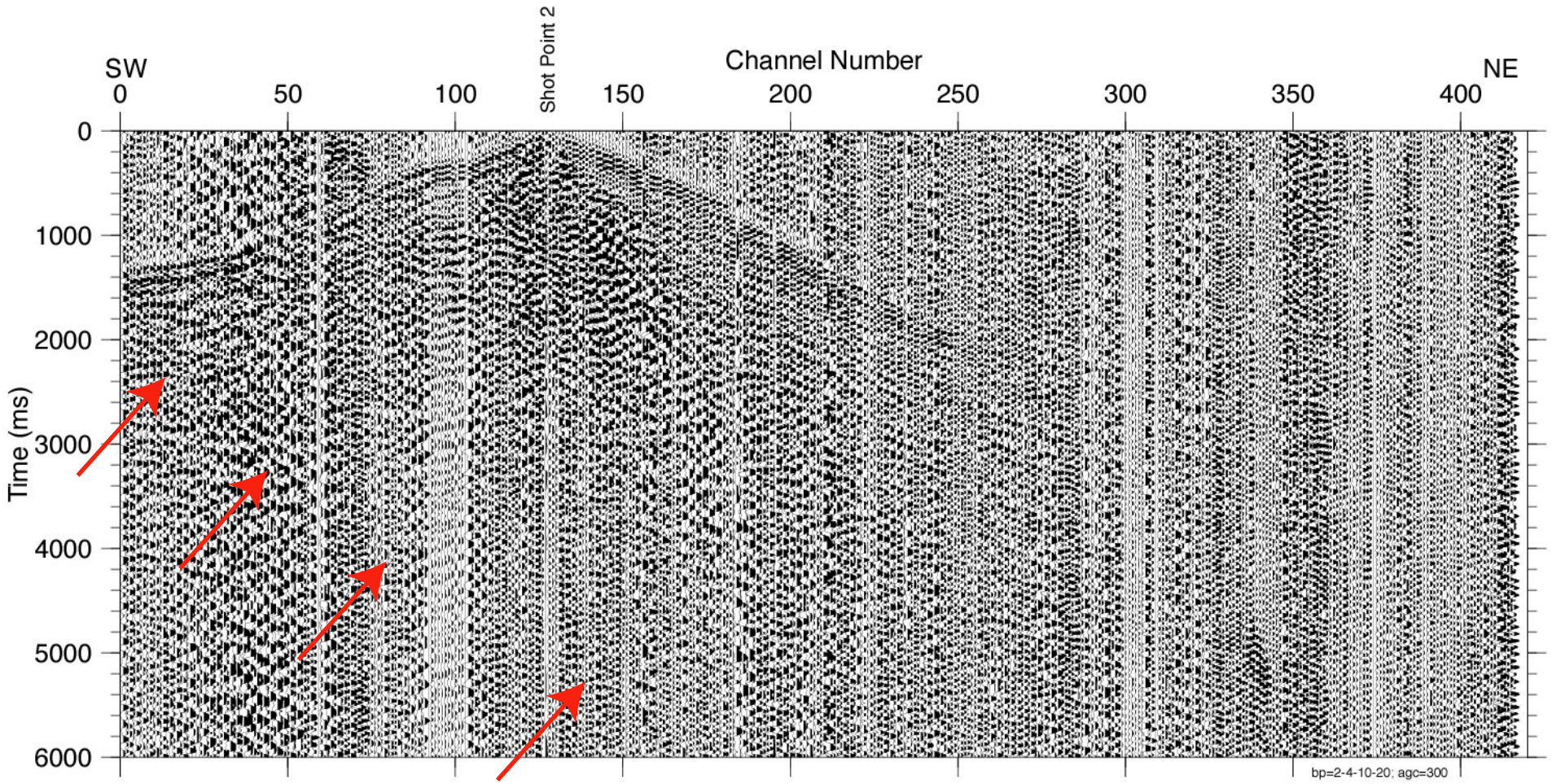
SW
NE
Channel Number
Shot Point 2
0
50
100
150
200
250
300
350
400
Time (ms)
0
1000
2000
3000
4000
5000
6000
bp=2-4-10-20; agc=300

Fig. 3b

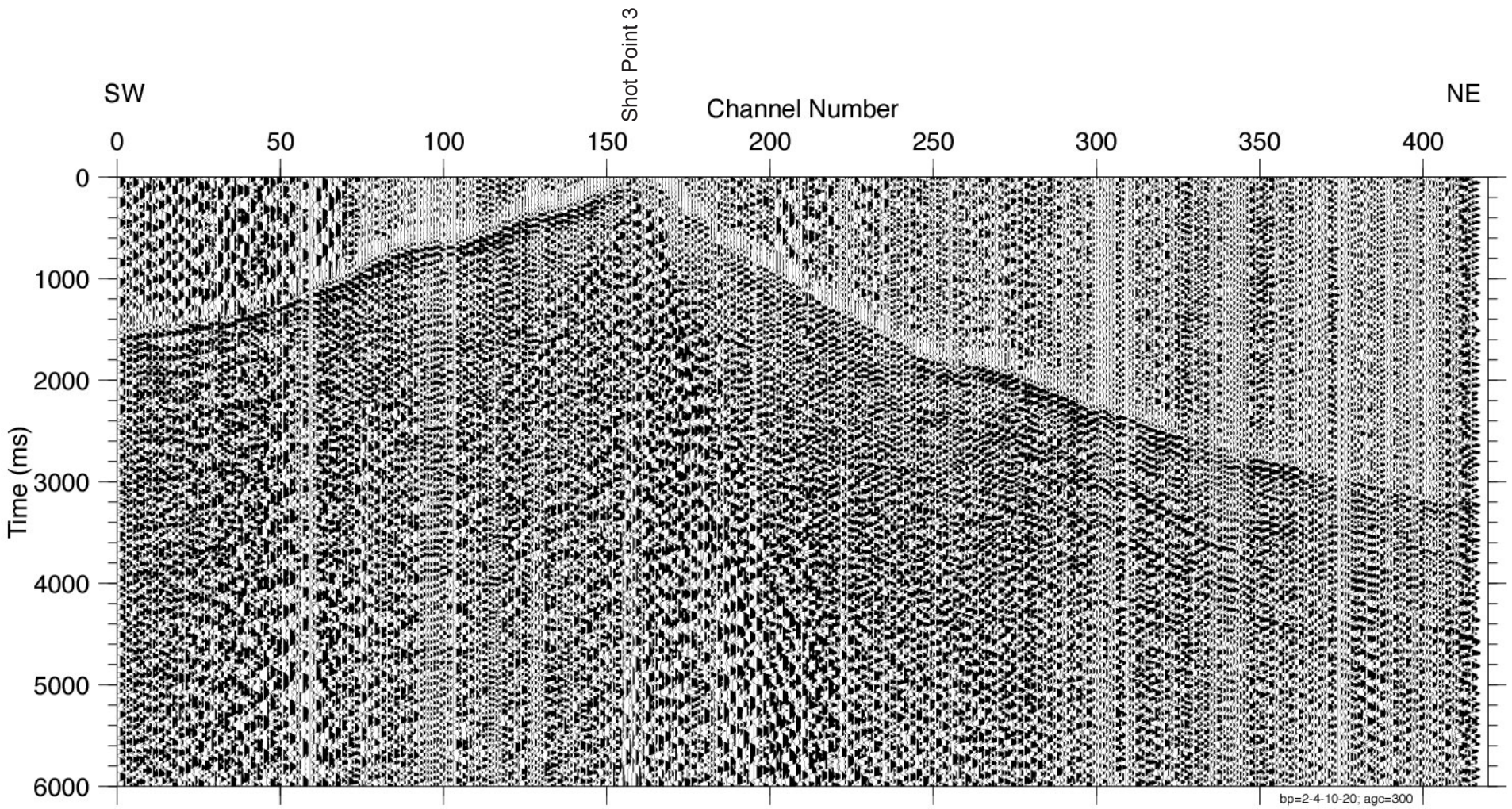
SW
Shot Point 3
Channel Number
NE
0
50
100
150
200
250
300
350
400
0
1000
2000
3000
4000
5000
6000
Time (ms)
bp=2-4-10-20; agc=300

Fig. 3c

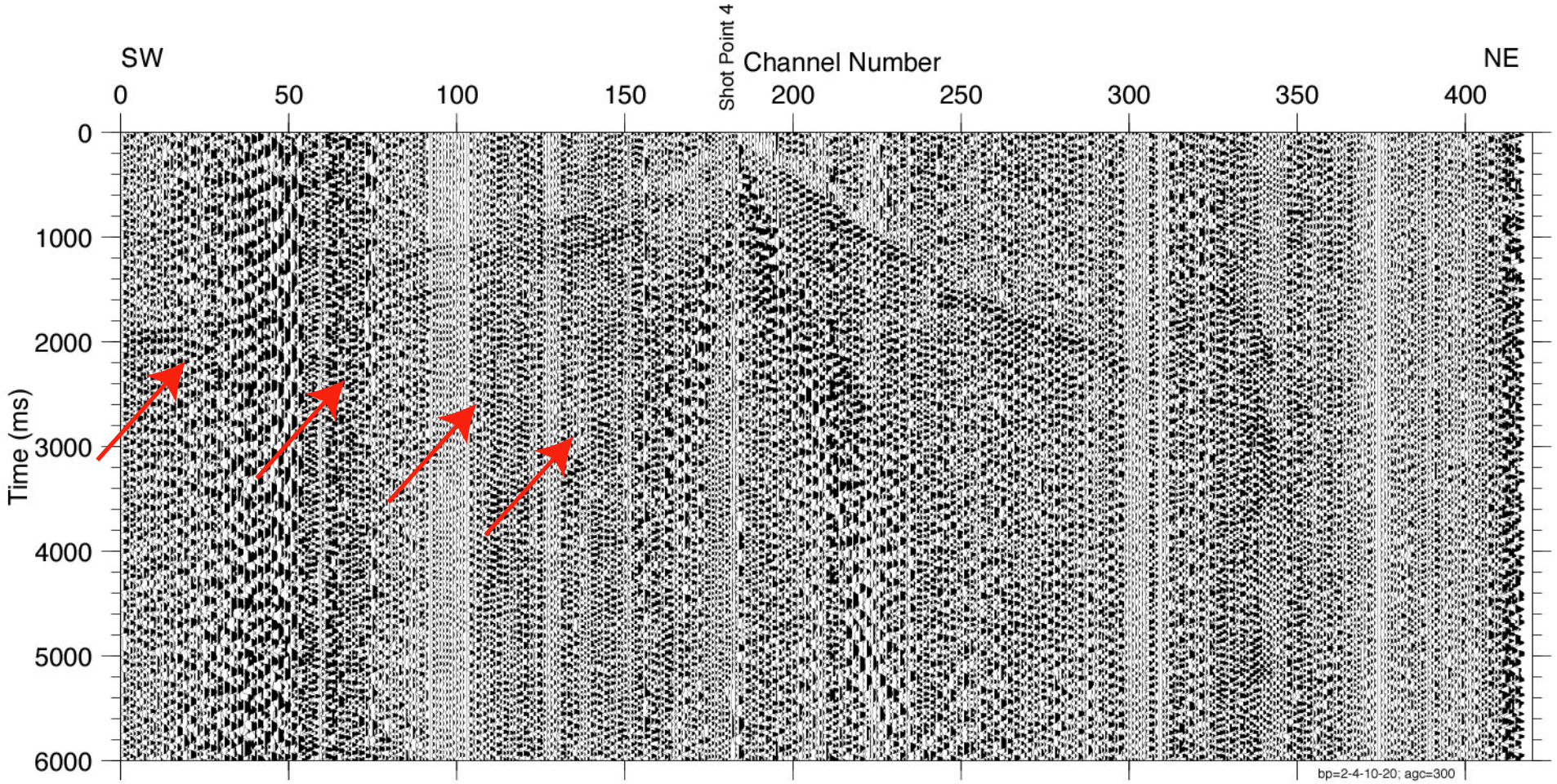
SW
Shot Point 4
Channel Number
NE
0
50
100
150
200
250
300
350
400
Time (ms)
0
1000
2000
3000
4000
5000
6000
bp=2-4-10-20; agc=300

Fig. 3d

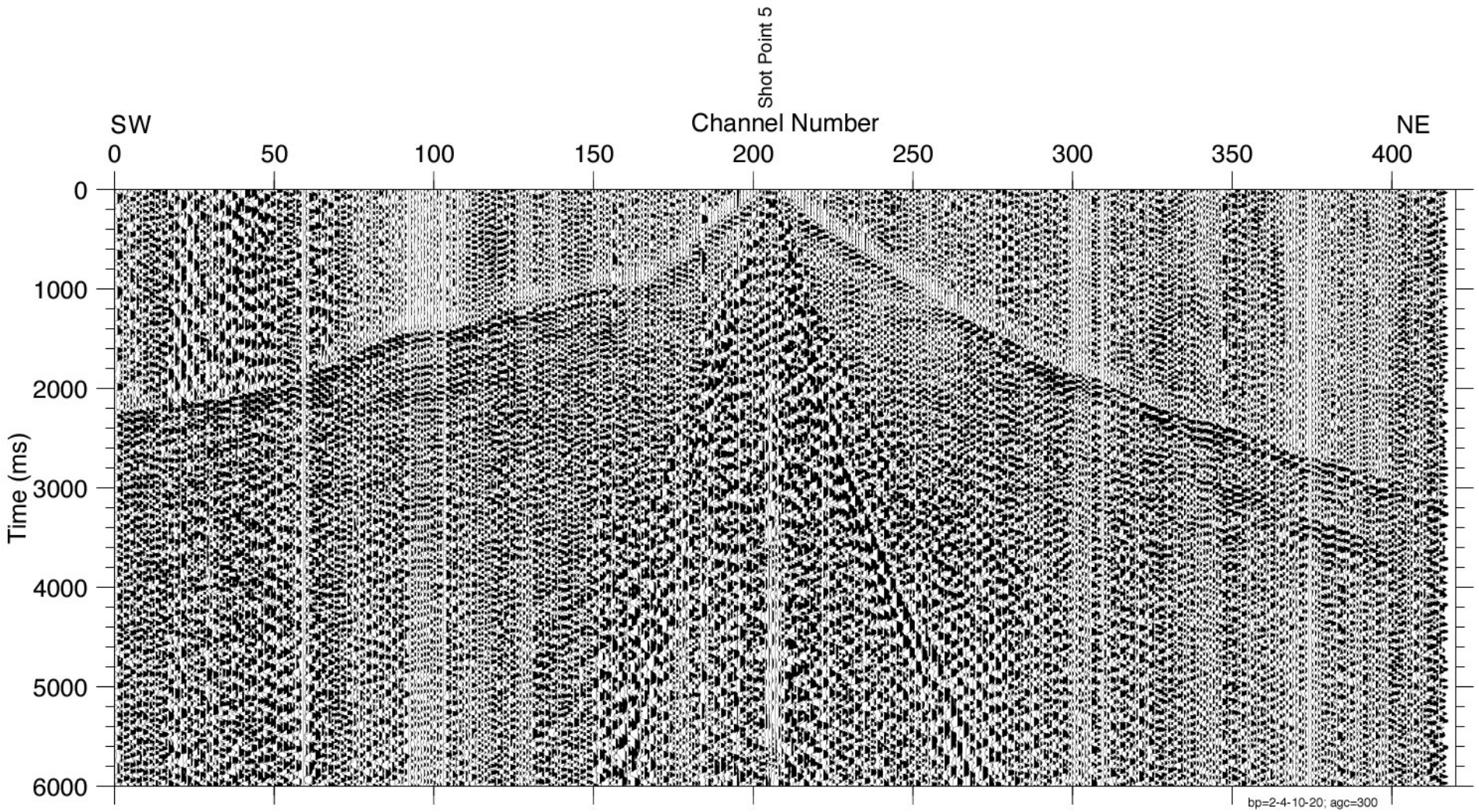
Shot Point 5
SW
Channel Number
NE
0
50
100
150
200
250
300
350
400
0
1000
2000
3000
4000
5000
6000
Time (ms)
bp=2-4-10-20; agc=300

Fig. 3e

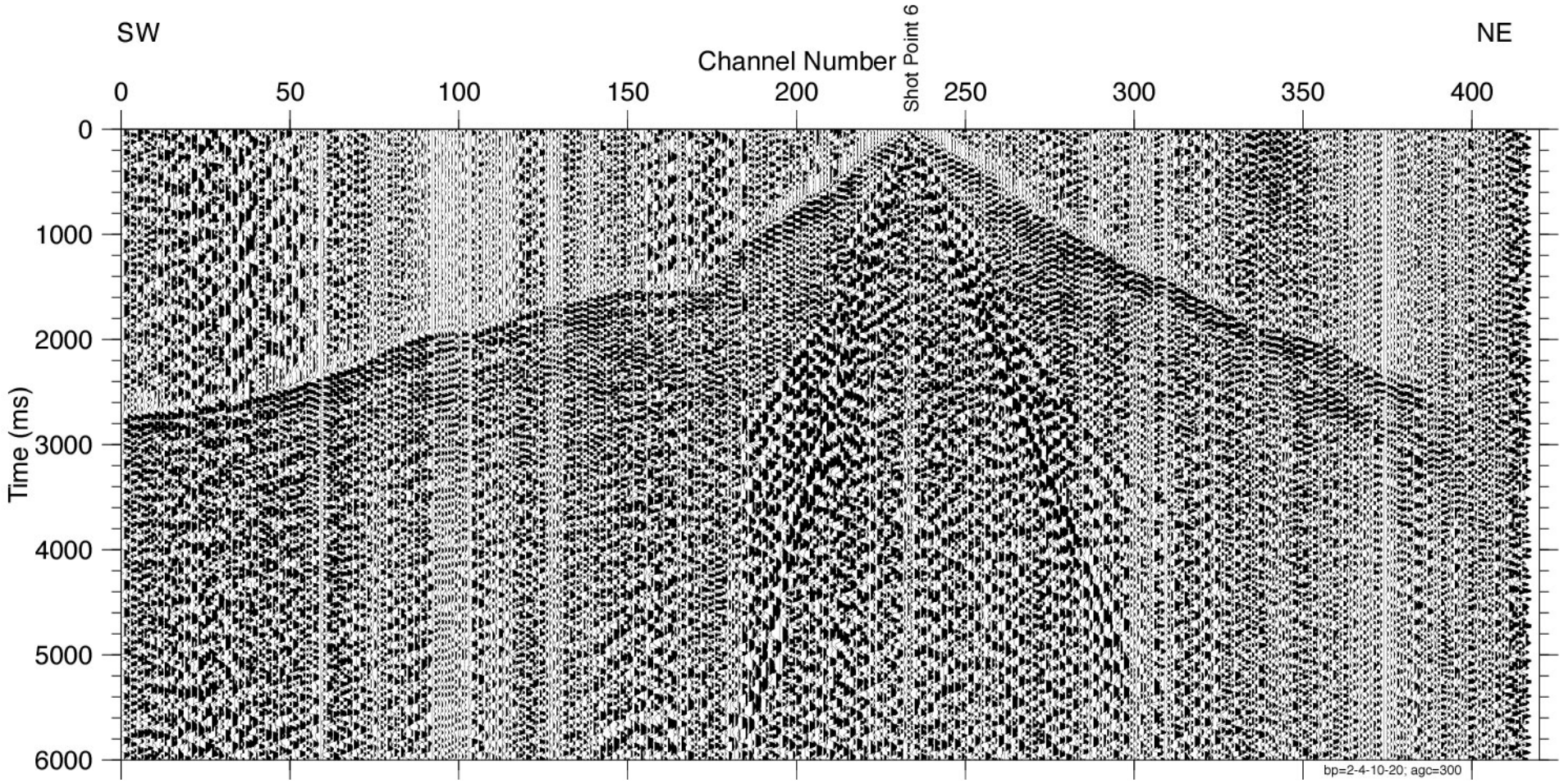
SW
NE
Channel Number
Shot Point 6
0
50
100
150
200
250
300
350
400
Time (ms)
0
1000
2000
3000
4000
5000
6000
bp=2-4-10-20; agc=300

Fig. 3f

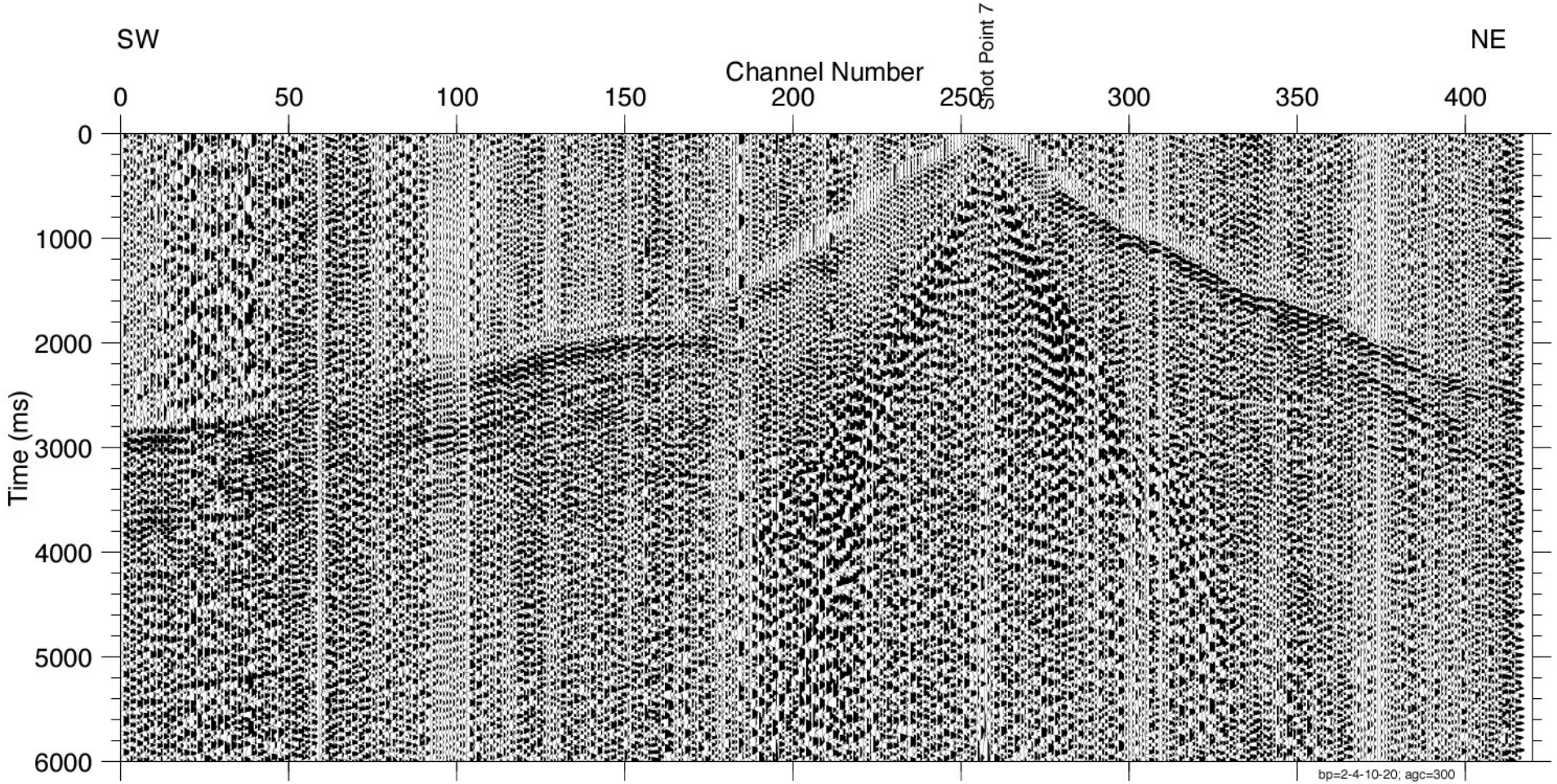
SW
NE
Channel Number
Shot Point 7
0
50
100
150
200
250
300
350
400
Time (ms)
0
1000
2000
3000
4000
5000
6000
bp=2-4-10-20; agc=300

Fig. 3g

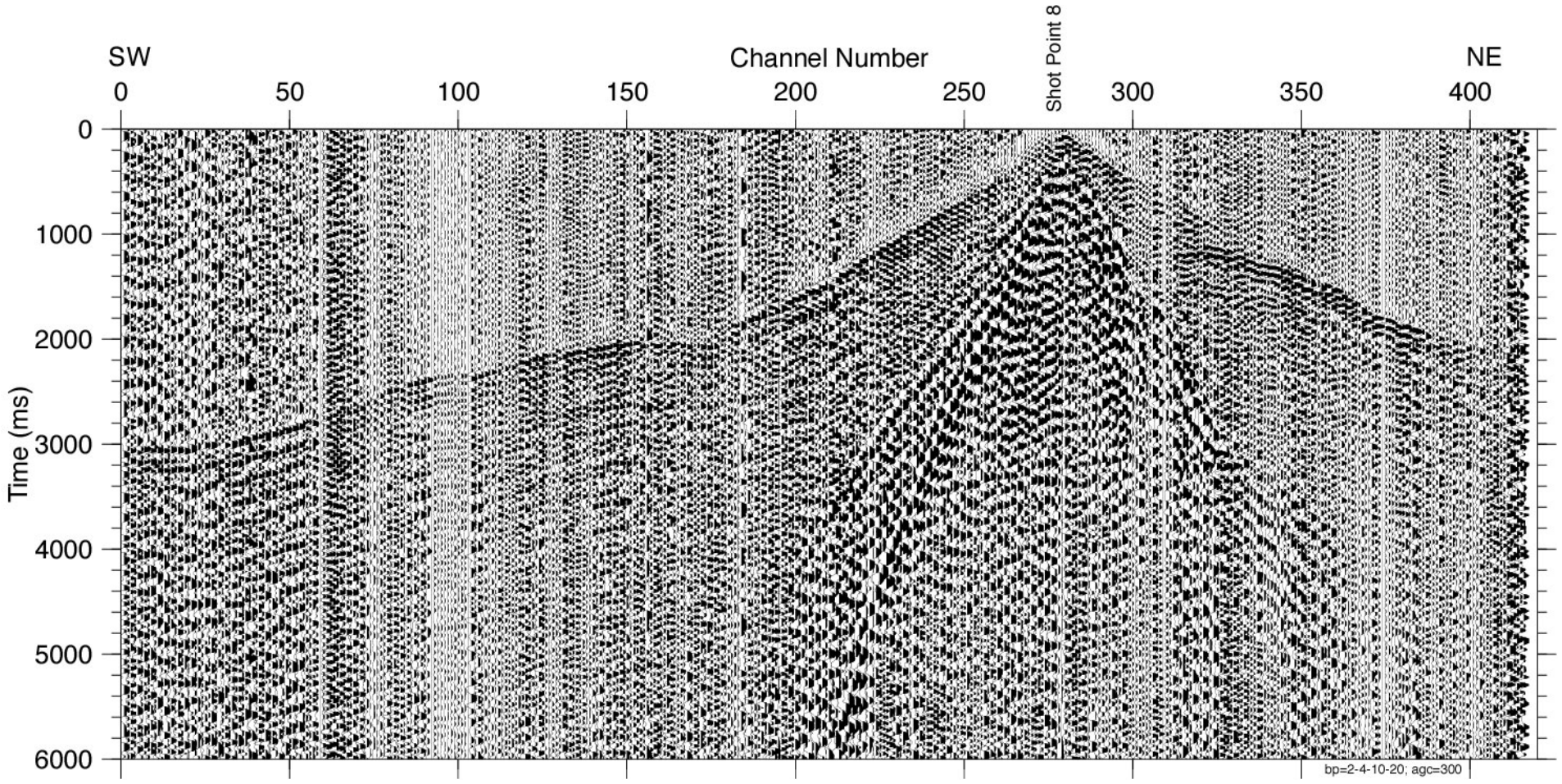
SW
Channel Number
NE
Shot Point 8
0
50
100
150
200
250
300
350
400
Time (ms)
0
1000
2000
3000
4000
5000
6000
bp=2-4-10-20; agc=300

Fig. 3h

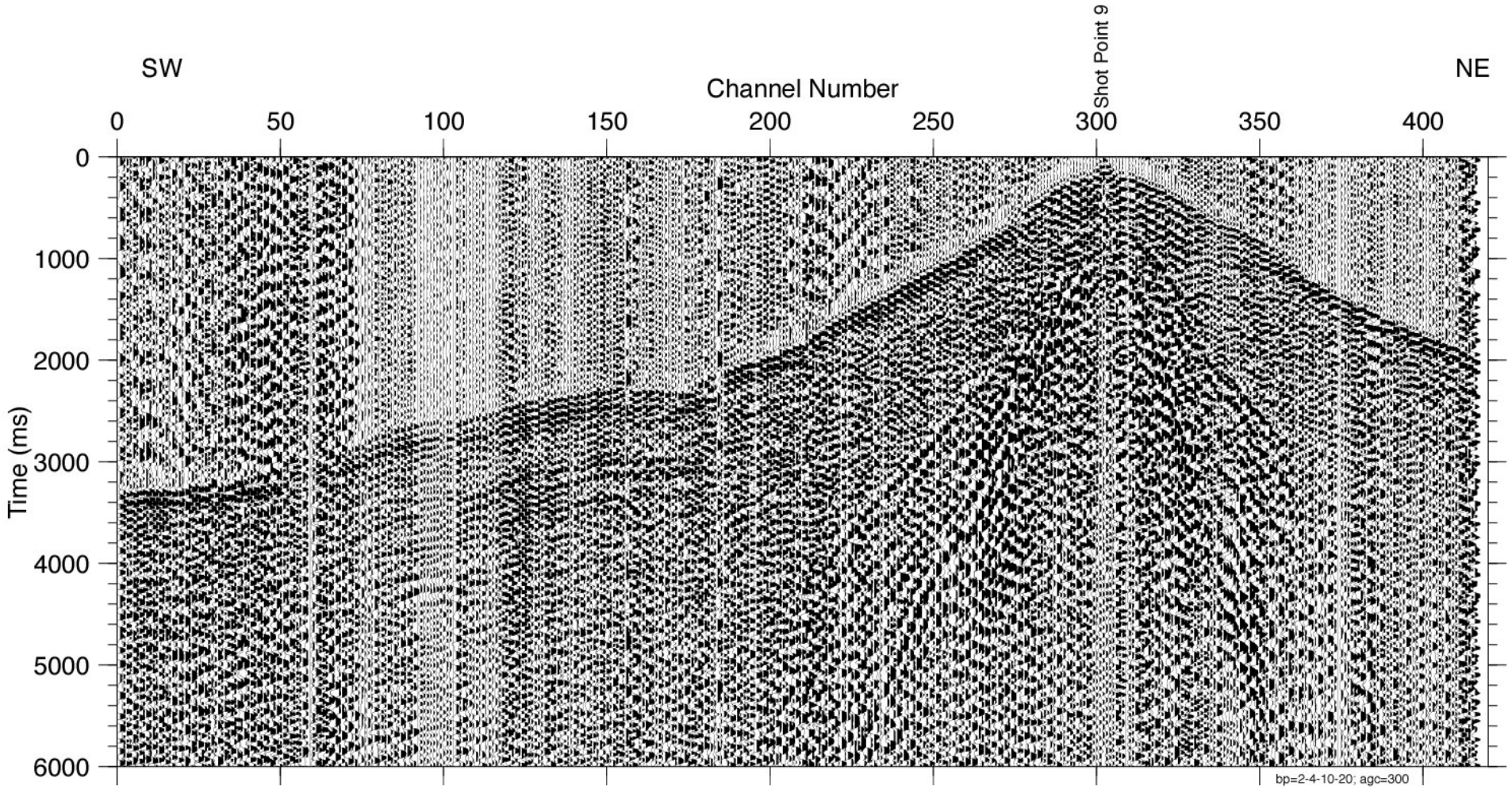
SW
NE
Channel Number
Shot Point 9
0
50
100
150
200
250
300
350
400
Time (ms)
0
1000
2000
3000
4000
5000
6000
bp=2-4-10-20; agc=300

Fig. 3i

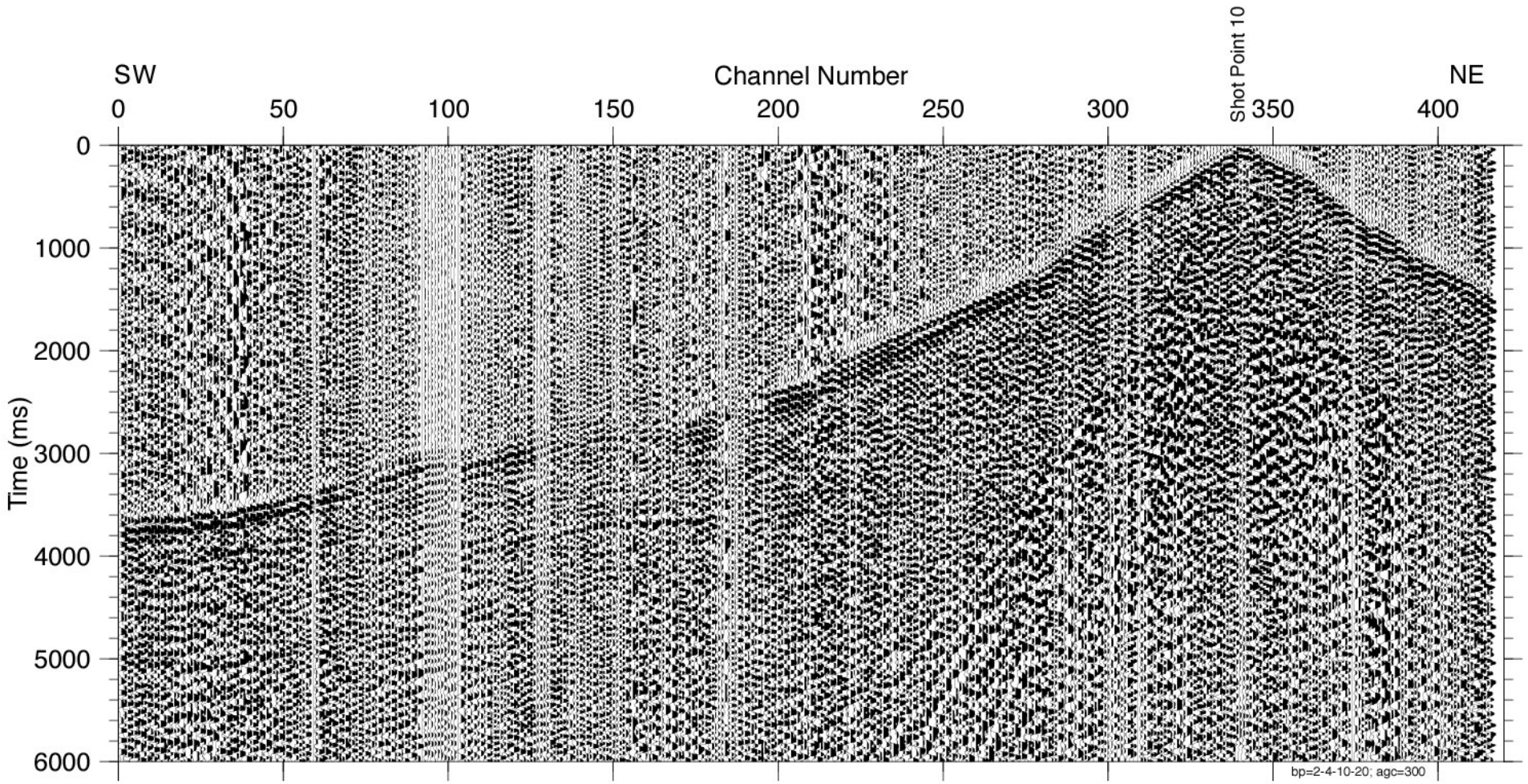
SW
Channel Number
NE
Shot Point 10
0
50
100
150
200
250
300
350
400
Time (ms)
0
1000
2000
3000
4000
5000
6000
bp=2-4-10-20; agc=300

Fig. 3j

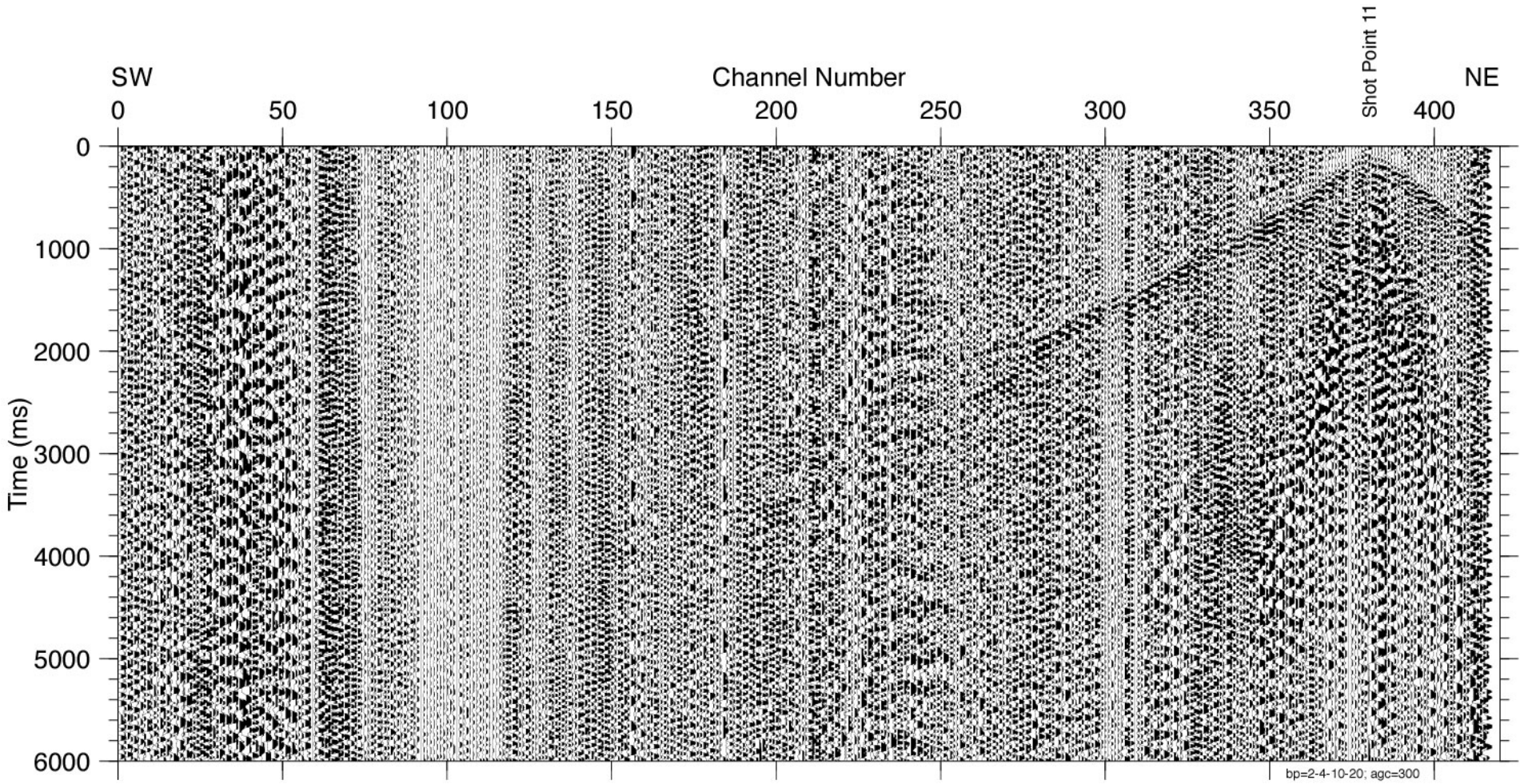
SW
Channel Number
NE
Shot Point 11
0
50
100
150
200
250
300
350
400
Time (ms)
0
1000
2000
3000
4000
5000
6000
bp=2-4-10-20; agc=300

Fig. 3k

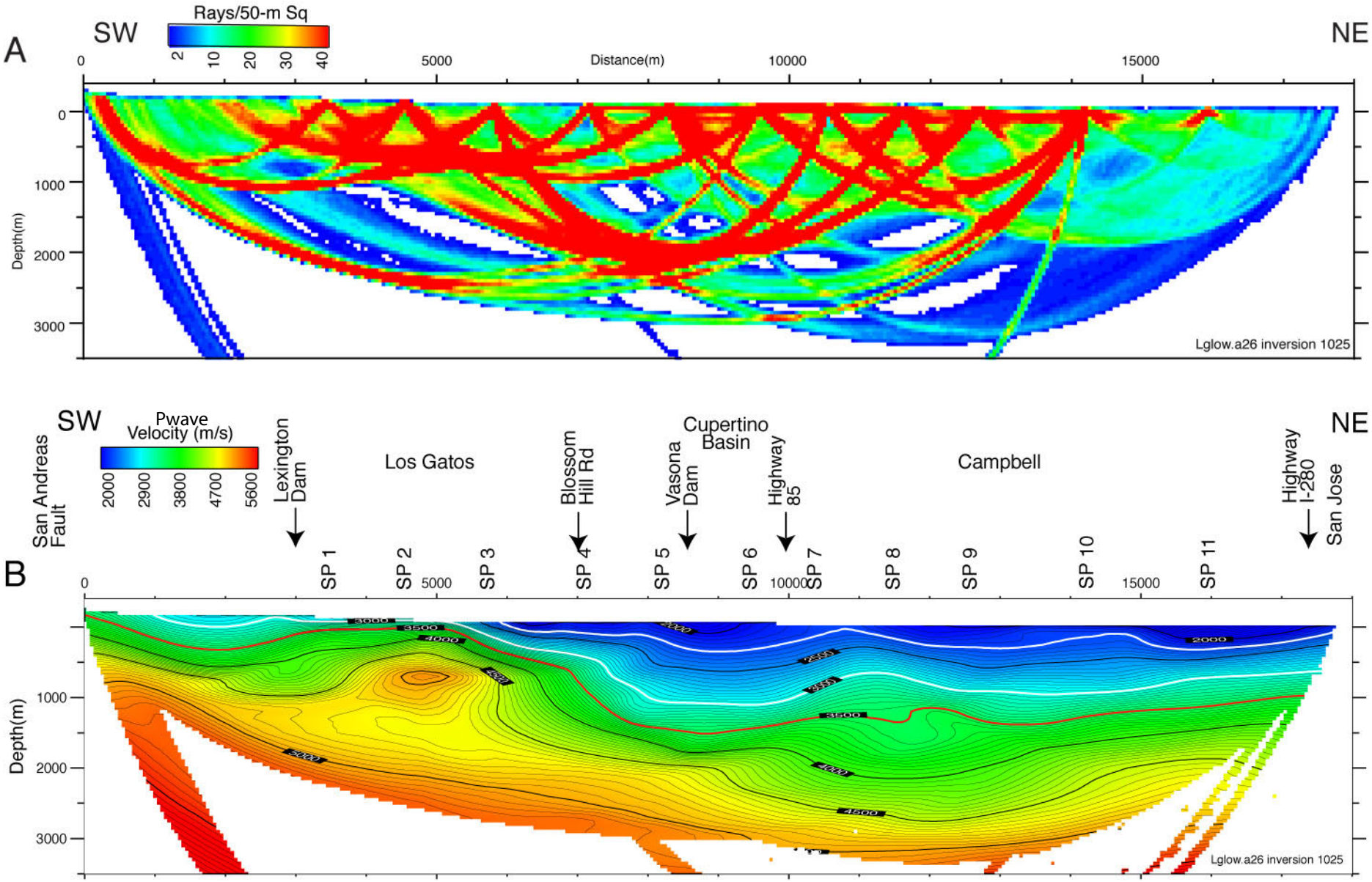
A
SW
NE
Rays/50-m Sq
2
10
20
30
40
0
5000
Distance(m)
10000
15000
Depth(m)
0
1000
2000
3000
Lglow.a26 inversion 1025
B
SW
NE
Pwave
Velocity (m/s)
2000
2900
3800
4700
5600
San Andreas
Fault
Lexington
Dam
Los Gatos
Blossom
Hill Rd
Vasona
Dam
Cupertino
Basin
Highway
85
Campbell
Highway
I-280
San Jose
SP 1
SP 2
SP 3
SP 4
SP 5
SP 6
SP 7
SP 8
SP 9
SP 10
SP 11
0
5000
10000
15000
Depth(m)
1000
2000
3000
2000
2500
3000
3500
4000
4600
5000
Lglow.a26 inversion 1025

Fig. 4

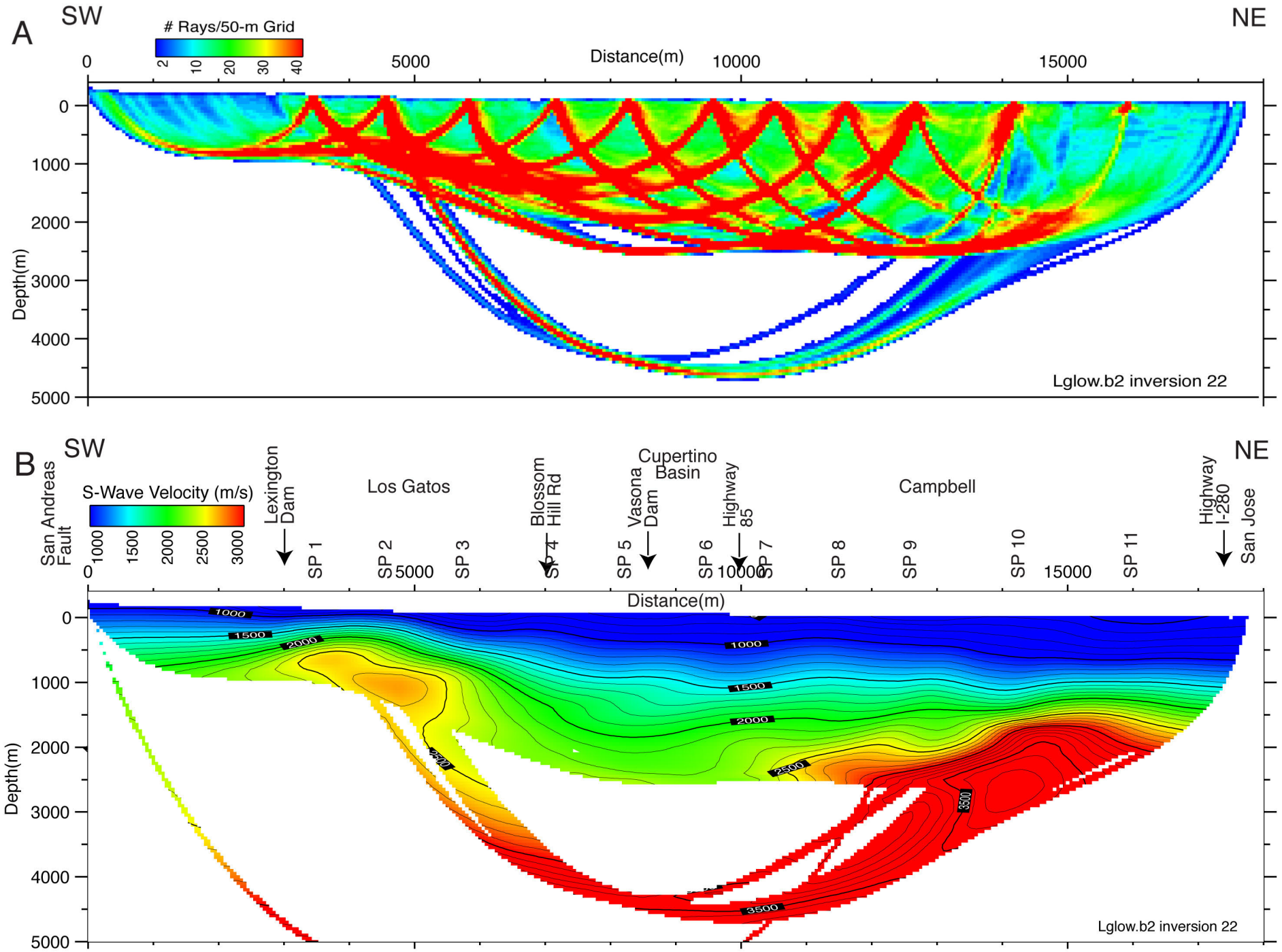
A
SW
NE
Rays/50-m Grid
2
10
20
30
40
0
5000
Distance(m)
10000
15000
Depth(m)
0
1000
2000
3000
4000
5000
Lglow.b2 inversion 22
B
SW
NE
S-Wave Velocity (m/s)
1000
1500
2000
2500
3000
San Andreas Fault
Lexington Dam
Los Gatos
Blossom Hill Rd
Vasona Dam
Cupertino Basin
Highway 85
Campbell
Highway I-280
San Jose
SP 1
SP 2
SP 3
SP 4
SP 5
SP 6
SP 7
SP 8
SP 9
SP 10
SP 11
0
5000
10000
15000
Distance(m)
Depth(m)
0
1000
2000
3000
4000
5000
1000
1500
2000
2500
3500
Lglow.b2 inversion 22

Fig. 5

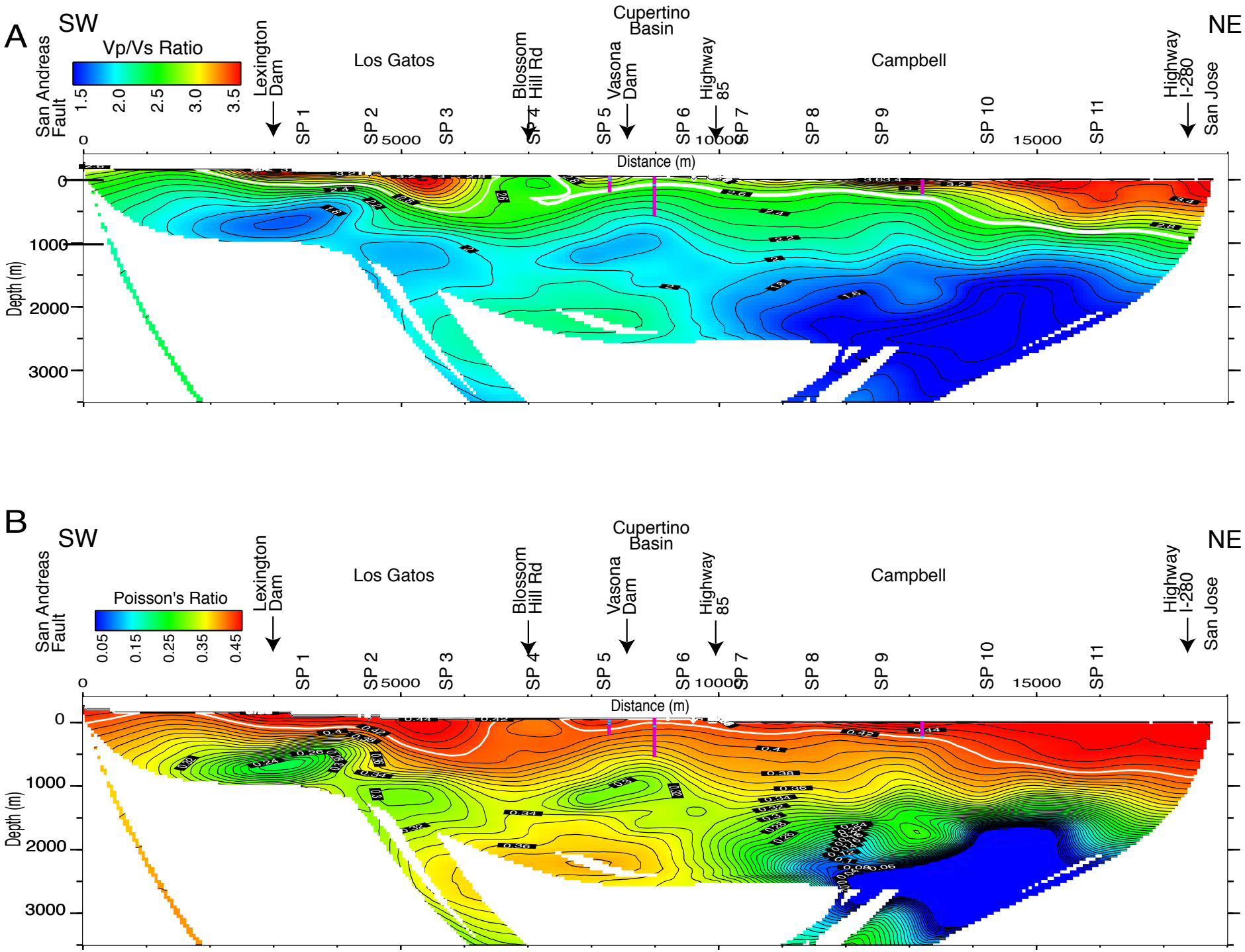
A
SW
NE
Vp/Vs Ratio
1.5
2.0
2.5
3.0
3.5
San Andreas Fault
Lexington Dam
Los Gatos
Blossom Hill Rd
Cupertino Basin
Vasona Dam
Highway 85
Campbell
Highway I-280
San Jose
SP 1
SP 2
SP 3
SP 4
SP 5
SP 6
SP 7
SP 8
SP 9
SP 10
SP 11
0
5000
10000
15000
Distance (m)
Depth (m)
0
1000
2000
3000
B
SW
NE
Poisson's Ratio
0.05
0.15
0.25
0.35
0.45
San Andreas Fault
Lexington Dam
Los Gatos
Blossom Hill Rd
Cupertino Basin
Vasona Dam
Highway 85
Campbell
Highway I-280
San Jose
SP 1
SP 2
SP 3
SP 4
SP 5
SP 6
SP 7
SP 8
SP 9
SP 10
SP 11
0
5000
10000
15000
Distance (m)
Depth (m)
0
1000
2000
3000

Fig. 6

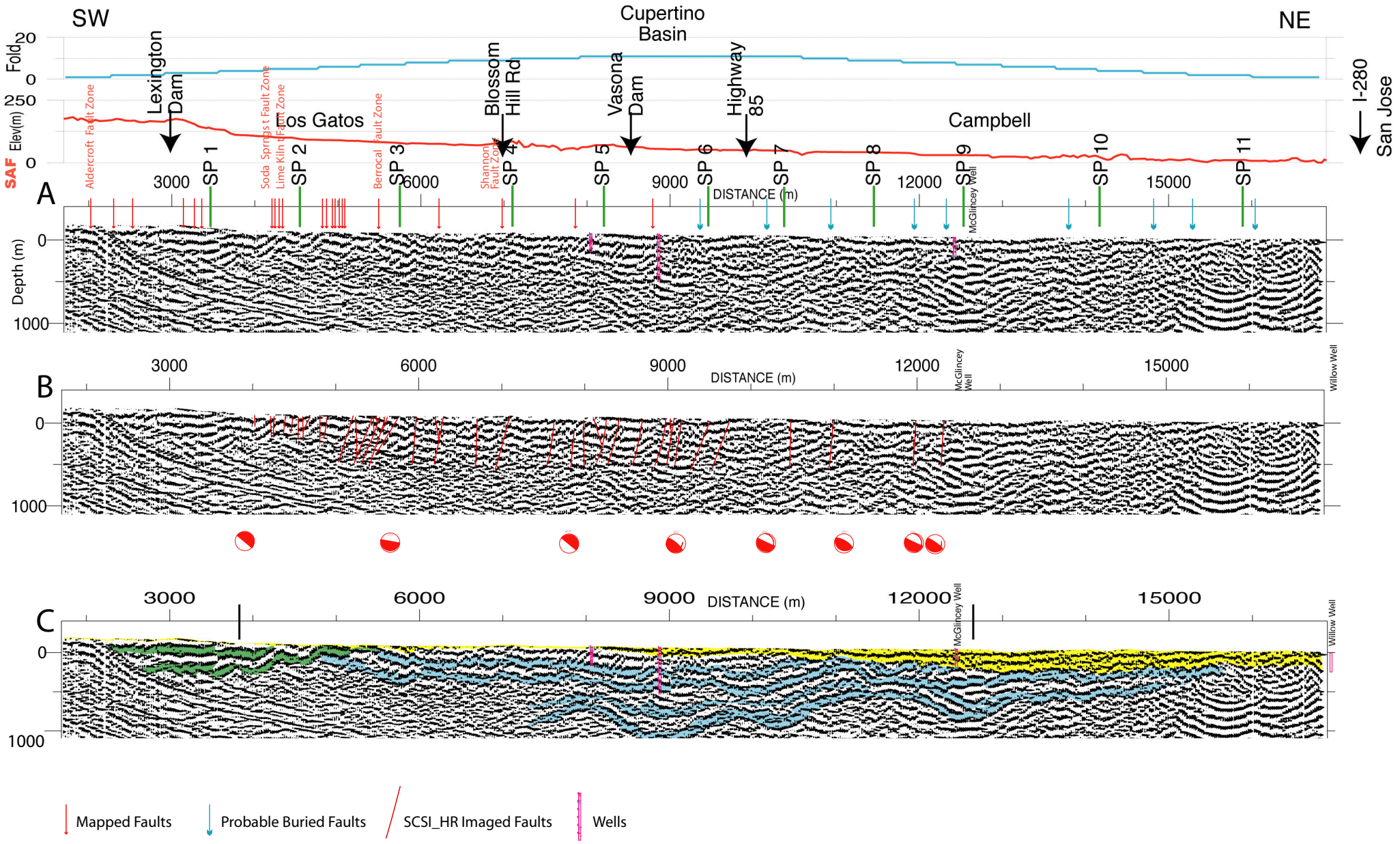
SW
NE
Cupertino Basin
Fold
Elev(m)
SAF
Aldercroft Fault Zone
Lexington Dam
Soda Springs t Fault Zone
Lime Kiln t Fault Zone
Los Gatos
Berrocal Fault Zone
Blossom Hill Rd
Shannon Fault Zone
Vasona Dam
Highway 85
Campbell
I-280
San Jose
SP 1
SP 2
SP 3
SP 4
SP 5
SP 6
SP 7
SP 8
SP 9
SP 10
SP 11
3000
6000
9000
12000
15000
DISTANCE (m)
McGlincey Well
Willow Well
A
B
C
Depth (m)
Mapped Faults
Probable Buried Faults
SCSI_HR Imaged Faults
Wells

Fig. 7

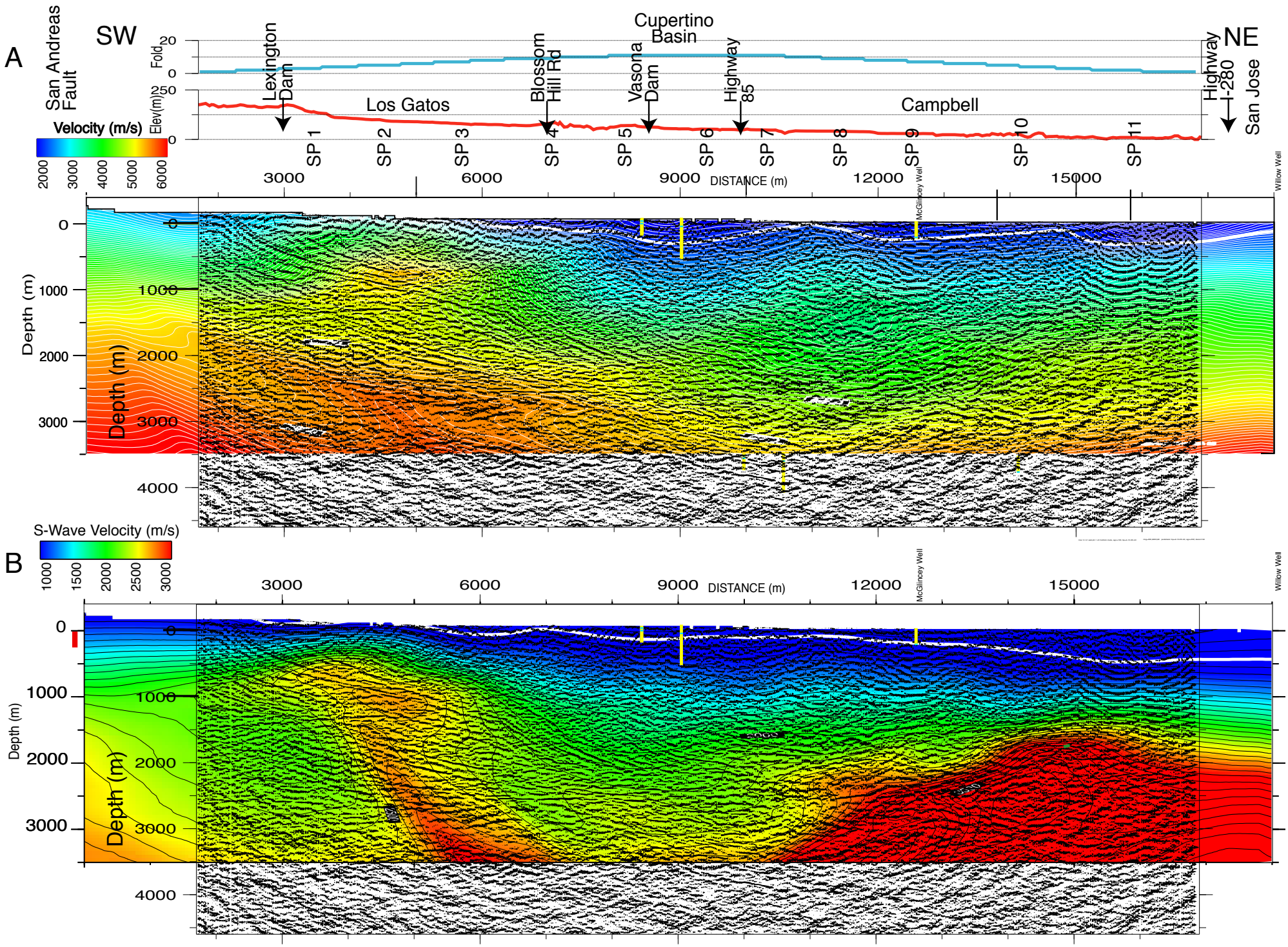
A
SW
NE
San Andreas Fault
Fold
Elev(m)
Velocity (m/s)
2000
3000
4000
5000
6000
Lexington Dam
Los Gatos
Blossom Hill Rd
Cupertino Basin
Vasona Dam
Highway 85
Campbell
Highway I-280
San Jose
SP 1
SP 2
SP 3
SP 4
SP 5
SP 6
SP 7
SP 8
SP 9
SP 10
SP 11
DISTANCE (m)
Depth (m)
McGlincey Well
Willow Well
S-Wave Velocity (m/s)
1000
1500
2000
2500
3000
B

Fig. 8

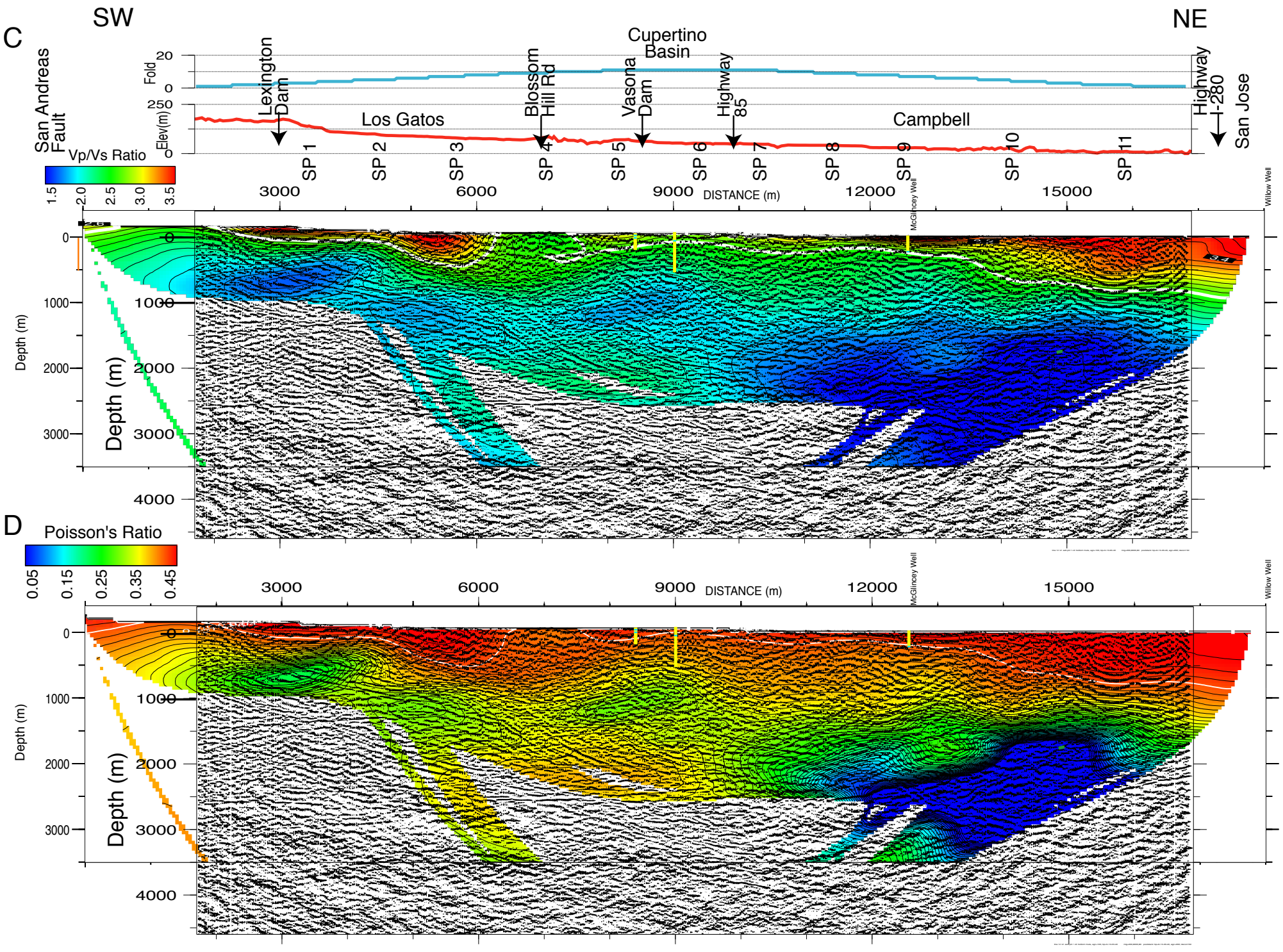
C
SW
NE
San Andreas Fault
Vp/Vs Ratio
1.5
2.0
2.5
3.0
3.5
Fold
20
0
Elev(m)
250
0
Lexington Dam
Los Gatos
Blossom Hill Rd
Cupertino Basin
Vasona Dam
Highway 85
Campbell
Highway I-280
San Jose
SP 1
SP 2
SP 3
SP 4
SP 5
SP 6
SP 7
SP 8
SP 9
SP 10
SP 11
3000
6000
9000
DISTANCE (m)
12000
15000
McGlincey Well
Willow Well
Depth (m)
0
1000
2000
3000
4000
D
Poisson's Ratio
0.05
0.15
0.25
0.35
0.45
3000
6000
9000
DISTANCE (m)
12000
15000
McGlincey Well
Willow Well
Depth (m)
0
1000
2000
3000
4000

Fig. 8

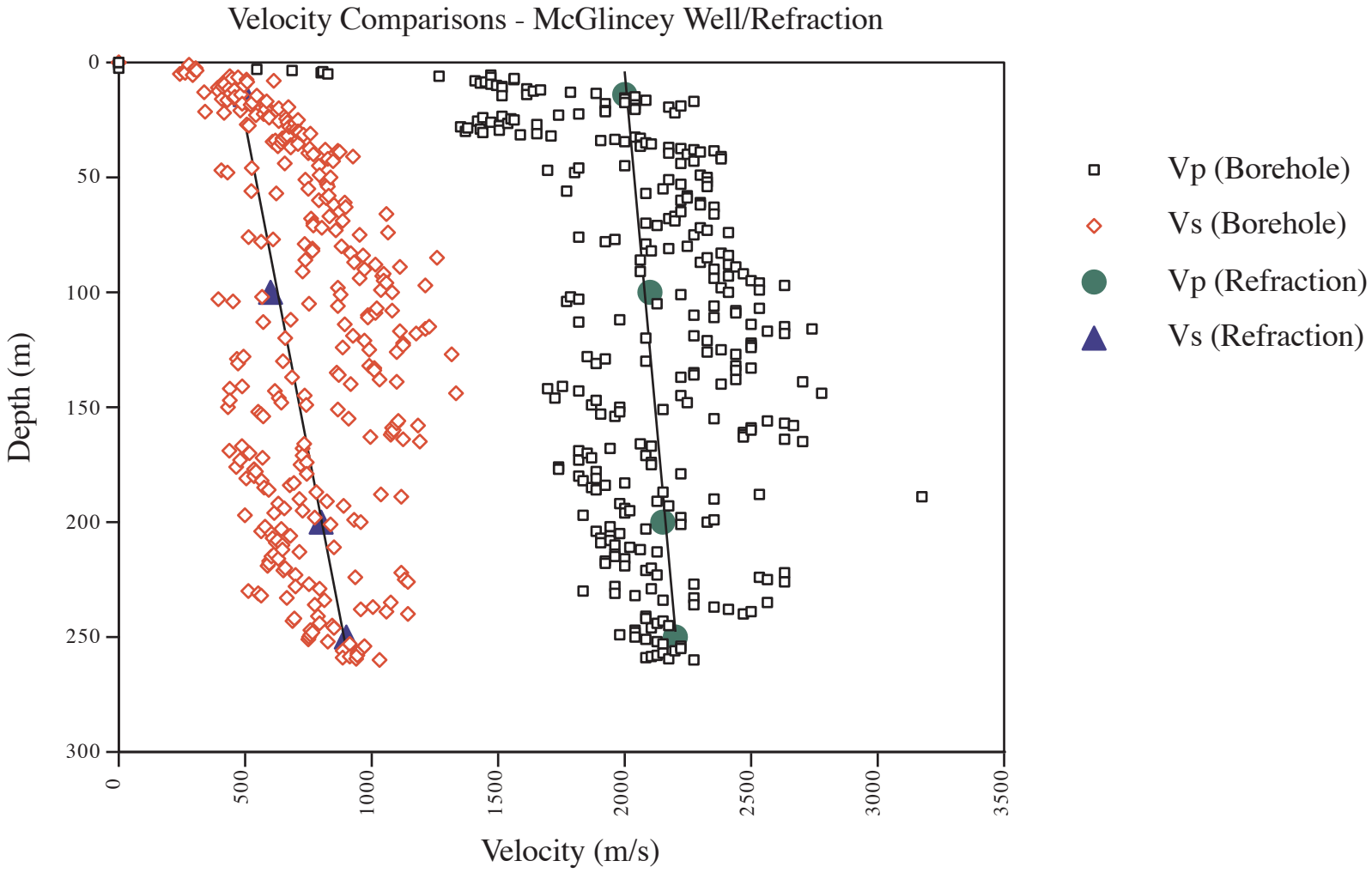
Velocity Comparisons - McGlincey Well/Refraction
Depth (m)
0
50
100
150
200
250
300
0
500
1000
1500
2000
2500
3000
3500
Velocity (m/s)
Vp (Borehole)
Vs (Borehole)
Vp (Refraction)
Vs (Refraction)

Fig. 9

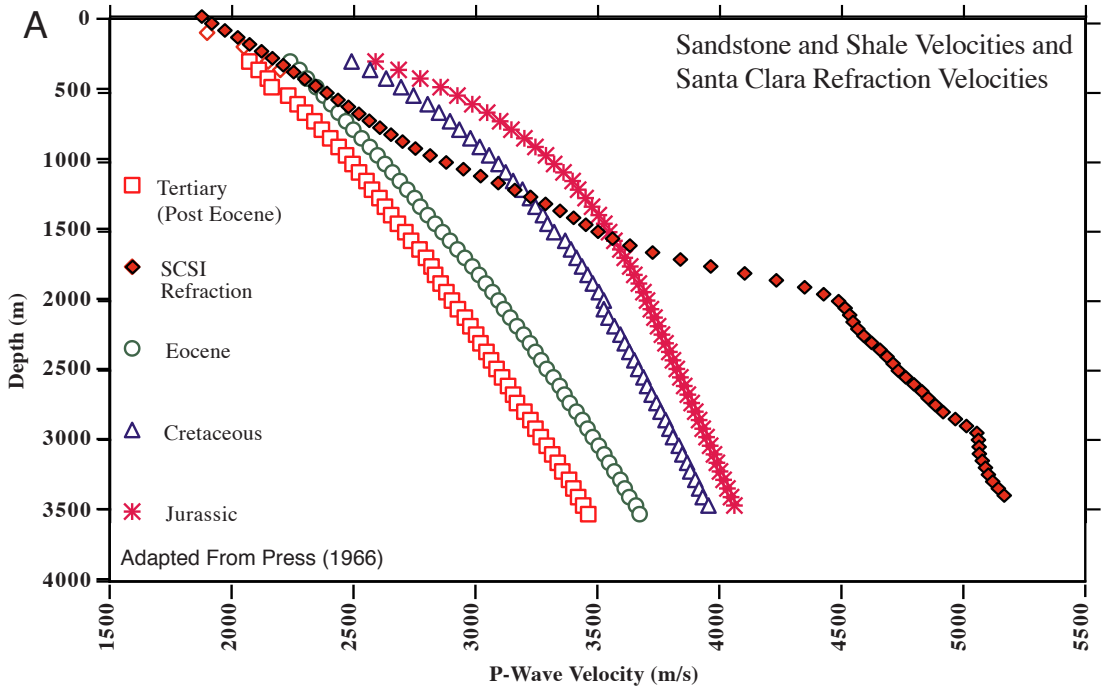
A
Sandstone and Shale Velocities and
Santa Clara Refraction Velocities
Tertiary
(Post Eocene)
SCSI
Refraction
Eocene
Cretaceous
Jurassic
Adapted From Press (1966)
Depth (m)
P-Wave Velocity (m/s)
0
500
1000
1500
2000
2500
3000
3500
4000
1500
2000
2500
3000
3500
4000
4500
5000
5500

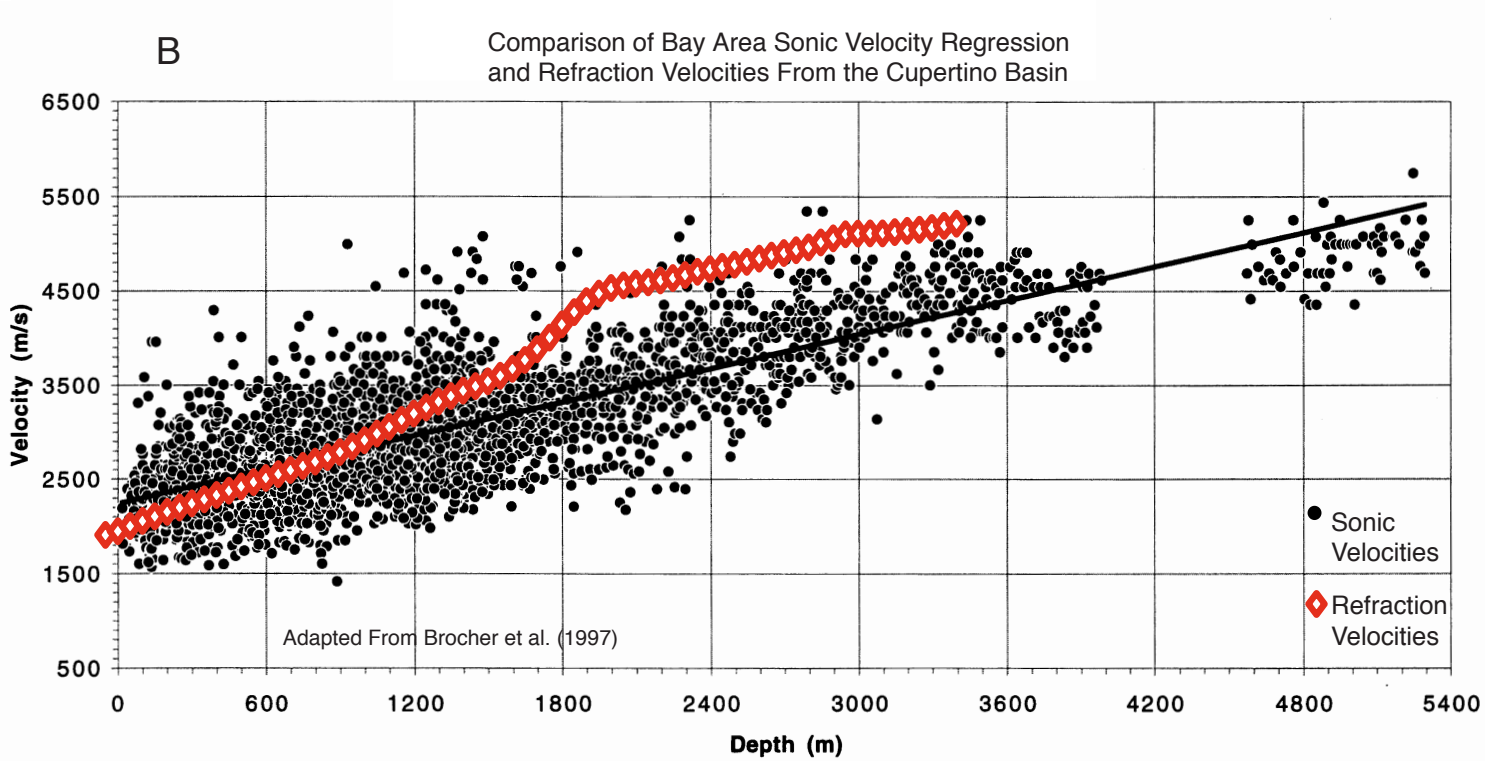
B
Comparison of Bay Area Sonic Velocity Regression
and Refraction Velocities From the Cupertino Basin
Sonic
Velocities
Refraction
Velocities
Adapted From Brocher et al. (1997)
Velocity (m/s)
Depth (m)
6500
5500
4500
3500
2500
1500
500
0
600
1200
1800
2400
3000
3600
4200
4800
5400

Fig. 10

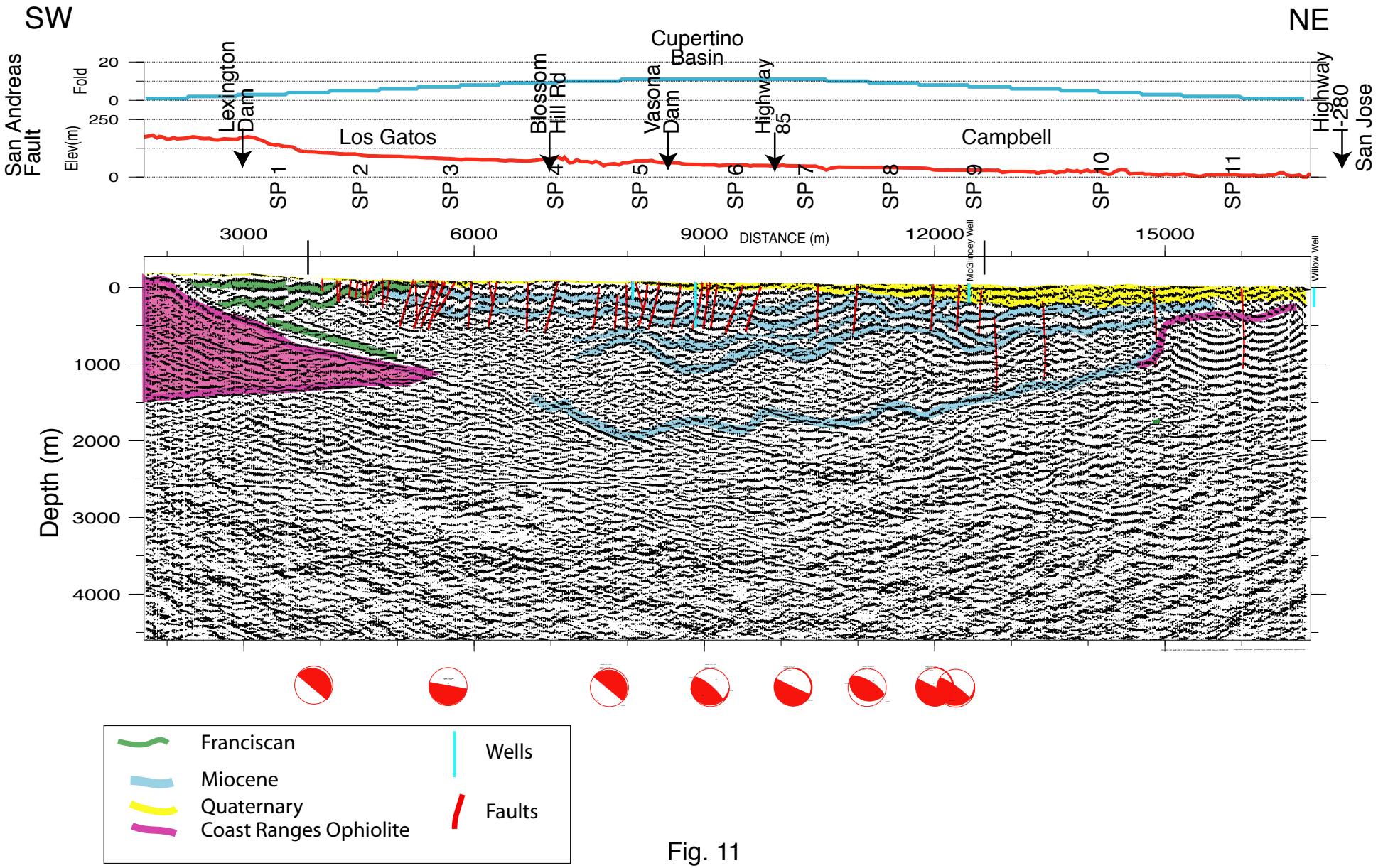
SW
NE
San Andreas Fault
Fold
Elev(m)
Lexington Dam
Los Gatos
Blossom Hill Rd
Cupertino Basin
Vasona Dam
Highway 85
Campbell
Highway I-280
San Jose
SP 1
SP 2
SP 3
SP 4
SP 5
SP 6
SP 7
SP 8
SP 9
SP 10
SP 11
DISTANCE (m)
McGlincey Well
Willow Well
Depth (m)
Franciscan
Miocene
Quaternary
Coast Ranges Ophiolite
Wells
Faults

Fig. 11

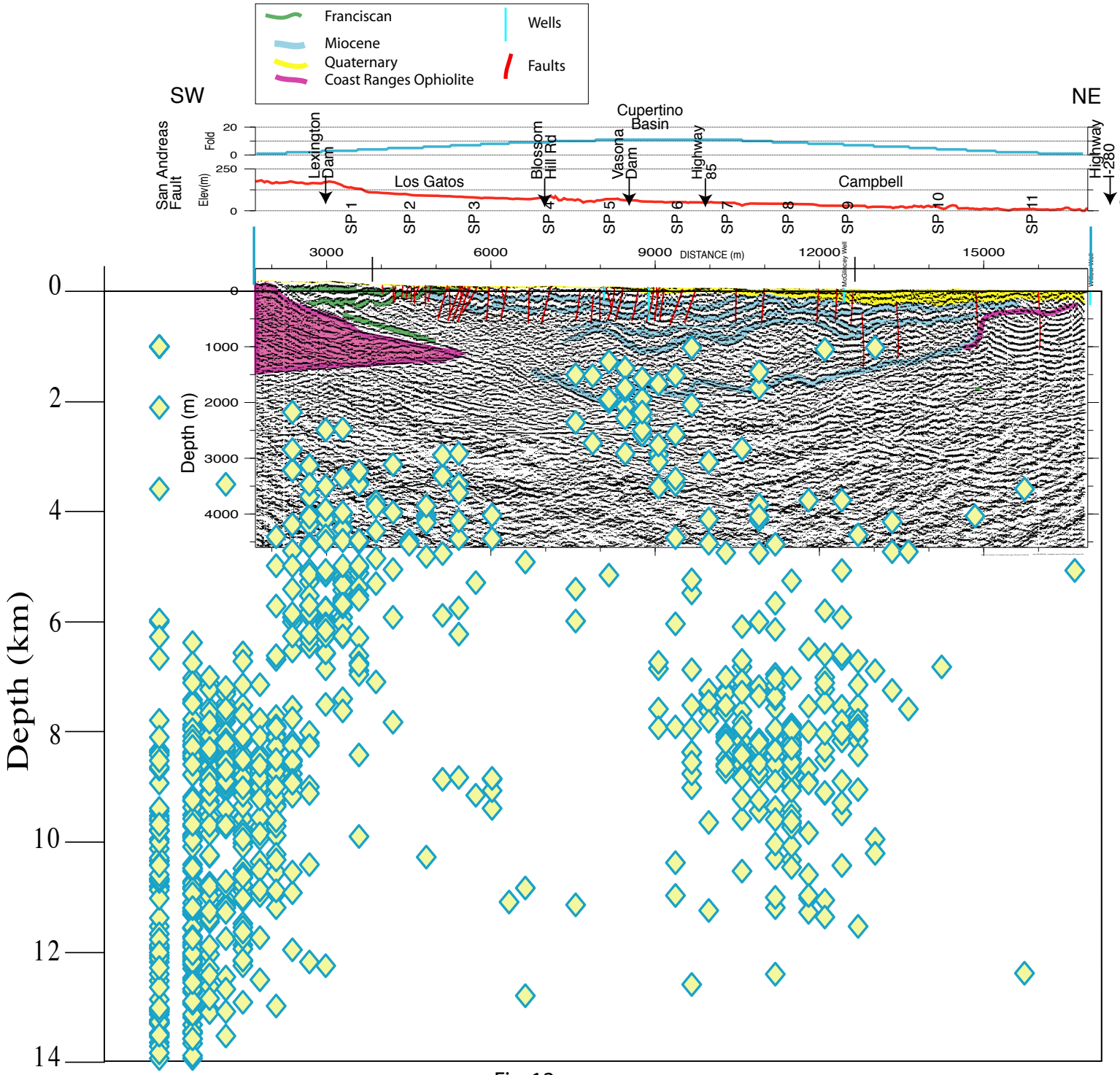
Franciscan
Miocene
Quaternary
Coast Ranges Ophiolite
Wells
Faults
SW
NE
Cupertino Basin
San Andreas Fault
Fold
Elev(m)
Lexington Dam
Blossom Hill Rd
Vasona Dam
Highway 85
Highway I-280
San Jose
Los Gatos
Campbell
SP 1
SP 2
SP 3
SP 4
SP 5
SP 6
SP 7
SP 8
SP 9
SP 10
SP 11
DISTANCE (m)
Depth (m)
Depth (km)

Fig. 12

Appendix 1 Shot Point Locations

Shot Point Number	Nearest Station	Dist(m) Along Profile	Lateral Dist (m) From Profile	Elevation (m)	UTM Northing	UTM Easting
1001	99	3440.79	0	140.22	4118014.9	589542.1
1002	127	4552.43	-103.18	116	4119058	589940
1003	158	5828.47	-53.07	74	4120181	590548
1004	182	7152.01	184.29	76	4121264	591345
1005	205	8288.63	-3.83	70.94	4122367	591677.7
1006	233	9561.46	-175.57	51.87	4123585	592085.2
1007	257	10533.85	127.25	0.43	4124324	592786
1008	279	11616.69	-51.03	39.73	4125374.4	593103.8
1009	302	12667.49	135.68	24	4126235	593735
1010	342	14196.01	82.82	15	4127630	594362
1011	379	15925.97	0	14	4129219	595051

Appendix 2 Seismograph Locations Along Profile

Station #	Dist (m) Along Profile	Lateral Dist (m) From Profile	Elevation (m)
1	0	2597.63	251
2	24.47	2549.94	259
3	44.44	2506.7	243
4	80.04	2465.79	247
5	106.63	2436	238
6	146.2	2403.17	226
7	166.02	2382.29	228
8	186.29	2360.06	230
9	192.39	2318.06	231
10	162.75	2269.12	224
11	225.21	2223.92	231
12	258.55	2187.47	228
13	283.45	2142.91	222
14	282	2092.36	222
15	285.88	2045.88	219
16	316.13	2003.15	206
17	296.7	1965.9	193
18	319	1909.25	203
19	365.5	1910.9	199
20	408.56	1891.96	203
21	444.1	1860	201
22	489.79	1848.67	192
23	539	1846.77	191
24	559	1799.05	184
25	583.42	1758.06	171
26	602.96	1711.68	171
27	650.12	1680.69	172
28	684.29	1654.98	167
29	727.39	1629.33	178
30	761.65	1587.97	173
31	781.62	1544.72	172
32	808.25	1508.22	175
33	839.85	1463.71	172
34	882.09	1434.03	178
35	926.02	1419.12	181
36	977.52	1408.28	181
37	1024.98	1400.55	180
38	1070.29	1379.38	179
39	1112.95	1352.84	186
40	1153.84	1324.93	191
41	1175.13	1284.38	189
42	1213.36	1251.09	186
43	1244.48	1212.39	173
44	1283.54	1189.84	157
45	1321.27	1164.6	169
46	1358.99	1141.6	181
47	1406.2	1103.9	190

48	1430.6	1067.39	186
49	1459.96	1022.86	177
50	1491.07	986.4	179
51	1531.95	958.5	179
52	1582.57	945.87	172
53	1632.23	942.62	179
54	1680.27	915.66	175
55	1727.31	902.56	176
56	1770.84	880.04	180
57	1810.42	847.21	182
58	1836.25	795.5	172
59	1868.25	758.6	170
60	1898.5	715.86	176
61	1930.47	683.43	175
62	1961.18	639.36	167
63	2002.52	610.12	164
64	2044.71	587.15	166
65	2082.98	549.39	171
66	2106.22	483.35	171
67	2132.15	418.23	166
68	2164.24	367.91	170
69	2219.89	338.32	168
70	2278.21	311.87	170
71	2336.42	301.08	175
72	2385.81	272.34	173
73	2440.85	266.45	168
74	2494.18	250.26	167
75	2549.75	234.08	168
76	2608.46	215.24	162
77	2665.82	198.18	161
78	2738.37	182.56	166
79	2859.87	271.03	164
80	2913.63	257.97	164
81	2950.48	230.94	170
82	2974.46	189.06	175
83	2993.19	129.7	171
84	3046.87	127.83	175
85	3087.3	101.26	173
86	3137.45	92.21	171
87	3184.91	84.47	165
88	3233.76	68.25	157
89	3274.17	43.92	154
90	3319.12	10.68	145
91	3371.06	0.74	141
92	3398.74	-18.89	138.44
93	3409.76	-21.18	138.12
94	3417.07	-23.55	138.05
95	3420.43	-24.87	138.19
96	3431.72	-28.19	138.27
97	3443.42	-32.94	137.86
98	3455.57	-36.57	137.47
99	3443.66	-0.96	140.26

100	3465.58	-42.05	137.02
101	3479.12	-47.37	135.9
102	3488	-51.52	135.33
103	3496.89	-55.66	135
104	3479.4	-35.92	136.48
105	3523.75	-59.96	133.48
106	3580.65	-56.18	131.82
107	3636.01	-7.51	130.45
108	3710.88	11.95	116.04
109	3763.66	-16.45	111
110	3822.76	-33.36	110
111	3877.37	-46.73	109.78
112	3925.8	-65.86	108.96
113	3961.13	-99.84	107.86
114	3998.17	-134.43	106.86
115	4040.94	-170.28	105.91
116	4086.23	-194.66	105.47
117	4133.59	-208.03	104.55
118	4188.66	-204.58	103.28
119	4236.84	-180.02	101.43
120	4278.69	-152.01	100.56
121	4329.12	-148.72	99.56
122	4397.93	-145.89	100.1
123	4445.95	-163.82	99.95
124	4495.41	-171.31	96.96
125	4544.55	-195.81	93.98
126	4526.01	-97.99	119
127	4552	-106.31	114
128	4599.09	-126.12	114
129	4651.05	-138.3	120
130	4697.18	-148.73	111
131	4582.15	-228.11	92.37
132	4620.1	-259.03	92.01
133	4656.03	-295.42	91.65
134	4691.64	-330.42	91.51
135	4730.04	-361.12	91.32
136	4774.96	-383.54	91.26
137	4822.71	-394.98	90.41
138	4873.37	-393.48	90.12
139	4969.34	-373.25	89.55
140	5018.49	-359.86	89.41
141	5065.36	-339.33	88.5
142	5106.31	-310.66	87.65
143	5149.54	-287.79	87.4
144	5201.87	-267.94	86.67
145	5245.76	-244.39	87.05
146	5290.57	-210.37	85.36
147	5335.78	-190.26	84.59
148	5380.57	-167.15	83.73
149	5428.33	-153.19	83.63
150	5474.99	-134.9	83.32
151	5525.35	-114.31	81.7

152	5577.28	-95.71	81.18
153	5627.61	-78.79	80.06
154	5675.07	-59.11	79.69
155	5717.56	-33.42	78.93
156	5761.09	-8.35	77.88
157	5804.66	16.8	76.83
158	5828.47	-53.07	75
159	5848.27	41.83	75.78
160	5889.16	-66.76	77.89
161	5902.52	61.73	75.67
162	5936.62	-67.91	76.96
163	5957.03	76.5	75.18
164	5986.57	-67.63	77.13
165	6010.86	99.17	74.33
166	6041.6	-64.04	76.36
167	6091.68	-63.03	74.83
168	6141.32	-62.25	75.16
169	6191.84	-60.13	75.2
170	6240.69	-55.06	75.16
171	6298.79	-49.08	74.2
172	6334.66	-2.65	72.1
173	6370.84	43.75	70
174	6411.03	73.58	70.15
175	6453.47	100.07	72.12
176	6498.7	118.17	72.17
177	6547.71	118.36	70.92
178	6606.62	111.02	70.23
179	6665.52	103.67	69.54
180	6724.57	107.74	69.86
181	7104.38	150.88	85
182	7152.04	179.82	76
183	7178.2	146.9	86
184	7242.31	55.2	62
185	7291.11	47.92	64
186	7335.87	41.51	75
187	7390.92	35.62	67
188	7438.41	23.41	67
189	7483.2	12.53	67
190	7540.18	-14.37	62
191	7585.7	1.14	68
192	7635.28	9.07	62
193	7685.33	15.67	49
194	7734.52	16	55
195	7784.19	12.75	57
196	7833.85	9.5	58
197	7883.89	16.1	53
198	7938.98	17.54	62.06
199	7993.89	19.52	62.2
200	8043.38	0.97	64.83
201	8100.31	-12.2	69.85
202	8147.19	-6.16	69.8
203	8205	-3.49	69.99

204	8257.87	-5.2	70.3
205	8284.14	-1.62	70.94
206	8316.65	-0.56	72.01
207	8356.5	-8.12	66.32
208	8396.71	17.91	64.68
209	8436.97	44.03	63.04
210	8486.97	83.18	62.48
211	8528.66	115.62	62.28
212	8576.47	142.59	62.66
213	8632.2	128.34	61.57
214	8668.88	87.12	61.6
215	8706.64	-23.04	57.92
216	8757.77	-98.33	55.4
217	8801.23	-123.26	55.19
218	8845.99	-155.74	55.02
219	8892.6	-184.68	54.57
220	8937.75	-215.24	54.44
221	8982	-244.24	53.23
222	9031.46	-263.76	53.52
223	9080.24	-276.05	53.54
224	9125.47	-291.04	53.58
225	9188.47	-296.39	49.68
226	9230.33	-282.87	50.55
227	9272.06	-269.4	51.43
228	9317.94	-254.96	52.54
229	9365.69	-240.11	52.02
230	9413.71	-224.72	51.89
231	9461.42	-210.63	51.67
232	9509.31	-195.28	51.83
233	9562.78	-173.54	51.49
234	9603.85	-202.21	47.74
235	9632.09	-258.55	50.54
236	9683.11	-276.95	50.49
237	9734.12	-295.34	50.43
238	9781.12	-314.22	50.23
239	9827.13	-333.5	50.16
240	9875.64	-344.31	47.4
241	9923.61	-355.75	47.34
242	9967.88	-361.36	49.21
243	10017.05	-357.45	52.32
244	10065.97	-349.52	49.2
245	10113.16	-337.18	49.13
246	10154.88	-309.66	48.59
247	10195.96	-280.5	48.49
248	10232.19	-247.39	47.92
249	10270.12	-214.89	47.85
250	10311.81	-188.81	47.54
251	10359.52	-175.38	47.14
252	10403.42	-152.06	47.19
253	10445.21	-133.94	47.4
254	10402.85	53.48	46
255	10466.55	92.37	44

256	10496.82	113.14	42
257	10533.86	125.02	40
258	10586.84	94.51	31
259	10649.11	78.38	39
260	10747.89	52.65	43.27
261	10787.57	85.3	43.03
262	10827.94	114.59	42.74
263	10870.24	141.71	42.49
264	10920.18	156.71	42.38
265	10973.96	160.47	42.46
266	11019.1	157.77	42.33
267	11067.33	154.78	42.18
268	11117.22	151.54	41.9
269	11166.8	147.89	41.91
270	11217.86	142.06	42.16
271	11265.58	135.76	41.94
272	11314.2	115.2	41.97
273	11360.11	97.3	41.67
274	11405.77	77.97	41.82
275	11452.31	60.22	41.59
276	11499.27	39.47	41.7
277	11545.71	24.21	40.23
278	11589.91	0.58	39.78
279	11620.31	-50.24	39.75
280	11674.46	-28.73	39.47
281	11721.32	-47.42	39.26
282	11768.33	-62.4	39.12
283	11821.63	-68.22	38.92
284	11870.58	-64.32	38.45
285	11942.36	-78.33	35.55
286	11998.54	-73.08	30.96
287	12045.47	-81.22	30.17
288	12093.89	-93.33	30.05
289	12142.22	-104.95	29.97
290	12189.7	-122.16	30.25
291	12236.74	-134.59	30.05
292	12287.8	-145.88	30
293	12336.27	-157.9	30
294	12384.74	-169.92	30
295	12433.21	-181.94	29.99
296	12478.36	-192.1	29.84
297	12529.78	-204.68	29.99
298	12578.26	-211.47	29.73
299	12630.04	-216.31	29.32
300	12645.62	-4	34
301	12600.73	88.27	33
302	12670.17	136.59	24
303	12729.11	84.21	31
304	12788.03	34.07	31
305	12852.65	-65.68	28
306	12679.3	-219.7	29.82
307	12729.43	-219.27	29.37

308	12781.11	-216.83	29.3
309	12829.74	-211.76	29.44
310	12877.65	-193.86	20
311	12925.9	-186.39	22
312	12975.89	-170.85	24
313	13023.19	-156.22	23
314	13069.61	-141.15	24
315	13115.09	-121.17	24
316	13160.13	-102.09	24
317	13206.98	-86.12	23
318	13252.94	-69.72	22
319	13294.92	-61.39	23
320	13343.95	-36.46	16
321	13390.82	-22.73	21
322	13437.68	-9	21
323	13476.46	10.93	25
324	13523.33	24.66	25
325	13577.42	28.16	18
326	13637.95	71.94	18
327	13650.92	71.13	23
328	13690.36	58.43	22
329	13726.17	54.19	30
330	13817.48	42.73	24
331	13855.49	42.98	28
332	13900.67	41.94	20
333	13949.86	42.27	27
334	13992.36	40.32	30
335	14039.84	28.11	23
336	14077.59	0.64	38
337	14110.62	11.14	28
338	14138.63	36.37	26
339	14170.38	103.22	23
340	14178.83	110.21	23.5
341	14187.28	117.2	24
342	14223.5	118.33	15
343	14266.38	126.22	11
344	14307.86	142.6	14
345	14340.99	137.45	22
346	14379.46	136.37	28
347	14432.67	138.07	33
348	14463.53	137.38	15
349	14495.28	138.48	30
350	14541.73	146.84	13
351	14581.54	146.22	14.5
352	14616.05	134.82	16
353	14647.05	114.01	15
354	14679.89	85.6	15
355	14712.27	58.54	16
356	14738.39	30.09	12
357	14764.02	9.69	15
358	14807.07	-7.02	13
359	14844.7	-16.61	10

360	14883.59	-14.56	11
361	14919.29	-3.14	8
362	15014.11	-2.95	13
363	15124.96	4.94	9
364	15156.18	18.57	10
365	15203.94	31.85	12
366	15252.18	41.57	14
367	15308.02	50.89	9
368	15353.49	73.1	7
369	15411.14	79.3	4
370	15462.45	97.53	2
371	15513.83	104.58	7
372	15559.82	116.52	10
373	15615.7	119.13	8
374	15668.83	132	10
375	15714.33	149.75	10
376	15763.44	163.49	10
377	15812.54	177.24	10
378	15898.01	101.78	14
379	15912.58	63.42	10
380	15919.72	-1.38	19
381	15861.19	192.32	10
382	15910.3	203.83	11
383	15962.1	216.25	8
384	16012.55	228.22	7
385	16063.91	239.74	7
386	16113.01	253.48	7
387	16163.45	267.68	8
388	16213.92	277.41	5
389	16264.37	291.61	6
390	16312.6	301.33	6
391	16347.85	314.08	9
392	16396.51	326.93	8
393	16446.96	338.89	11
394	16493.39	351.73	18
395	16544.29	364.59	18
396	16593.38	380.57	8
397	16647.85	393.9	5
398	16699.64	406.32	6
399	16751	417.85	9
400	16796.98	429.78	0
401	16844.73	445.31	0
402	16876.02	447.75	12
403	16930.48	463.32	7
404	16983.17	475.3	3
405	17032.27	489.04	1
406	17081.37	502.79	2
407	17133.6	518.34	5
408	17188.02	538.38	3
409	17234.07	541.37	2
410	17324.67	569.26	8
411	17373.34	579.87	5

412	17423.83	587.36	3
413	17561.34	622.27	4
414	17606.89	633.31	6
415	17648.37	649.68	5
416	17700.16	662.1	6

Appendix 3 Seismograph UTM Locations

PASSCAL Seismograph Number	Station #	UTM Northing	UTM Easting	Elevation (m)	Geo. Freq.
553	2	4113781	590355	281	4.5
557	3	4113824	590323	289	40
554	4	4113861	590293	273	4.5
551	5	4113911	590272	277	40
559	6	4113948	590257	268	4.5
442	7	4113998	590245	256	40
560	8	4114025	590235	258	4.5
561	9	4114053	590224	260	40
562	10	4114077	590189	261	4.5
696	11	4114072	590132	254	40
558	12	4114148	590119	261	4.5
555	13	4114194	590101	258	40
552	14	4114236	590072	252	4.5
556	15	4114257	590026	252	40
563	16	4114281	589986	249	4.5
102	17	4114327	589961	236	40
100	18	4114326	589919	223	4.5
101	19	4114371	589878	233	40
110	20	4114412	589900	229	4.5
106	21	4114459	589902	233	40
109	22	4114505	589889	231	4.5
105	23	4114551	589899	222	40
103	24	4114596	589919	221	4.5
108	25	4114635	589885	214	40
107	26	4114675	589859	201	4.5
104	27	4114713	589826	201	40
111	28	4114769	589819	202	4.5
574	29	4114811	589811	197	40
455	30	4114861	589807	208	4.5
133	31	4114910	589785	203	40
41	32	4114947	589755	202	4.5
456	33	4114987	589734	205	40
52	34	4115035	589708	202	4.5
134	35	4115086	589700	208	40
207	36	4115132	589706	211	4.5
70	37	4115183	589719	211	40
201	38	4115229	589733	210	4.5
180	39	4115279	589734	209	40
66	40	4115329	589729	216	4.5
175	41	4115378	589722	221	40
580	42	4115415	589695	219	4.5
573	43	4115464	589682	216	40
517	44.2	4115509	589661	203	4.5
578	44	4115554	589658	187	40
209	45	4115599	589652	199	4.5
567	46	4115643	589648	211	40
47	47	4115702	589635	220	4.5

485	48	4115740	589613	216	40
507	49	4115786	589586	207	4.5
460	50	4115830	589567	209	40
132	51	4115879	589560	209	4.5
587	52	4115930	589571	202	40
433	53	4115976	589590	209	4.5
149	54	4116031	589587	205	40
524	55	4116079	589596	206	4.5
511	56	4116128	589595	210	40
501	57	4116178	589583	212	4.5
566	58	4116224	589548	202	40
50	59	4116269	589529	200	4.5
59	60	4116315	589504	206	40
576	61	4116358	589489	205	4.5
38	62	4116405	589463	197	40
436	63	4116455	589455	194	4.5
401	64	4116503	589453	196	40
483	65	4116554	589436	201	4.5
404	66	4116604	589387	201	40
458	67	4116656	589340	196	4.5
412	68	4116707	589309	200	40
139	69	4116770	589307	198	4.5
183	70	4116834	589309	200	40
607	71	4116891	589325	205	4.5
406	72	4116948	589321	203	40
596	73	4117000	589340	198	4.5
403	74	4117055	589349	197	40
579	75	4117112	589359	198	4.5
582	76	4117173	589368	192	40
593	77	4117232	589378	191	4.5
409	78	4117304	589396	196	40
604	79	4117374	589529	194	4.5
408	80	4117428	589541	194	40
605	81	4117473	589533	200	4.5
407	82	4117513	589506	205	40
428	83	4117556	589461	201	4.5
610	84	4117605	589483	205	40
402	85	4117653	589477	203	4.5
522	86	4117702	589491	201	40
492	87	4117748	589505	195	4.5
411	88	4117799	589512	187	40
177	89	4117846	589508	184	4.5
609	90	4117901	589498	175	40
497	91	4117952	589512	171	4.5
450	92	4118004	589510.5	168.05	40
74	10001	4117985.5	589506.6	168.44	99
431	10002	4117996.4	589509.4	168.12	99
743	10003	4118007.6	589510.8	168.19	99
116	10004	4118019.2	589512.8	168.27	99
681	10005	4118031.8	589513.7	167.86	99
130	10006	4118044.3	589515.8	167.47	99
121	10007	4118055.7	589515.3	167.02	99

529	10008	4118070.2	589516.5	165.9	99
664	10009	4118080	589516.7	165.33	99
750	10010	4118089.8	589516.9	165	99
445	93	4118017.9	589542.5	170.26	40
879	94	4118065.4	589526.9	166.48	4.5
413	94.5	4118115.8	589524.9	163.48	40
447	95	4118165.2	589553.4	161.82	4.5
405	96	4118193.4	589621.5	160.45	40
482	97	4118252	589672	146.04	4.5
597	98	4118311.9	589669.8	141	40
80	99	4118372.4	589680.7	140	4.5
57	100	4118427.3	589692.8	139.78	40
451	101	4118479.2	589697	138.96	4.5
594	102	4118525.9	589682.1	137.86	40
830	103	4118574.4	589667.4	136.86	4.5
165	20001	4119032	589933	149	99
464	20002	4119059	589937	144	99
178	20003	4119110	589940	144	99
486	20004	4119162	589952	150	99
73	20005	4119208	589963	141	99
844	104	4118628.6	589654.1	135.91	99
136	105	4118680	589652.2	135.47	4.5
417	106	4118728.4	589661.1	134.55	40
81	107	4118776.3	589688.5	133.28	4.5
46	108	4118808.7	589731.8	131.43	40
86	109	4118833.9	589775.4	130.56	4.5
508	110	4118877.7	589800.6	129.56	40
79	111	4118938.2	589833.5	130.1	4.5
55	112	4118989.2	589838.6	129.95	40
85	113	4119036.9	589853.7	126.96	4.5
512	114	4119091.8	589853.4	123.98	40
82	115	4119139.8	589841	122.37	4.5
506	116	4119187.5	589830	122.01	4.5
78	117	4119235.8	589813.2	121.65	4.5
49	118	4119283.2	589797.5	121.51	40
75	119	4119331.2	589786.9	121.32	4.5
441	120	4119381.4	589786.6	121.26	40
84	121	4119429.3	589797.4	120.41	4.5
425	122	4119474.1	589821.1	120.12	40
514	124	4119551.3	589881.6	119.55	40
45	125	4119589.5	589915.3	119.41	4.5
840	126	4119622.5	589954.4	118.5	40
40	127	4119646.6	589998.2	117.65	4.5
503	128	4119675.3	590037.8	117.4	40
523	129	4119713.5	590078.7	116.67	4.5
414	130	4119742.5	590119.2	117.05	40
148	131	4119767.7	590169.5	115.36	4.5
418	132	4119799.4	590207.5	114.59	40
513	133	4119829.4	590248	113.73	4.5
500	134	4119866.1	590281.6	113.63	40
77	135	4119899.9	590318.6	113.32	4.5
518	136	4119936	590359.3	111.7	40

25	137	4119974.4	590398.9	111.18	4.5
419	138	4120012.1	590436.3	110.06	40
30	139	4120046	590474.9	109.69	4.5
581	140	4120072.8	590516.7	108.93	40
83	141	4120100.8	590558.4	107.88	4.5
420	142	4120128.8	590600.2	106.83	40
843	143	4120156.9	590641.9	105.78	4.5
424	144	4120196.8	590683.7	105.67	40
841	145	4120239.2	590721	105.18	4.5
422	146	4120277.5	590765.1	104.33	40
505	147	4120181	590548	115	4.5
504	148	4120241.5	590562.5	107.89	40
89	149	4120284.6	590582.4	106.96	4.5
87	150	4120329.3	590604.7	107.13	40
93	151	4120377.1	590632.2	106.36	4.5
416	152	4120421.6	590655.2	104.83	40
143	153	4120465.8	590677.8	105.16	4.5
421	154	4120510.2	590702	105.2	40
544	155	4120551.8	590728.1	105.16	4.5
415	156	4120601.3	590759.1	104.2	40
141	157	4120613	590816.6	102.1	4.5
172	158	4120625	590874.2	100	40
546	159	4120647.9	590918.7	100.15	4.5
577	160	4120674.3	590961.2	102.12	40
488	161	4120706.9	590997.4	102.17	4.5
34	162	4120750.8	591019.2	100.92	40
27	163	4120806.9	591038.6	100.23	4.5
590	164	4120863	591058	99.54	40
547	165	4120914.2	591087.7	99.86	4.5
832	40001	4121236	591294	115	99
612	40002	4121266	591341	106	99
757	40003	4121304	591323	116	99
90	401	4121402	591269	92	4.5
474	402	4121449	591284	94	40
88	403	4121492	591298	105	4.5
469	404	4121544	591317	97	40
154	405	4121592	591327	97	4.5
95	406	4121637	591337	97	40
542	407	4121700	591338	92	4.5
33	408	4121734	591372	98	40
203	409	4121775	591401	92	4.5
569	410	4121817	591429	79	40
435	411	4121861	591451	85	4.5
570	412	4121907	591470	87	40
540	413	4121953	591489	88	4.5
568	414	4121995	591517	83	40
69	415	4122043.8	591542.6	92.06	4.5
36	416	4122092.2	591568.6	92.2	40
541	417	4122144.8	591573.8	94.83	4.5
571	418	4122201.7	591587.1	99.85	40
545	419	4122241.1	591613.2	99.8	4.5
589	420	4122291.8	591641.1	99.99	40

29	421	4122340	591662.9	100.3	4.5
31	422	4122362	591677.7	100.94	40
510	423	4122390.7	591693	102.01	4.5
881	424	4122429.8	591703.8	96.32	40
548	425	4122454.4	591744.9	94.68	4.5
525	426	4122479	591786.1	93.04	40
868	427	4122506.6	591843.3	92.48	4.5
480	428	4122529.7	591890.8	92.28	40
127	429	4122560.7	591936.1	92.66	4.5
871	430	4122617	591947.9	91.57	40
400	431	4122668.1	591927.1	91.6	4.5
391	432	4122750.6	591844.9	87.92	40
54	433	4122829.7	591799.9	85.4	4.5
394	434	4122879.7	591796.7	85.19	40
867	435	4122934.2	591787.3	85.02	4.5
393	436	4122988.8	591781.9	84.57	40
125	437	4123042.8	591774.4	84.44	4.5
392	438	4123095.3	591767.9	83.23	40
481	439	4123148.3	591772.2	83.52	4.5
60	440	4123197.5	591782.7	83.54	40
861	441	4123244.7	591789.2	83.58	4.5
874	442	4123303.6	591812.2	79.68	40
863	443	4123335.2	591842.8	80.55	4.5
839	444	4123366.7	591873.3	81.43	40
876	445	4123401.5	591906.5	82.54	4.5
140	446	4123437.8	591940.9	82.02	40
72	447	4123474.1	591975.9	81.89	4.5
397	448	4123510.7	592009.6	81.67	40
146	449	4123546.9	592044.5	81.83	4.5
198	601	4123585.3	592087.6	81.49	40
550	602	4123634.8	592080	77.74	4.5
509	604	4123685	592041.9	80.54	4.5
176	605	4123738.9	592047.9	80.49	40
443	606	4123792.8	592053.9	80.43	4.5
444	607	4123843.3	592057.7	80.23	40
187	608	4123893.1	592060.7	80.16	4.5
196	609	4123941.4	592072.4	77.4	40
195	610	4123989.5	592083.3	77.34	4.5
193	611	4124031.7	592097.8	79.21	40
189	612	4124074.1	592123	82.32	4.5
197	613	4124114.5	592151.7	79.2	40
199	614	4124151.4	592183.6	79.13	4.5
191	615	4124176.7	592226.7	78.59	40
188	616	4124200.7	592271	78.49	4.5
99	617	4124218.6	592316.7	77.92	40
96	618	4124238.3	592362.6	77.85	4.5
465	619	4124264.2	592404.4	77.54	40
475	620	4124301.1	592437.5	77.14	4.5
466	621	4124330.2	592477.8	77.19	40
92	622	4124359.7	592512.5	77.4	4.5
94	623	4124239	592662	76	40
498	625	4124279	592725	74	40

97	626	4124297	592757	72	4.5
399	701	4124325	592784	70	40
208	702	4124386	592780	61	4.5
206	703	4124449	592793	69	40
76	704	4124549	592813.5	73.27	4.5
179	705	4124570.2	592860.3	73.03	40
26	706	4124593.5	592904.4	72.74	4.5
734	707	4124619.5	592947.4	72.49	40
543	708	4124657.7	592982.9	72.38	4.5
423	709	4124704.3	593010	72.46	40
128	710	4124746	593027.5	72.33	4.5
585	711	4124790.6	593046.1	72.18	40
539	712	4124836.8	593065.2	71.9	4.5
866	713	4124882.9	593083.8	71.91	40
865	714	4124931.3	593101.1	72.16	4.5
438	715	4124976.9	593116.5	71.94	40
549	716	4125029.6	593119.5	71.97	4.5
205	717	4125078.7	593123.7	71.67	40
389	718	4125128.2	593126.5	71.82	4.5
395	719	4125177.8	593131.1	71.59	40
862	720	4125229.1	593133.2	71.7	4.5
71	721	4125277.5	593140	70.23	40
864	722	4125327.6	593138.3	69.78	4.5
463	801	4125377.3	593106.1	69.75	40
35	802	4125416.4	593149.3	69.47	4.5
32	803	4125466.7	593153.2	69.26	40
390	804	4125515.5	593160.5	69.12	4.5
755	805	4125565.9	593178.8	68.92	40
598	806	4125608.1	593203.9	68.45	40
833	807	4125678.7	593223	65.55	4.5
741	808	4125726.8	593252.5	60.96	40
502	809	4125772.5	593265.9	60.17	40
221	810	4125821.3	593276.4	60.05	4.5
212	811	4125869.8	593287.3	59.97	40
487	812	4125920	593292.8	60.25	40
124	813	4125967.7	593302.4	60.05	4.5
211	814	4126018.5	593314.8	60	40
532	815	4126067.3	593325.4	60	40
224	816	4126116.1	593336	60	4.5
530	817	4126164.9	593346.6	59.99	40
168	818	4126209.9	593357.4	59.84	40
113	819	4126261.6	593368.8	59.99	4.5
526	820	4126308.1	593384.1	59.73	40
223	821	4126356.7	593402.6	59.32	40
214	822	4126402.4	593421.3	59.82	4.5
158	823	4126447.2	593443.8	59.37	40
760	824	4126492.5	593468.8	59.3	40
837	825	4126533.9	593494.8	59.44	4.5
150	826	4126569	593532	50	40
534	827	4126609	593560	52	40
490	90001	4126277	593600	64	99
753	90002	4126196	593663	63	99

135	90003	4126237	593737	54	99
754	90004	4126313	593716	61	99
43	90005	4126388	593697	61	99
166	90006	4126490	593636	58	99
120	828	4126647	593596	54	4.5
521	829	4126683	593630	53	40
672	830	4126718	593664	54	40
117	831	4126750	593702	54	4.5
592	832	4126782	593739	54	40
623	833	4126817	593774	53	40
126	834	4126851	593809	52	4.5
742	835	4126885	593835	53	40
531	836	4126918	593879	46	40
123	837	4126954	593912	51	4.5
457	838	4126990	593945	51	40
586	839	4127016	593980	55	40
216	840	4127052	594013	55	4.5
156	841	4127099	594040	48	40
479	842	4127134	594106	48	40
440	843	4127146	594111	53	4.5
144	844	4127187	594117	52	40
614	845	4127221	594129	60	40
119	846	4127308	594159	54	4.5
519	847	4127342	594176	58	40
44	848	4127383	594195	50	40
477	849	4127427	594217	57	4.5
468	850	4127466	594234	60	40
528	851	4127514	594244	53	40
679	852	4127560	594236	68	40
219	853	4127585	594260	58	4.5
112	854	4127599	594295	56	40
747	10101	4127598	594369	53	99
744	10102	4127602.5	594379	53.5	99
138	10103	4127607	594389	54	99
740	2074	4127639	594406	45	40
159	2073	4127674	594432	41	40
155	2072	4127704	594465	44	4.5
432	2071	4127736	594475	52	40
439	2070	4127771	594491	58	40
875	2069	4127818	594516	63	4.5
153	2068	4127846	594529	45	40
583	2067	4127874	594544	60	40
202	2066	4127912	594572	43	4.5
495	2065	4127948	594589	4.5	40
186	2064	4127984	594594	46	40
68	2063	4128021	594589	45	4.5
484	2062	4128063	594578	45	40
62	2061	4128104	594568	46	40
204	2060	4128140	594554	42	4.5
494	2059	4128172	594547	45	40
473	2058	4128218	594551	43	40
538	2057	4128256	594559	40	4.5

137	2056	4128290	594578	41	40
732	2055	4128317	594604	38	40
67	2054	4128402	594646	43	4.5
662	2053	4128498	594702	39	40
665	2052	4128520	594728	40	40
145	2051	4128557	594761	42	4.5
619	2050	4128596	594791	44	40
210	2049	4128642	594824	39	40
878	2048	4128673	594864	37	4.5
611	2047	4128722	594895	34	40
736	2046	4128760	594934	32	40
448	2045	4128803	594963	37	4.5
410	2044	4128839	594994	40	40
157	2043	4128888	595021	38	40
185	2042	4128930	595056	40	4.5
427	2041	4128963	595092	40	40
745	2040	4129001	595126	40	40
618	2039	4129039	595160	40	40
761	2038	4129076	595195	40	4.5
751	2037	4129115	595227	41	40
462	2036	4129156	595261	38	4.5
620	11001	4129149	595130	44	99
452	11002	4129179	595102	40	99
173	11003	4129214	595047	49	99
151	2035	4129196	595294	37	4.5
515	2034	4129237	595327	37	40
613	2033	4129275	595361	37	40
835	2032	4129314	595396	38	4.5
472	2031	4129355	595427	35	40
446	2030	4129394	595462	36	40
615	2029	4129433	595492	36	40
192	2028	4129459	595519	39	4.5
668	2027	4129497	595552	38	40
42	2026	4129537	595585	41	40
453	2025	4129573	595617	48	40
220	2024	4129613	595651	48	4.5
164	2023	4129650	595687	38	40
735	2022	4129693	595723	35	40
181	2021	4129734	595757	36	40
430	2020	4129775	595790	39	4.5
667	2019	4129811	595821	30	40
115	2018	4129847	595856	30	40
114	2017	4129874	595872	42	40
520	2016	4129916	595910	37	4.5
48	2015	4129958	595944	33	40
56	2014	4129996	595978	31	40
142	2013	4130034	596012	32	40
595	2012	4130074	596049	35	4.5
622	2011	4130114	596091	33	40
152	2010	4130154	596114	32	40
122	2009	4130223	596179	38	40
91	2008	4130262	596210	35	4.5

459	2007	4130304	596239	33	4.5
222	2004	4130412	596331	34	4.5
215	2003	4130448	596361	36	4.5
535	2002	4130478	596394	35	4.5
845	2001	4130519	596428	36	4.5